2008-04-28

Optimal sensor/actuator placement and switching schemes for control of flexible structures

Raffaele Potami
Worcester Polytechnic Institute

Optimal sensor/actuator placement and switching schemes for control of flexible structures

by

Raffaele Potami

A Thesis

Submitted to the Faculty

of the

WORCESTER POLYTECHNIC INSTITUTE

In partial fulfillment of the requirements for the

Degree of Doctor of Philosophy

in

Mechanical Engineering

by

April 2008

APPROVED:

Professor Michael A. Demetriou, Main Advisor

Professor Mark W. Richman, Committee Member

Professor Islam Hussein, Committee Member

Professor Karolos M. Grigoriadis, Committee Member

Professor Nikolaos A. Gatsonis,Graduate Committee Rep.

Abstract

The vibration control problem for flexible structures is examined within the context of overall controller performance and power reduction. First, the issue of optimal sensor and actuator placement is considered along with its associated control robustness aspects. Then the option of alternately activating subsets of the available devices is investigated. Such option is considered in order to better address the effects of spatiotemporally varying disturbances acting on a flexible structure while reducing the overall energy consumption.

Towards the solution to the problem of optimal device placement, three different approaches are proposed. First, a computationally efficient scheme for the simultaneous placement of multiple devices is presented. The second approach proposes a strategy for the optimal placement of sensors and collocated sensor/actuator pairs, taking into account the influence of the spatial distribution of disturbances. The third approach provides a solution to the actuator location problem by incorporating considerations with respect to preferred spatial regions within the flexible structure.

Then the second problem named above is considered. Activating a subset of the available and optimally placed actuators and sensors in a flexible structure provides enhanced performance with reduced energy consumption. Such approach of switching on and off different actuating devices, depending on their local-in-time authority, results in a hybrid system. Therefore the proposed work draws on existing results on hybrid systems and includes an additional degree of freedom, whereby both the actuating devices and the control signals allocated to them are switched in and out. To enable this switching an activation strategy, which insures also that stability-under-switching is guaranteed, is required. Three different strategies are

considered for such actuators allocation: first a cost-to-go index is considered, then a cost function based on the mechanical energy of the flexible structure and finally a performance index based on the maximum deviation of the transverse displacement.

A flexible aluminum plate was chosen to validate and test the proposed approaches. The set up utilized four pairs of collocated piezoceramic patches that serve to provide sensing and actuating capabilities. Extensive numerical simulations were performed for both the placement strategies and the switching policies proposed, in order to predict the behavior of the flexible plate and provide the optimal actuator and sensor locations that were to be affixed on the flexible structure.

Finally, to complete the validation process a sequence of experimental tests were performed. The objective of these tests was to compare the performance of the proposed hybrid control system to traditional non switched control schemes. In order to provide a repeatable perturbation, four of the piezoceramic patches were allocated to simulate a spatiotemporally varying disturbance, while the remaining four patches were used as sensors and controlling actuators. The experimental results showed a significant performance improvement for the switched controller over the traditional controller. Moreover the switched controller exhibited improved robustness towards spatiotemporally varying disturbances while the traditional controller showed a significant loss of controller performance. The improvement achieved in vibration control problems could be extended to a wider range of applications. In particular, although this study was concentrated on a rectangular thin plate, the proposed strategies can be applied to *any* structure and more generally to any plant whose dynamics can be represented by a second order linear system. For example, by removing the restriction of spatially fixed actuators and sensors, the proposed theory can be applied to the problem of unmanned vehicles control.

Acknowledgements

I would like to gratefully thank my advisor Prof. Demetriou for his guidance during my academic studies at WPI.

I would like to thank my family and my wife for all the moral and practical support they provided during those years.

I am also grateful to all the members of the Aerospace group of ME Dept. for being an always stimulating source of knowledge and help at the same time. Thanks to Randy and Sia for their invaluably help with computer problems and to Barbara Furhman, Pamela St Louis and Barbara Edilberti for their precious help with the bureaucracy world.

Contents

List of Figures

List of Tables

Chapter 1

Introduction

1.1 Objectives and Literature Review

The objective of this work is to propose new schemes to optimize the overall performance of control systems and in particular flexible structures. Vibration control problems were chosen to apply these new schemes due to the wide range of existing applications. It is indeed possible to identify vibration phenomena in almost any engineering problem. For the majority of cases, vibration is an unwelcome component of the designed operating conditions and, if left uncontrolled, it can result in serious damage or loss of efficiency. A well known example is the Tacoma Narrows Bridge which collapsed due to wind induced vibration [1].

Active or passive strategies can be used in order to control and reduce structures' vibration. Reducing the stress induced by vibration results in an extended lifetime, noise reduction, lighter structural design and weight reduction; this directly translates in improving system efficiency and performances. Examples can be found in several fields [2] such as the automotive industry [3, 4, 5, 6], the aeronautical industry [7, 8] or the aerospace field [9, 10]. Also, vibration control has relevant applications

Figure 1.1: Solar sail: example of flexible structure in space application (BBC News 5/14/2002)

in other fields, for example building safety [11, 12, 13] against earthquakes.

The objective of this work can be achieved by two separate steps described in the following paragraphs.

1.1.1 Architecture design for control systems

The first step to improve vibration control of a flexible structure is to optimize its architecture design. Two main components can be distinguished in this phase: the *structure's geometry* and the *network of sensors and actuators* linked to the structure.

One way to increase control system's efficiency is to optimize the structure's shape and geometry. Several geometries have been investigated in the past years such as the case of the beam [14, 15, 16], the plate [17, 18, 19] or more complex shapes such as shell [20] or toroidal configurations [21]. Another approach to improve struc-

tural vibration control is to optimize sensors and actuators capabilities. Different options are available for such components and interesting contributions have come from the use of smart materials [22, 23, 24, 25, 26, 27]. Placement of the actuating devices was found to play a fundamental role over the global control capability and it has been the object of intense study in the past years, see [28, 29, 19]. The goal is to determine the device's location that guarantees optimality for the closed loop system. This is accomplished by defining a performance index, which accounts for the vibration control effect over the global structure behavior, and by optimizing such index. Several choices for the performance index have been proposed. An index based on modal controllability is used to optimally locate an acting bracing system in civil structures [30] or to place piezoelectric patches on a cantilever beam [18]. In [31] the performance index is intended to maximize the spatial controllability of piezoelectric patches. A similar approach is to minimize capital and installation costs with the constraint of stability for the overall system. This is done in [32] for chemical reactors.

The optimization strategies referenced above do not account for possible perturbations affecting the structure, which is a common condition in real applications. A placement strategy that does not account for such influence may not guarantee optimality for the closed loop. To avoid this problem, the disturbance's influence should be included in the performance index. This was done in [33] where the minimized index is the H_∞ norm of the transfer function between the disturbance and the state's variables. The disturbance effect is accounted for, but the optimization is still dependent on the arbitrary choice made for such disturbance. Unless the spatial distribution of disturbance is known *a priori*, an arbitrary choice may again result in loss of optimality.

A different challenge when selecting the placement of multiple devices is to ac-

count for their mutual influence. Placement of multiple actuators can be determined by looking for the optimal placement of each single element. In certain cases, the locations found may not be optimal when the full set of devices is simultaneously affixed and utilized. This is due to the influence that the actuators may have over the structure's properties and therefore the optimality function. For example the addition of piezoceramic patches changes the mass and stiffness distributions of the structure.

Three strategies are presented here to address the problems highlighted above. The first one is based on maximizing modal controllability for a given number of modes. The actuators' placement is computed simultaneously for all the available devices, accounting for their mutual influences over the plate's behavior. In the second approach, a more general procedure is considered where the effect of disturbances is included in the optimization process. A spatial distribution of disturbance is calculated as the worst admissible case; this guarantees robustness against unknown disturbances. The third placement policy guarantees overall vibration reduction while enhancing stability over preselected spatial regions of the structure. This is equivalent to globally ensuring spatial controllability and at the same time maximizing preselected modal controllability. The common goal is to optimally and efficiently design the control system's architecture. Two optimization problems are encountered, maximizing the performance index and defining the spatial component for the disturbance distribution. In order to find the locations that maximize the performance, a brute force optimization is used over a grid of possible candidate locations. The second optimization problem is solved by using the *Matlab*® Optimization Toolbox. Numerical studies were performed simulating a square aluminum plate one meter wide with a set of piezoelectric patches as sensing and actuating devices.

The final result is a closed loop system where the original plant is interfaced with a network of sensors and actuators. The strategies proposed in this work are applied to the case of flexible structures, however it is important to highlight how those approaches can be applied to *any* structure and more generally to any plant whose dynamics is represented by a second order linear system.

1.1.2 Switching rules for hybrid control system

In several situations it may not be possible or convenient to simultaneously activate the entire set of available actuators. For example, one may have a limited power supply and not be able to use the entire set of these devices.

Moreover, different actuators may own different levels of efficiency, depending, for example, on external disturbances or different stages of the main plant process. In such cases, one may want to use only a subset of efficient actuators. Typically this subset is not composed by the same elements for the entire time domain. It is therefore required to determine an activation strategy that identifies the efficient actuators to be turned on during the time domain of interest. The second step of this work is therefore to provide the hybrid system with a switching strategy to define in real time the actuators activation sequence.

The most general definition of a hybrid system is a dynamic system that exhibits both continuous and discrete dynamic behavior. This is the case of a system provided with a network of sensors and actuators that can be alternately activated. The control system described above exhibits a continuous dynamics behavior when a subset of sensors and actuators are used. If at a certain discrete time the elements of such subset are modified, the system dynamics will also exhibit a discrete behavior.

In several cases, the switching sequence may not be determined by a human

supervisor. For example, this could be due to high switching frequency or excessive computations required at each switch. In this situation an automated controller is required to define the sequence of devices to be activated.

Several options can be considered for the activation policies. For example, one may look for the sequence that maximizes the results, increases stability or minimizes cost functions. Example of hybrid systems can be found in almost any field such as medical care [34], chemistry [35], electronics, marine [36], automotive or aeronautical [37], etc etc.

Hybrid system switching presents two main challenges. The first one is to identify the sequence of subsystems to be activated. The second challenge is to define the time sequence or switching times. Several solutions have been explored in the past years, such as the ones proposed in [38] and [39]. The goal here is to provide the controller with a set of decision rules enabling its ability to autonomously determine the subsystems activation sequence. Switching sequences can be defined for both sensing and controlling subsystems, but due to the higher impact of the actuators efficiency on the overall system performance, only the second class of subsystems is considered. Several switching strategies have been proposed. In [40], the supervisor strategy for a discrete hybrid system is based on minimizing a tracking error signal. In [34], the switching logic is focused on optimizing a performance index related to the H_∞ control theory. A different choice for the index to be minimized is made in [36]. The switching logic for discrete systems is designed using a finite horizon technique. A model predictive approach is presented in [41] to generate the switched control law for discrete time hybrid systems. Action dependent heuristic dynamic programming is instead used in [42] to obtain a solution to the dynamic problem of generating a switching law.

Another important aspect of switched system's design is considered in [35, 43].

A set of constraints and rules for the switching algorithm are introduced in order to ensure stability under switching. In [44] feedback gains for the controlling subsystems are defined in a way such that the overall switched system is stable. The stability issue in hybrid systems has been investigated by several authors. In [37], a common non traditional Lyapunov function is used to guarantee stability for the switched system. A switching law based on defining a common Lyapunov function is proposed in [45] to ensure stability for linear systems. Lie algebra is used instead in [46] to generate a common Lyapunov function and prove stability for the system. A different solution is proposed in [47]. It consists in identifying the "worst" or least stable solution for the switched system and verify that it still fulfils the minimum requirements of stability.

In this work three different approaches to implement an autonomous switching controller are presented. The first switching policy is based on plant's global properties. It defines the activation sequence minimizing a cost function for the system. The goal with the second policy is to chose the activation sequence that minimizes the plant's kinetic energy. Finally the third law is based on local structure behavior. It enables the controlling devices closest to the area of the structure where the disturbance effect is maximum. Differently from what was found in most of the works referred above, the proposed algorithms were validated with *both* numerical simulations and experimental tests. The structure selected for the tests was a thin aluminium plate and piezoelectric material patches were used both as sensing and actuating devices. This material can be used in several industrial applications [48] and has been intensively used for controlling vibration in flexible structures [49].

1.2 Chapter Organization

The dynamics of the flexible thin plate considered in this thesis is presented in the following chapter. Chapter 2 includes the finite element model used and the model considered to represent the piezoelectric patches. After a brief introduction, three placement strategies are described in details in the third chapter. Final section of Chapter 3 includes the relative numerical test performed for each of the presented strategies. Chapter 4 is dedicated to hybrid switched systems. After an overview on hybrid systems three switching policies are described. In this chapter are also presented the results from the performed numerical simulation and the experimental tests. Finally conclusions and future developments are presented in last chapter.

Chapter 2

Thin Plate Model

2.1 Dynamics of the Thin Plate

In this section the dynamics of a thin, flexible plate is described. The plate dimensions are indicated by $L_\xi = a, L_\zeta = b$. The choice a thin plate was made due to its simplified mathematical model. The following general assumption are implicitly

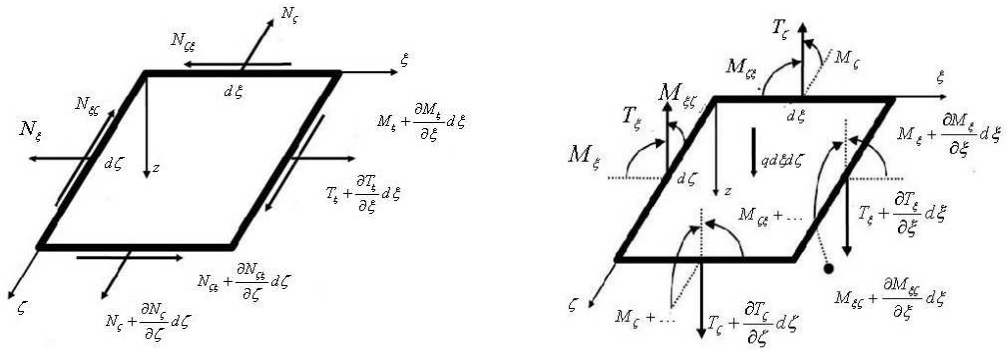

Figure 2.1: In and out of plane forces

made by using the thin plate theory [50]:

- The plate is thin in the sense that the thickness is small compared to the other characteristic lengths.

- The plate thickness is uniform so that three-dimensional stress effects are ignored.
- The plate is composed by homogenous and isotropic material with linear, elastic properties.
- The plate deforms through flexural deformation. The deformations are small in comparison with the thickness.

Piezoelectric patches, affixed on the plate, are used as sensors and actuators. It is assumed that the piezoelectric patches thickness is small compared to the plate thickness.

In Figure 2.1 the forces N, T and moments M acting over a representative plate element are presented. First it is considered the static problem. With reference to Figure 2.1 the equilibrium of forces in z direction is given by

$$\frac{\partial T_\xi}{\partial \xi} + \frac{\partial T_\zeta}{\partial \zeta} + q = 0. \tag{2.1}$$

Additionally, from the equilibrium of moments in ξ and ζ directions,

$$T_\xi = \frac{\partial M_\xi}{\partial \xi} + \frac{\partial M_{\zeta\xi}}{\partial \zeta} \tag{2.2}$$

$$T_\zeta = \frac{\partial M_\zeta}{\partial \zeta} + \frac{\partial M_{\xi\zeta}}{\partial \xi} \tag{2.3}$$

We now introduce the relation between the displacement in z direction v and the moments $M_\xi, M_\zeta, M_{\xi\zeta}$

$$M_\xi = -D_E\left(\frac{\partial^2 v}{\partial \xi^2} + \nu\frac{\partial^2 v}{\partial \zeta^2}\right) \tag{2.4}$$

$$M_\zeta = -D_E\left(\frac{\partial^2 v}{\partial \zeta^2} + \nu\frac{\partial^2 v}{\partial \xi^2}\right) \tag{2.5}$$

$$M_{\xi,\zeta} = -(1-\nu)D_E\frac{\partial^2 v}{\partial \xi \zeta} \tag{2.6}$$

where D_E is the plate flexural rigidity

$$D_E = \frac{Eh^3}{12(1-\nu^2)} \tag{2.7}$$

with ν the Poisson's ratio, E the Young's elastic modulus and h the plate thickness.

Combining together equation (2.1)-(2.6) and introducing the inertial term, the dynamics of the plate is described by the following equation

$$\rho h\frac{\partial^2 v(\xi,\zeta,t)}{\partial t^2} + D_E\nabla^4 v(\xi,\zeta,t) = q(\xi,\zeta,t) \tag{2.8}$$

with ρ being the density of the material used.

The equation obtained so far does not include any damping effect. To complete the model air damping and the Kelvin-Voigt [51] damping components are introduced. The term $q(\xi,\zeta)$ represents the forces per unit of area acting over the plate. In our case the term q includes the control forces and the disturbance forces. The control action is delivered by the piezoelectric patches in term of the moments $M_{p\xi}$ and $M_{p\zeta}$. The disturbance is represented by the term $d(\xi,\zeta,t)$.

The plate equation finally becomes

$$\rho h \frac{\partial^2 v(\xi,\zeta,t)}{\partial t^2} + D_E \nabla^4 v(\xi,\zeta,t) + c_d \nabla^4 \frac{\partial v(\xi,\zeta,t)}{\partial t} = \frac{\partial^2 M_{p\xi}(t)}{\partial \xi^2} + \frac{\partial^2 M_{p\zeta}(t)}{\partial \zeta^2} + d(\xi,\zeta,t) \tag{2.9}$$

An approximated solution for this equation is provided in the next sections.

2.2 The Variational Form

First we assume that the approximated solution of equation (2.9) can be expressed in its separate spatial and temporal components.

$$v(\xi,\zeta,t) = \sum_{m=1}^{N_\xi} \sum_{n=1}^{N_\zeta} \phi_{mn}(\xi,\zeta) x_{mn}(t) \tag{2.10}$$

Substituting the approximated solution (2.10) in (2.9) we end up with a residual component due to the approximation introduced. Following the Galerkin method we then force all the residuals to be orthogonal to the base function ϕ_{mn}. This is done by taking the inner product between the residuals and the base function and set the result to be zero.

Equation (2.9) can now be written as a system of $N_m \times N_n$ equations, in the vector second order form

$$M(\xi,\zeta)\ddot{X}_{mn}(t) + D(\xi,\zeta)\dot{X}_{mn}(t) + K(\xi,\zeta)X_{mn}(t) = B(\xi,\zeta)U(t) + E(\xi,\zeta)W(t) \tag{2.11}$$

where $B(\xi,\zeta)$ and $E(\xi,\zeta)$ are the matrix representations of the control and disturbance distributions, respectively. Matrices M and K are respectively the mass and

stiffness matrices.

The expressions for the matrices obtained as a result of the above discretization are

$$
\begin{aligned}
K_s &= D_E \sum_{m=1}^{N_m} \sum_{n=1}^{N_n} \int_0^a \int_0^b \left(\frac{\partial^4 \phi_{mn}(\xi,\zeta)}{\partial \xi^4} + 2\frac{\partial^4 \phi_{mn}(\xi,\zeta)}{\partial \xi^2 \partial \zeta^2} + \frac{\partial^4 \phi_{mn}(\xi,\zeta)}{\partial \zeta^4} \right) \phi_{kl}(\xi,\zeta) d\xi d\zeta \\
M_s &= \rho h \sum_{m=1}^{N_m} \sum_{n=1}^{N_n} \int_0^a \int_0^b \phi_{mn}(\xi,\zeta)\phi_{kl}(\xi,\zeta) d\xi d\zeta \\
D_s &= \alpha_1 M + \alpha_2 K \\
E &= \int_0^a \int_0^b d(\xi,\zeta)\phi_{kl}(\xi,\zeta) d\xi d\zeta \\
B &= \int_0^a \int_0^b \left(\frac{\partial^2 M_{p\xi}}{\partial \xi^2} + \frac{\partial^2 M_{p\zeta}}{\partial \zeta^2} \right) \phi_{kl}(\xi,\zeta) d\xi d\zeta
\end{aligned}
\tag{2.12}
$$

with $k, m = 1, \ldots, N_m$ and $l, n = 1, \ldots, N_n$.

The damping matrix $[D]$ is proportional to the mass and stiffness matrices via the coefficient α_1 and α_2, and which models both Kelvin-Voigt viscoelastic damping and air damping.

The base function $\phi(\xi, \zeta)$, according to [52], can be decomposed into its two spatial directions ξ and ζ

$$\phi(\xi,\zeta) = \varphi(\xi)\psi(\zeta) \tag{2.13}$$

where φ and ψ can be chosen as the model shapes or finite elements satisfying the applied boundary conditions.

2.3 Piezoelectric Model

In this section we describe the ability of piezoelectric material to convert mechanical strains into electrical voltage and viceversa. In particular we present the mathematical model used to represent such relation between voltage and strain.

The dimension of the piezoelectric patch are defined as $L_{p\xi} \times L_{p\zeta} \times h_p$ as depicted in Figure 2.2.

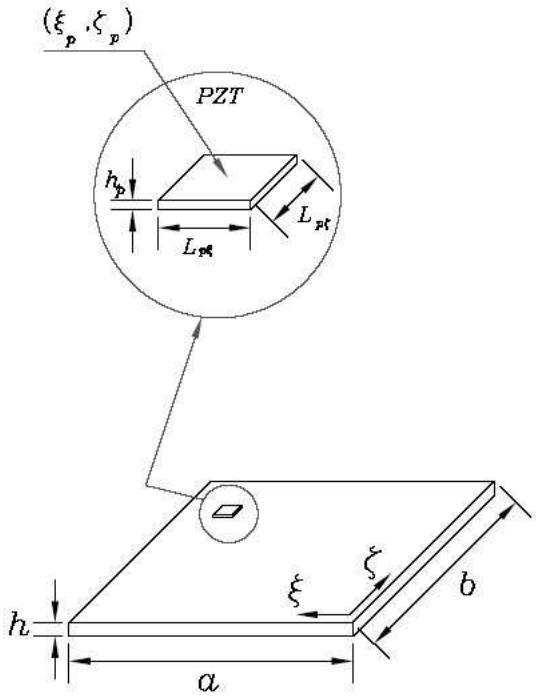

Figure 2.2: Plate with piezoelectric patch

The piezoelectric patch converts a supplied voltage in a change of its lengths and viceversa. In other words when a voltage is supplied to the piezo, it will deform by applying a moment to the structure. Alternatively if the structure is deformed, a moment will be applied to the piezo that will return a voltage.

According with [53, 54] the correlation between voltage and moment can be

expressed with the following equation (2.14)

$$M_p(t) = \frac{1}{2} E_p d_{31} w_p (h + h_p) \nu_p(\xi, \zeta, t) \tag{2.14}$$

where E_p is the Young's modulus of the piezoceramic patch, w_p is the width of the electrodes, d_{31} is the electric charge constant controlling the device extension and finally h and h_p are the plate and the piezoelectric thickness; the piezo patch considered is shown in Figure 2.3.

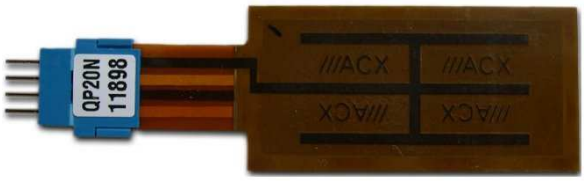

Figure 2.3: Piezoelectric patch

As already pointed out above it is assumed that the piezo thickness is much smaller than the plate thickness $h_p << h$. The term $\nu_p(\xi, \zeta, t)$ represent the applied voltage. This term can be decomposed in the spatial component and the time component $V_p(t)$. The spatial component is considered constant in the interval of the piezo length and reaches zero at its boundary according with a step function H as shown in the following equation.

$$\begin{aligned} \nu_p(\xi, \zeta, t) = V_p(t) \left[H\left(\xi - (\xi_p - L_{p\xi}/2)\right) - H\left(\xi - (\xi_p + L_{p\xi}/2)\right) \right] \times \\ \left[H\left(\zeta - (\zeta_p - L_{p\zeta}/2)\right) - H\left(\zeta - (\zeta_p + L_{p\zeta}/2)\right) \right] \end{aligned} \tag{2.15}$$

where the center of the piezo has been indicated with (ξ_p, ζ_p).

2.4 The Finite Element Model

In order to complete the discrete model discussed above we need to define the base functions (2.13). These functions are defined by using the finite elements methods. This choice was made instead of using modal shape due to the following reasons:

- There is not an analytical expression for the modal shapes of an all-clamped plate that includes the effects of the attached piezoelectric patches.
- The use of finite elements functions allows a much simpler approach to apply and change boundary conditions.
- The eigenfunctions describe the global behavior of the structure. This imply that they are defined over the full domain and often they tend to be complicated and uneasy to approach computationally.

A good choice for the finite element function is the cubic splines function as underlined in [55]. The following equations describe mathematically the splines function.

$$\varphi(\xi) = \begin{cases} 0 & \xi < \xi_c - 2h_c \\ (\xi + 2h_c - \xi_c)^3 & \xi_c - 2h_c < \xi < \xi_c - h_c \\ h_c^3 + 3h_c^2(\xi + h_c - \xi_c) + 3h_c(\xi + h_c - \xi_c)^2 - 3(\xi + h_c - \xi_c)^3 & \xi_c - h_c < \xi < \xi_c \\ h_c^3 + 3h_c^2(\xi_c - \xi + h_c) + 3h_c(\xi_c + h_c - \xi)^2 - 3(\xi_c + h_c - \xi)^3 & \xi_c < \xi < \xi_c + h_c \\ (\xi_c + 2h_c - \xi)^3 & \xi_c + h_c < \xi < \xi_c + 2h_c \\ 0 & \xi > \xi_c + 2h_c \end{cases} \tag{2.16}$$

where ξ_c is the center of a spline and h_c is the distance between the nodes.

2.5 Boundary and Initial Conditions

In order to complete the mathematical model proposed above we need to define initial and boundary condition for the problem considered.

The plate is assumed to have zero displacements and zero velocity at the initial time $t = 0$ as follows

$$v(\xi, \zeta, 0) = 0, \qquad \frac{\partial v(\xi, \zeta, 0)}{\partial t} = 0. \tag{2.17}$$

The boundary conditions for an all clamped plate are described by the following set of equations

$$v(0, \zeta, t) = 0, \qquad v(a, \zeta, t) = 0, \qquad v(\xi, 0, t) = 0, \qquad v(\xi, b, t) = 0, \tag{2.18}$$

$$\frac{\partial v(0, \zeta, t)}{\partial \xi} = 0, \quad \frac{\partial v(a, \zeta, t)}{\partial \xi} = 0, \quad \frac{\partial v(\xi, 0, t)}{\partial \zeta} = 0, \quad \frac{\partial v(\xi, b, t)}{\partial \zeta} = 0. \tag{2.19}$$

In order to apply such boundary conditions the base functions φ need to be modified such that the slope and the displacement are zero at the boundaries. The $(n + 3)$ original spline functions are changed to $(n - 1)$ transformed spline functions via the transformation

$$\begin{cases} \Phi_1 = -2\varphi_{-1} + \varphi_0 - \varphi_1 \\ \Phi_2 = \varphi_2 \\ \vdots \\ \Phi_{n-2} = \varphi_{n-2} \\ \Phi_{n-1} = -2\varphi_{n-1} + \varphi_n - \varphi_{n+1} \end{cases} \tag{2.20}$$

An example of the original and the transformed spline function and its derivative for the 1D case are shown in Figures 2.4 and 2.5.

Using an appropriate transformation matrix T it is possible to impose the boundary condition simply by pre and post multiplying the mass and stiffness matrices (2.12) by T. In the case of an all-clamped conditions such matrix is given by

$$T = \begin{bmatrix} -2 & 1 & -2 & 0 & \dots & 0 & 0 & 0 & 0 \\ 0 & 0 & 0 & 1 & 0 & 0 & 0 & 0 & 0 \\ 0 & 0 & 0 & 0 & \ddots & 0 & 0 & 0 & 0 \\ 0 & 0 & 0 & 0 & 0 & 1 & 0 & 0 & 0 \\ 0 & 0 & 0 & 0 & 0 & 0 & -2 & 1 & -2 \end{bmatrix} \tag{2.21}$$

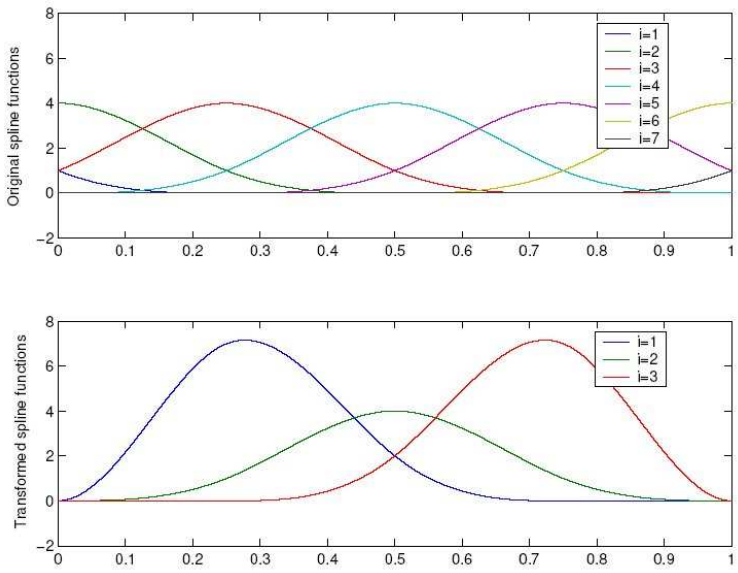

Figure 2.4: Original spline functions and its transformed form

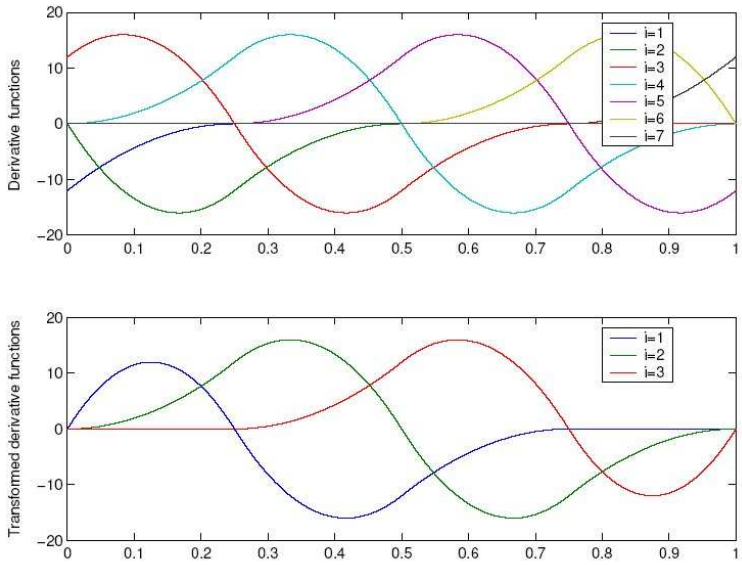

Figure 2.5: Derivative of the original spline functions and its transformed form

Chapter 3

Optimal Placement of Sensors and Collocated Sensors/Actuators

3.1 Introduction

In this chapter three algorithms to determine the optimal placement for sensing and actuating devices are presented. The goal is to determine a set of suitable positions (ξ_p, ζ_p) for each device.

In order to present such strategy it is necessary to reformulate the model equation (2.11) in a first order form as shown in equation (3.1)

$$\dot{x}(t) = A(\xi, \zeta)x(t) + B_1(\xi, \zeta)w(t) + B_2(\xi_p, \zeta_p)u(t) \tag{3.1}$$

where

$$x = \begin{bmatrix} X_{mn} \\ \dot{X}_{mn} \end{bmatrix}, \qquad A = \begin{bmatrix} 0 & I \\ -M^{-1}K & -M^{-1}D \end{bmatrix},$$

$$B_1 = \begin{bmatrix} 0 \\ M^{-1}E(\xi,\zeta) \end{bmatrix}, \qquad B_2 = \begin{bmatrix} 0 \\ M^{-1}B(\xi_p,\zeta_p) \end{bmatrix}. \tag{3.2}$$

The $[A]$ matrix includes the system's dynamics and properties. The spatial components of the disturbance forces are described in $[B_1]$ while the control forces are represented by the matrix $[B_2]$. Dependence on the piezo position (ξ_p, ζ_p) is made explicit to point out how a different placement of the actuating device affects the system.

The first objective is to find the best location for the piezo placement on the plate both as a sensing and actuating device. There are infinite possible locations for the piezo as described by the set

$$\Theta = \{(\xi,\zeta) \in [0,a] \times [0,b]\}$$

but the primary requirement is to enhance the system-theoretic properties of the piezo devices. The piezo position must therefore satisfy the condition of controllability for the system. This means that the contribution to the differential equation (2.9) from the term

$$\frac{\partial^2 M_{p\xi}}{\partial \xi^2} + \frac{\partial^2 M_{p\zeta}}{\partial \zeta^2} \tag{3.3}$$

must not be zero for a given piezo candidate position $(\xi_k, \zeta_k) \in \Theta$. Considering the weak form assuming $\phi_{mn}(\xi,\zeta) = \varphi_m(\xi)\psi_n(\zeta)$, it is possible to write the controllability condition as

$$\int_0^a \int_0^b \left(\frac{\partial^2 M_{p\xi}}{\partial \xi^2} + \frac{\partial^2 M_{p\zeta}}{\partial \zeta^2} \right) U_{ij}(\xi,\zeta) d\xi d\zeta = \left(\varphi_i'(\xi_k + L_\xi/2) - \varphi_i'(\xi_k - L_\xi/2) \right)$$

$$\times \int_{\zeta_k - L_\zeta/2}^{\zeta_k + L_\zeta/2} \psi_j(\zeta) d_{31} V_p d\zeta + \int_{\xi_k - L_\xi/2}^{\xi_k + L_\xi/2} \varphi_i(\xi) d_{32} V_p d\xi \times \left(\psi_j'(\zeta_k + L_\zeta/2) - \psi_j'(\zeta_k - L_\zeta/2) \right) \neq 0 \tag{3.4}$$

where L_ξ and L_ζ are the piezo lengths, d_{31} and d_{32} denote the mechanical strain in the ξ and ζ directions experienced by a piezoelectric element per unit of electrical energy applied V_p. A set of candidate positions, both for sensors and actuators, is therefore defined with respect to the following condition

$$\Theta_{ad} = \left\{ (\xi, \zeta) \in \Theta : \int_0^a \int_0^b \left(\frac{\partial^2 M_{p\xi}}{\partial \xi^2} + \frac{\partial^2 M_{p\zeta}}{\partial \zeta^2} \right) \neq 0 \right\}. \tag{3.5}$$

For the symmetry of the problem the previous condition ensures also that sensor candidate locations do not result in a zero reading from the devices.

Three different solutions to the actuators and sensors placement problem are presented in the following sections.

3.2 Simultaneous placement of multiple actuator devices

In this section it is considered the simultaneous placement of multiple devices on the flexible plate. It is assumed that n_g clusters or groups of actuators are available on the structure. The total number of actuators n_a on the plate is given by

$$n_a = \textstyle\sum_{k=1}^{n_g} q_k$$

where q_k is the number of actuators for the k^{th} cluster. Moreover, it is chosen to have the same number of actuators $q_k = q$ in each group. At any time piezoelectric effects, such as mass and stiffness contributions, are accounted in the structure model. This implies that the $[A]$ matrix in equation (3.1) is a function of the piezo positions $(\xi_p, \zeta_p)_{i=1\ldots n_a}$.

With reference to equation (3.1), it is possible to associate a specific vector B_2 to each single actuator $(\xi_p, \zeta_p)_i$. Corresponding to the n_a available actuators there

are n_a associated control vectors B_2.

The input term for the k^{th} group of actuators in state space form is therefore given by the matrix

$$B_{2k}(\xi_p, \zeta_p) = \begin{bmatrix} 0 & 0 & \dots & 0 \\ M^{-1}B_2(\xi_{p_k1}, \zeta_{p_k1}) & M^{-1}B_2(\xi_{p_k2}, \zeta_{p_k2}) & \dots & M^{-1}B_2(\xi_{p_kq_k}, \zeta_{p_kq_k}). \end{bmatrix} \tag{3.6}$$

To each group of actuators correspond a matrix B_{2k} whose columns are the single actuators vectors B_2

Grouping together these matrixes for all the n_g clusters it is obtained

$$\widehat{B}_2(\xi_p, \zeta_p) = \begin{bmatrix} \underbrace{B_{21(\xi_{p_1}, \zeta_{p_1})}}_{\text{group 1}} & \underbrace{B_{22(\xi_{p_2}, \zeta_{p_2})}}_{\text{group 2}} & \dots & \underbrace{B_{2g(\xi_{pn_g}, \zeta_{pn_g})}}_{\text{group } n_g} \end{bmatrix} \tag{3.7}$$

The algorithm is composed of two steps: first defining the locations for all the assigned devices n_a; second grouping together the actuators in n_g clusters each composed of q elements.

Placing simultaneously n_a actuators can be done by running $N_s = n_a$ separate searches. Such strategy simplifies the placement procedure, but neglects the mutual influence between the n_a actuators and their combined effect on the structure's mass and damping. Combinatory approaches should be used to consider these mutual influences for the location-optimized measures. Approaching such problem requires the solution of at most

$$\begin{pmatrix} n_{ad} \\ q_1 \end{pmatrix} + \begin{pmatrix} n_{ad} - q_1 \\ q_2 \end{pmatrix} + \ldots + \begin{pmatrix} n_{ad} - \sum_{i=1}^{n_g-1} q_i \\ q_{n_g} \end{pmatrix} =$$

$$\begin{pmatrix} n_{ad} \\ q_1 \end{pmatrix} + \sum_{i=2}^{n_g} \begin{pmatrix} n_{ad} - \sum_{j=1}^{i-1} q_i \\ q_i \end{pmatrix} \tag{3.8}$$

location-optimized measures in order to place the considered n_a actuators. This

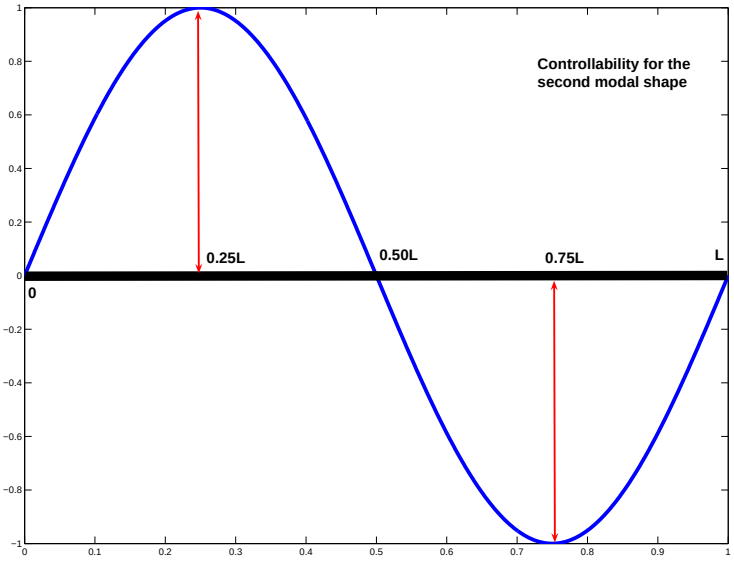

Figure 3.1: Second modal shape for a clamped-clamped beam

placement approach therefore requires an extremely high computational cost.

A procedure that is computationally feasible and minimizes the design and algorithmic complexity was instead considered. The idea is to assign a "value" for any candidate placement representing its ability to affect specific modes. This approach was validated on previous works such as [56]. Addressing a finite number of modes, many candidate locations might have the same controllability index. For

example, one may think the second mode for a clamped-clamped beam represented in the schematic Figure 3.1. In this case both the location at $0.25L$ and $0.75L$ of the length have the same control authority while the controllability is zero for the location at $0.50L$.

It is chosen to consider only the first five modes for the case under analysis. The modal shapes for the only flexible rectangular all clamped plate are given by [52, 57]

$$v_{i,j}(\xi,\zeta) = \sin\left(\frac{i\pi\xi}{a}\right)\sin\left(\frac{j\pi\zeta}{b}\right), \qquad i,j = 1,2,\ldots,\infty \tag{3.9}$$

To initialize the problem, locations are assigned corresponding to the maximum modal shape deformation given by (4.12). The overall structure's properties are now affected by the contribution to the stiffness and mass from the piezo, the wires and the control action. The originally found optimal locations may be not anymore optimal and they need to be recalculated. This leads to an iterative process described in the following algorithm 1

Algorithm 1

1: for a given mode, find the location(s) associated with the maximum absolute value of the modal function $(\xi,\zeta) = \arg\{\max_{(\xi,\zeta)\in\Theta_{ad}} |v_{i,j}(\xi,\zeta)|\}$

2: repeat step 1 for the remaining modes of interest

3: assign the devices on the found locations separately for each considered mode and repeat step 1

Any actuator will therefore optimally address at least one of the considered modal shapes.

Remark 3.2.1: The iteration is set to terminate when two successive iterates yield the same location or the difference between the values from the iterations is below a fixed threshold. The devices influence over the global properties strongly depends from the structure rigidity and the devices mass contributions. Due to this

dependency, the convergence of the iterative method may not exist if such effect is excessive. In such cases the methodology does not provide a unique optimal set of positions but rather a selection of positions with a higher level of controllability for the selected number of modal shapes.

The second step is to group the n_a actuators in n_g clusters. Such choice requires that each cluster attains a certain independent level of control authority over all the selected modal shapes. This requirement is necessary to guarantee, independently from the activated cluster, stability and controllability for the overall structure. This is achieved by selecting in any group at least one optimally located actuator for any modal shape.

Remark 3.2.2: In some cases, different groups shared the same location, as it happens that there is only one location that provides the maximum for a given modal shape.

3.3 Optimal Sensor and collocated Sensor/Actuator placement

A procedure to simultaneously place multiple actuators was described in the previous section. The proposed solution presents some limits. In particular only a limited number of modal shapes, chosen a priori, can be considered. An arbitrary choice of these modal shapes may lead to neglect some of the important phenomena and consequently to a final loss of optimality.

The loss of control optimality, or in the worse cases stability, is due to the effects of the neglected dynamics. This phenomena was earlier investigated from Balas in [58] that termed it as *spillover effect*. An interesting note exploring the relation between spillover, control robustness and global stability was presented in [59]. Such

phenomena was deeply investigated in the past years. For example the effects of spillover over robustness of sensors systems was analyzed in [60]. When dealing with actuator placement such problems should be accounted for. In [61], for example, extra constraints are introduced for the minimum controllability required on high frequency components for a candidate actuator location. An hybrid controller is proposed to reduce the effects of spillover in [62]. Here a traditional modal controller is combined with a negative velocity feedback to address both the low and high frequency vibration modes. In [63] a distributed controlling system, based on energy dissipation by internal flowing fluid, is proposed to avoid the spillover limits. An analytical solution is instead proposed by Moheimani and Halim [64]to compensate the error induced by the truncation of a discrete model.

A common condition for mechanical system is to be perturbed by some kind of unwanted disturbance. The spatial distribution and the temporal component of such disturbance are generally unknown. Different distributions of disturbance may have different effects over the system. For example exciting different states or different part of the system. Neglecting those effects may results in loss of optimality for the piezo placement. The next strategies, including the influence of disturbances, address the problems of sensor and couple sensor/actuator placement avoiding such losses.

3.3.1 Optimal sensor placement

The problem of designing a sensor network is now addressed. Sensing devices are usually a necessary component of mechanical systems. The information acquired may be used only for monitoring the system or for providing information to a human interface. In the most advanced cases the sensor readings can be used to define an autonomous feedback control strategy. In general obtaining a good sensing per-

formance is a required condition. The placement of sensors can substantially impact its overall performance. In this section a strategy for optimal sensors placement is summarized.

In general it is not possible to obtain sensing information for the overall states of the systems but only a partial set. This is accounted for by assuming only partial state availability as described by the following expression

$$y(t) = C(\xi_p, \zeta_p)x(t) \tag{3.10}$$

The term $y(t)$ represents the system output or in other words the available information gathered from the sensors.

In many applications the localized information, provided by the sensors, may not be sufficient and it could be required to reconstruct the behavior of the global system. This can be done by considering an observer or state estimator. The state estimator utilizes the sensors information as input and generates as output the estimated full state information $\widehat{x}(t)$. The state estimator considered is described by the following set of equations, more details about state estimation can be found in[65, 66].

No control moment ($u(t) = 0$) is considered in this model.

$$\dot{\widehat{x}}(t) = A\widehat{x}(t) + L(\xi_p, \zeta_p)(y(t) - \widehat{y}(t)) \qquad \widehat{y}(t) = C(\xi_p, \zeta_p)\widehat{x}(t) \tag{3.11}$$

Equation (3.11) describes a dynamical system mirroring the original plant. The full estimated states are available from such system. If by hypotheses the initial conditions were known and there was not any form of disturbance involved, the estimated states $\widehat{x}(t)$ would coincide with the actual state $x(t)$. In general however such conditions are not verified and a correction term $L(\xi_p, \zeta_p)(y(t) - \widehat{y}(t))$ is introduced. This correction term is proportional to the difference between the plant output $y(t)$

and the output calculated from the estimated state space variables $\widehat{y}(t)$.

The sensor location $(\xi_p, \zeta_p)-$ parameterized Kalman filter gain $L(\xi_p, \zeta_p)$ is given by

$$L(\xi_p, \zeta_p) = \widetilde{X}(\xi_p, \zeta_p) C^T(\xi_p, \zeta_p) N^{-1} \tag{3.12}$$

with $\widetilde{X}(\xi_p, \zeta_p)$ being the solution to the following filter Riccati equation

$$A\widetilde{X}(\xi_p, \zeta_p) + \widetilde{X}(\xi_p, \zeta_p) A^T - \widetilde{X}(\xi_p, \zeta_p) C^T N^{-1} C \widetilde{X}(\xi_p, \zeta_p) + Q = 0. \tag{3.13}$$

The weight Q is related to the disturbance distribution acting over the plate, $Q = B_1 B_1^T$.

The following expression for the observer error e is found by combining equations (3.11), (3.10) and (3.1)

$$\dot{e(t)} = (A - L(\xi_p, \zeta_p) C(\xi_p, \zeta_p)) e(t) + B_1(\xi, \zeta) w(t) \tag{3.14}$$

It can be noticed that the observer error is affected by *both* the location of the sensor (ξ_p, ζ_p) and the spatial distribution of disturbance $B_1(\xi, \zeta)$. The optimal location is chosen to be the one that minimizes the effects of the disturbance on the observer error. In order to implement such idea it is required to define a measure of the observer error. The choice made was to consider the H_2 norm of the transfer function $T_{ew}(s; \xi_p, \zeta_p)$.

The transfer function of a particular system describes the system properties in frequency domain. For example considering a single input single output system (SISO) the corresponding transfer function express the system output $y(s)$ respect to a specific input $u(s)$. Systems with multiple inputs and multiple outputs (MIMO) are characterized by a matrix of transfer functions associated with the different

inputs/outputs.

In particular it is considered the transfer function that relates the observer error respect to a given disturbance distribution.

$$T_{ew}(s;\xi_p,\zeta_p) = I\left(sI - \left(A - L\left(\xi_p,\zeta_p\right)C\left(\xi_p,\zeta_p\right)\right)\right)^{-1} B_1(\xi,\zeta)$$

Using the H_2 norm guarantees an integral measure of the considered function. In all the strategies proposed in this work the idea is to optimize the system response over the complete frequency domain rather than for a specific component (H_∞ norm).

From [65] the norm can be expressed as

$$\|T_{ew}(s;\xi_p,\zeta_p)\|_2^2 = B_1^T(\xi,\zeta)\widetilde{P}(\xi_p,\zeta_p)B_1(\xi,\zeta) \tag{3.15}$$

where the matrix $\widetilde{P}(\xi_p,\zeta_p)$ is the solution of the Grammian

$$(A - L(\xi_p,\zeta_p)C(\xi_p,\zeta_p))^T\widetilde{P}(\xi_p,\zeta_p) + \widetilde{P}(\xi_p,\zeta_p)(A - L(\xi_p,\zeta_p)C(\xi_p,\zeta_p)) + I = 0 \tag{3.16}$$

It is not considered any output error in model (3.10). The optimal position for the sensor is finally given by

$$\left(\xi^{opt},\zeta^{opt}\right) = \arg\{\min_{(\xi,\zeta)\in\Theta_{ad}} \|T_{ew}\|_2^2|\} \tag{3.17}$$

Solving the previous optimization problem is equivalent to selecting the sensors' configuration that provides the best global sensing capabilities. In other words the sensor placement from (3.17) produces the "optimal input" for the observer (3.11) improving the accuracy of the final full state estimation $\widehat{x}$.

Remark 3.3.1: The disturbance distribution $B_1(\xi, \zeta)$ is assumed to be known. Usually this assumption is not verified. In such cases one may consider to find the worst admissible case for such disturbance. This would provide also robustness against unknown distributions.

3.3.2 Worst distribution of disturbances

In order to find the worst distribution of disturbances one starts again from the basic equation (3.1) where the control term is zero $u(t) = 0$

$$\dot{x} = Ax + B_1(\xi, \zeta)w(t) \tag{3.18}$$

This equation describes the behavior of the system under the effect of active disturbance with spatial component B_1 and temporal component $w(t)$.

The idea is to find the spatial distribution vector $B_1(\xi, \zeta)$ that, for a given temporal component of the disturbance $w(t) \in L_2$, maximizes the effect of $w(t)$ on the entire state $x(t)$. In a similar fashion to what done above this objective can be achieved by maximizing the H_2 norm of the open loop transfer function from the system (3.18)

$$T_{xw}(s; \xi, \zeta) = (sI - A)^{-1} B_1(\xi, \zeta) \tag{3.19}$$

To ensure a certain regularity for the disturbance distribution it is introduced the constraint $d(\xi, \zeta) \in L_2$. The expression for the worst admissible disturbance becomes

$$B_1^{worst}(\xi, \zeta) = \arg \{ \max_{B_1 \in L_2} \|T_{xw}(s, \xi, \zeta)\|_2^2 \} \tag{3.20}$$

The H_2 norm is evaluated solving the following Lyapunov equation associated to

system (3.18)

$$AX_w(\xi,\zeta) + X_w(\xi,\zeta)A^T + B_1(\xi,\zeta)B_1(\xi,\zeta)^T \tag{3.21}$$

with the norm given by the expression

$$\|T_{xw}(s;\xi,\zeta)\|_2^2 = trace\,(X_w(\xi,\zeta)) \tag{3.22}$$

The elements of the vector B_1^{worst} are obtained by solving the constrained nonlinear optimization problem described in (3.20). The problem is solved with a sequential quadratic programming (SQP) method and solving a quadratic programming (QP) subproblem at each iteration [67, 68]. The code was implemented using the control toolbox from $Matlab$®.

3.3.3 Spatially robust optimal sensor placement

The next step is to combine the results obtained above for sensor placement procedure. Using the worst case disturbance it is possible to improve the strategy including robustness against unknown disturbance distributions. Using the previous result one may now look for the optimal sensor placement against the worst admissible spatial disturbance distribution.

Following the steps described in Section 3.3, a general approach for the optimal location is given by

$$\left(\xi^{opt},\zeta^{opt}\right) = \arg\{\min_{(\xi,\zeta)\in\Theta_{ad}} \|T_{ew}^{worst}\|_2^2|\} \tag{3.23}$$

with

$$\|T_{ew}^{worst}(s,\xi_p,\zeta_p)\|_2^2 = trace\left(B_1^{worst}(\xi,\zeta)^T\widetilde{P}(\xi_p,\zeta_p)B_1^{worst}(\xi,\zeta)\right) \tag{3.24}$$

with $\widetilde{P}(\xi_p, \zeta_p)$ being the solution to equation (3.16). The locations found are now optimal with respect to the worst case disturbance.

3.3.4 Optimal sensor/actuator pair placement

When active control is considered along with sensors it is required to provide a network of actuators. In this section it is addressed both the actuator and sensor placement. The idea is to find the optimal position for the subsystem sensor-actuator such that the global disturbance's effect on a controlled structure is minimized. In order to find the optimal placement for both sensor and actuator, the associated combinatoric optimization problem should be solved. In other words this requires to find the coordinates $(\xi_{piezo}^{opt}, \zeta_{piezo}^{opt})$ and $(\xi_{sens}^{opt}, \zeta_{sens}^{opt})$ maximizing the coupled sensor-actuator performances/actions. To quantify this computational load one may assume a finite number of candidate positions $N_{sens} = 400, N_{act} = 400$ and for such choice the required combinatorial function to be evaluated are $N_{Funct} = N_{sens} \cdot N_{act} = 160000$. Solving this composite problem may lead to unfeasible or excessive computational effort. To avoid such problem the assumption of collocated actuator and sensor is made. This constraint is expressed by the equation (3.25)

$$C(\xi, \zeta) = B_2^T(\xi, \zeta) \tag{3.25}$$

and implies that $N_{Funct} = N_{sens} = N_{act}$ eliminating the possible permutations between different sensor and actuator locations.

The closed loop form of the system presented in Figure 3.2 is now considered. The system output $y(t)$ is processed by the observer described above that returns an estimate of the complete state space variable set $\widehat{x}(t)$. This information is provided to the controller that return a control law signal $u(t)$ for the actuator.

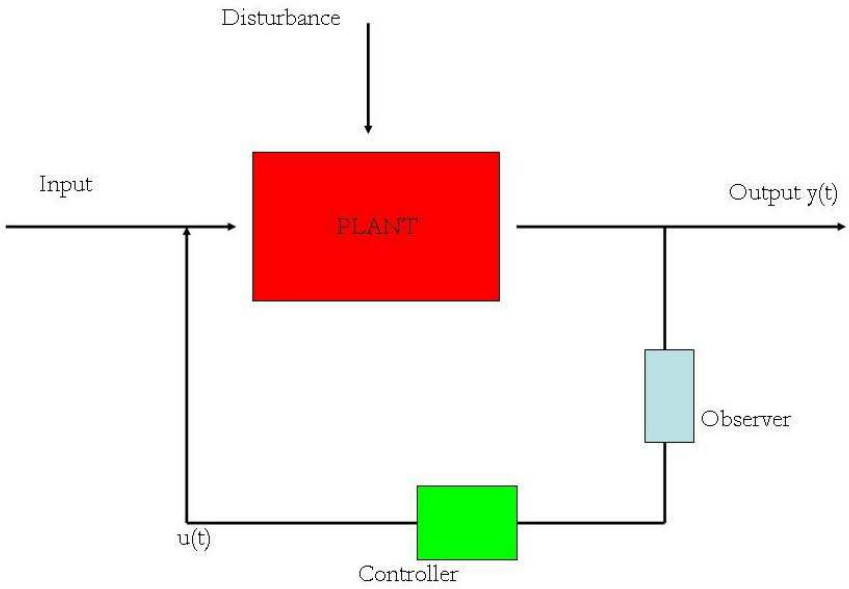

Figure 3.2: Scheme of a closed loop system

To define a control law for system (3.1,3.10) a dynamic compensator with an observed based feedback is therefore required. This global structure obtained by coupling an observer and a controller together is called compensator. The control law $u(t) = -B_2 K\widehat{x}(t)$, provided from the compensator and based on the estimated state variables, is finally sent to the actuators. The compensator behavior is described by the following first order differential equation

$$\dot{\bar{x}}(t) = \bar{A}\bar{x}(t) + B_1(\bar{\xi}, \zeta)W(t) \tag{3.26}$$

where $\bar{x}$ represents the augmented state vector error and the augmented matrixes $\bar{A}$ and $\bar{B}_1$ are shown below.

$$\bar{A} = \begin{bmatrix} A - B_2K & B_2K \\ 0 & A - LC \end{bmatrix} \qquad \bar{B_1}(\xi, \zeta) = \begin{bmatrix} B_1(\xi, \zeta) \\ B_1(\xi, \zeta) \end{bmatrix}. \tag{3.27}$$

K represents the LQR feedback gain associated with the state equation (3.1). The system's dynamics is influenced by the actual location of actuators and sensors. A specific compensator with its own dynamics is associated to any candidate actuator-sensor location. Moreover the devices locally affect stiffness and mass properties of the structure. System (3.26) must therefore be recalculated for each candidate position considered.

The observer gain L is obtained as before (3.12) while the controller gain is given by $K = R^{-1}B_2^T X_c$ with X_c the solution of the Riccati equation

$$A^T X_c + X_c A - X_c B_2 R^{-1} B_2^T X_c + Q = 0 \tag{3.28}$$

In [66] to achieve an optimal placement the effect of the disturbance w over the output $y = C(\xi_p, \zeta_p)x(t)$ was minimized. In a similar fashion to find the optimal position it is searched for the candidate position that minimizes the augmented state $\bar{x}$ against the disturbance w. This not only provides robustness for the controller against disturbances but also minimizes the observer error represented by the second half of the state variable $\bar{x}$.

It is considered again the H_2 norm of the transfer function

$$T_{\bar{x}w}^{\xi_p,\zeta_p}(s) = I(sI - \bar{A})^{-1}B_1(\xi, \zeta) \tag{3.29}$$

as optimality index for the actuator/sensor placement.

The best placement for the collocated pair is therefore the one that minimizes the following norm

$$\|T_{\bar{x}w}\|_2^2 = trace\left(B_1^T(\xi, \zeta)\bar{X}(\xi_p, \zeta_p)B_1(\xi, \zeta)\right) \tag{3.30}$$

where the matrix $\bar{X}(\xi_p, \zeta_p)$ is the solution of the related Grammian observability

equation

$$\bar{A}^T\bar{X} + \bar{X}\bar{A} + I = 0 \tag{3.31}$$

The placement strategy can be summarized by

$$\left(\xi^{opt}, \zeta^{opt}\right) = \arg\{\min_{(\xi,\zeta)\in\Theta_{ad}} \|T_{\bar{x}w}\|_2^2|\} \tag{3.32}$$

The disturbance distribution $B_1(\xi, \zeta)$ is calculated as the worst case possible for the open loop system. Analogous to section 4.2, the worst distribution is chosen to maximize the effect of the disturbance both on the plant's states and on the observer error. The worst distribution is given as

$$B_1^{worst}(\xi, \zeta) = \arg\left(\max \|T_{\bar{x}w}(s, \xi, \zeta)\|_2^2\right) \tag{3.33}$$

$$T_{\bar{x}w}(s, \xi, \zeta) = (sI - \bar{A})^{-1}B_1(\xi, \zeta) \tag{3.34}$$

The system's properties are related to actuator and sensor position. Once a placement is found the worst disturbance calculated may not be anymore the "worst" for the new closed loop. Updated worst case disturbance needs to be recalculated along with a new optimal placement. This leads to an iterative process described by the following algorithm

Remark 3.3.2: Similar to the previous case, convergence is again dependent on structure properties and discretization choices. However the considered algorithm still provides a way to identify a set of optimal positions ensuring controllability and robustness. Numerical results presented later evidence and clarify such concept.

Remark 3.3.3: The proposed algorithms involves an optimization process.

Algorithm 2

1: Calculate the worst distribution disturbance using (3.33) for the open loop system, i.e.
$B_2(\xi_p, \zeta_p) = 0$

2: Solve (3.32) for the optimal collocated pair actuator/sensor location (ξ^{opt}, ζ^{opt})

3: Compute the new worst disturbance distribution using (3.33)

4: Solve (3.32) for the new optimal placement with the new worst disturbance distribution

5: If $|\,(\xi^{opt}, \zeta^{opt})_{new} - (\xi^{opt}, \zeta^{opt})_{old}\,| \leq Tolerance$ then exit, else go to step 3

The basic approach considered here, is to define a grid of candidate locations and run a brute optimization process. This is equivalent to searching for the grid location that provides the minimum cost function value. The accuracy is strongly dependent on the fitting level of the grid used. In particular defining the distance $D_{piezo} = \sqrt{(\xi_p^i - \xi_p^{i-1})^2 + (\zeta_p^i - \zeta_p^{i-1})^2}$, if for any grid node i it is verified that $D_{piezo} \leq L_{piezo}$, with L_{piezo} being the length of the active device part, then the optimization search is sufficiently accurate. However, for large scale problems, as a 3D or larger dimension structure, this optimization approach does not guarantee sufficient accuracy or may result in excessive computational cost. In such cases one can define a coarse grid and use the locations set as initial condition to run a more accurate research method. A choice for such optimization method could be the conjugate gradient method or the gradient projection technique. Interesting results for large scale optimizations problems can be found from Jorge More[69] or Gaohang Yu [70]. A third possibility is offered by the use of genetic algorithm approach[71]. In this case a family of possible candidate locations over the all structure could be used as initial condition. This could prevent the optimization search to result only into a local minima.

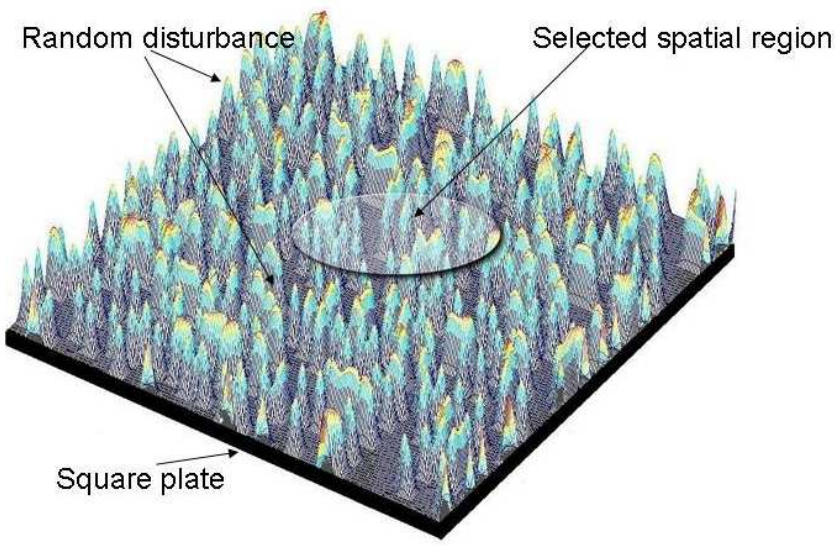

Figure 3.3: Enhanced stability over assigned spatial regions

3.4 Optimal actuator placement over assigned spatial regions

In certain cases it is required to enhance stability over designed regions of a structure. To accomplish such goal one may locally increase the control action on those designed regions. This choice may result in overall loss of controllability for the system as shown in the following example. Consider for example the case illustrated in Figure 3.3; the desired region is the middle of a square plate, subject to a random disturbing force. In such situation one could choose as optimal location the center itself. In this case the controller would not have any authority on important modes such as the second and third ones and consequently there would be an overall loss of performance.

The proposed strategy guarantees both local stability enhancement and overall

control performances. First it is considered the index $\|T_{xw}\|_2$ given by

$$T_{xw}^{\xi_p,\zeta_p}(s) = I\left(sI - \widetilde{A}(\xi_p,\zeta_p)\right)^{-1} B_1(\xi,\zeta) \tag{3.35}$$

where the spatial disturbance distribution was considered constant over the plate and $\widetilde{A}$ is the closed loop matrix for the system

$$\widetilde{A}(\xi_p,\zeta_p) = A(\xi_p,\zeta_p) - B_2(\xi_p,\zeta_p)K(\xi_p,\zeta_p) \tag{3.36}$$

the overall performance is ensured by selecting the candidate position (ξ^p,ζ^p) that minimizes the full state transfer function T_{xw}. We look for the placement that minimizes the effect of a given disturbance over the plant's states.

To introduce a significant measure for the transfer function, we consider again the H_2 norm as in (3.30). The optimal placement is obtained solving the optimization problem

$$\left(\xi^{opt},\zeta^{opt}\right) = \arg\left\{\min_{(\xi_p,\zeta_p)\in\Theta_{ad}} \|T_{xw}\|_2\right\} \tag{3.37}$$

The closed loop gain $\widetilde{K}$ is obtained from the LQR approach minimizing the cost to go function

$$J = \int_{t_0}^{\infty} [x^T(t)Qx(t) + u^T(t)Ru(t)]dt. \tag{3.38}$$

The previous index is minimized by the following expression

$$J^{min} = x^T(t_0)P(\xi^p,\zeta^p)x(t_0) \tag{3.39}$$

where the matrix $P(\xi^p, \zeta^p)$ is found solving the algebraic Riccati equation

$$\begin{aligned} &A^T(\xi^p, \zeta^p)P(\xi^p, \zeta^p) + P(\xi^p, \zeta^p)A(\xi^p, \zeta^p) + Q \\ &-P(\xi^p, \zeta^p)B_2^T(\xi^p, \zeta^p)R^{-1}B_2(\xi^p, \zeta^p)P(\xi^p, \zeta^p) = 0. \end{aligned} \tag{3.40}$$

The standard choice for the weight matrix Q is given by

$$Q = \begin{bmatrix} M_s & 0 \\ 0 & K_s \end{bmatrix} \tag{3.41}$$

where M_s affects the first n states of $x(t)$ (the velocity) and K_s the remaining n (the transversal deformation). In order to enhance the stability in selected spatial regions, the Q matrix can be modified as described below

$$\widetilde{Q} = \begin{bmatrix} \widetilde{M_s} & 0 \\ 0 & \widetilde{K}_s \end{bmatrix} \tag{3.42}$$

By opportune definition of $\widetilde{K}_s, \widetilde{M_s}$ it is possible to select some elements of the state vector $x(t)$ to have higher cost for the index (3.38). This is equivalent to penalize deformation and velocity for specific spatial regions on the cost index (3.38). The terms $\widetilde{K}$,$\widetilde{M}$ are obtained, similarly to (2.12), from

$$\begin{aligned} \widetilde{K}_s = D_E \sum_{m=1}^{N_m}\sum_{n=1}^{N_n} \int_0^a \int_0^b \left(\frac{\partial^4 V_{mn}(\xi,\zeta)}{\partial \xi^4} + 2\frac{\partial^4 V_{mn}(\xi,\zeta)}{\partial \xi^2 \partial \zeta^2} + \frac{\partial^4 V_{mn}(\xi,\zeta)}{\partial \zeta^4} \right) \\ V_{kl}(\xi,\zeta)\widetilde{f}_K(\xi,\zeta)d\xi d\zeta \end{aligned} \tag{3.43}$$

$$\widetilde{M_s} = \rho h \sum_{m=1}^{N_m}\sum_{n=1}^{N_n} \int_0^a \int_0^b V_{mn}(\xi,\zeta)V_{kl}(\xi,\zeta)\widetilde{f}_M(\xi,\zeta)d\xi d\zeta \tag{3.44}$$

The 2D weight functions $\widetilde{f}_K(\xi,\zeta), \widetilde{f}_M(\xi,\zeta)$, defined for $\xi \in (0,a), \zeta \in (0,b)$,

describe geometric surfaces. The functions assume maximum values for ξ, ζ corresponding to selected regions over the plate where the control effect should be maximized. For simplicity the two functions are assumed to identical $\widetilde{f}(\xi, \zeta) = \widetilde{f}_K(\xi, \zeta) = \widetilde{f}_M(\xi, \zeta)$.

The weight functions affect, through the closed loop gain K, the global optimality index J_{opt} defined above. The procedure to select the actuator location can be schematized from Algorithm 3

Algorithm 3

1: Define a grid of possible locations over the structure under consideration
2: Design a controller based on the LQR approach (3.38)-(3.44) for each candidate location
3: Compute the performance index map (3.37) for the introduced grid in order to find the optimal placement

This optimization problem has the same limits described for the previous case and a similar approach can be used for large scale problems.

3.5 Numerical Results

Numerical simulations were performed to validate the strategies described above. The case considered is a square, all clamped, aluminum plate of length $a = b = 1m$. This choice was made for its symmetry properties. This allows an easier a posteriori analysis for the obtained results. The approach presented above was used to create a discrete model. Up to $n = 25$ elements for each direction (ξ, ζ) were considered for the truncated expression (2.10).

Between the most important parameters, required to characterize the structure behavior, are the first natural frequencies. It was then a given choice to use those values to verify the accuracy achieved by the used discretization level. The values

Table 3.1: Analytical and numerical frequency

Analytical solution	Numerical solution
8.7626 Hz	8.7615 Hz
17.8734 Hz	17.8704 Hz
26.3682 Hz	26.3500 Hz
32.0411 Hz	32.0430 Hz

Table 3.2: Plate properties

Aluminium plate properties	
Length	$1m$
Width	$1m$
Thickness	$0.002m$
Density	$2700Kg/m^3$
Young's modulus	$70GPa$
Poisson ratio	0.35

found for the discrete model were compared with the values available from literature [57] for the case of a all clamped thin plate. No devices were included for this test and only the open loop matrices were computed. The natural frequencies ω_n were calculated solving the well knows equation

$$\omega_n = \frac{1}{2\pi}\sqrt{eig[K][M]^{-1}}$$

with $[M_s], [K_s]$ being the mass and stiffness matrices from the numerical model. Results are shown on Table 3.1 The aluminium plate's properties and geometry chosen for the numerical model are shown in Table 3.2 while Table 3.3 provides the piezo's properties. The spatial distribution of disturbance $B_1(\xi, \zeta)$ was similarly discretized as described in Section 2.1 using 50 piecewise constant functions for each direction. *Matlab* optimization and control predefined function were used for the numerical studies.

Table 3.3: Piezo properties

Piezo properties and coordinates	
Length	$0.0508m$
Width	$0.016078m$
Thickness	$0.000845m$
Density	$8140Kg/m^3$
Young's modulus	$55GPa$
Poisson ratio	0.25

Table 3.4: Coordinates for group of piezoelectric patches

group 1	(0.7143a,0.4286b)	(0.7143a,0.2857b)	(0.2143a,0.7857b)
group 2	(0.4643a,0.7500b)	(0.5357a,0.2857b)	(0.2857a,0.5714b)
group 3	(0.2857a,0.5714b)	(0.2857a,0.2857b)	(0.7143a,0.4286b)
group 4	(0.5a,0.5b)	*	*

3.5.1 Numerical Results for Algorithm 1

In this simulation, nine ($n_a = 9$) actuators were considered. Four different groups share the available actuators , each group having at most 3 devices. The assumption that any actuator could be shared by any group was made. Table 4 shows the actuator placements found for each group. Figure 3.4 shows part of the iterative process described above. The pictures depict the plate's 2nd modal shape corresponding to different actuator placements. The change in shape is due to the effect on the plate properties of changing actuators placements. Such effect is even amplified when the devices are wired to some centralized controller or a wireless device is associated with each actuator/sensor. This is due to the wires' additional influence over the plate's properties.

The optimal location for the first and the second two modal shapes can be easily identified. Some complexity may arise when looking for higher modes to which correspond several optimal locations or equivalently maximum deformation points. Once all the positions for the nine actuators were found, the patches were grouped

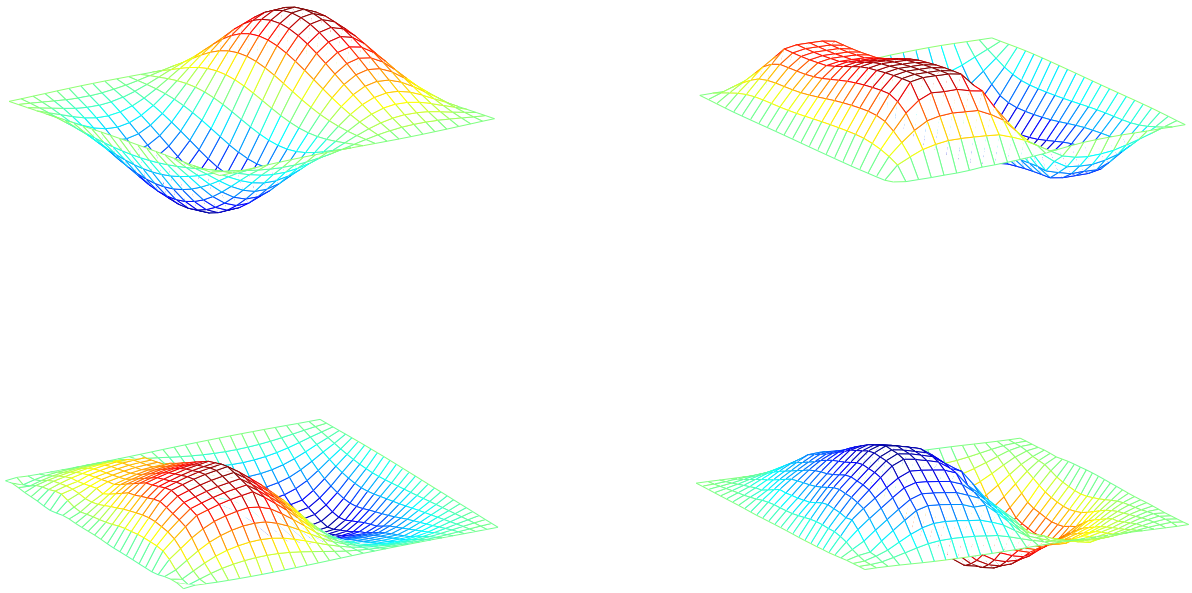

Figure 3.4: Actuator placement for the second modal shape.

together, as described on the previous table. Each group was designed to optimally address all the selected first modal shapes.

3.5.2 Numerical Results for Algorithms 2

A grid of 900 candidate locations over the plate was considered in these simulations. To each possible placement corresponds a specific model for the plant, as described above.

The first step was to generate the worst disturbance distribution by using the expression (3.20), shown on Figure 3.7. The distribution was used to find the optimal sensor's location shown in Figure 3.8. According to equation (3.23), the optimal location is given by the candidate position that minimizes the effect of the disturbance over the observer error (Z axis). The H_2 norm of the observer error shown on

this and the following pictures was normalized and the Z axis values were inverted for easier visualization.

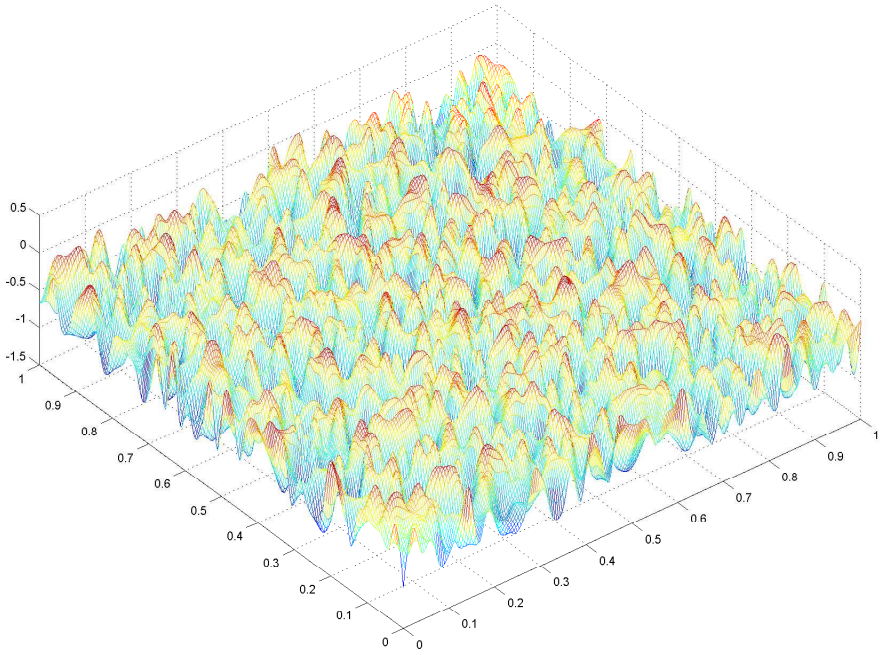

Figure 3.5: Random disturbance distribution

A second placement simulation was performed considering a disturbance distribution randomly generated, results are shown in Figures 3.5 and 3.6.

The following step was to look for the optimal placement of the collocated couple sensor/actuator. As described above an iterative process is required to identify the optimal placements. The results for optimal couple actuator/sensor placement are shown below. Figures 3.9,3.10,3.11 depict the iterative process described on section 4.4.

Four areas were identified as optimal location for placement of couple actuator/sensor. It can be noticed how the locations close to the plate's quarters result to be optimal for the considered case. This result can be justified for the case of a

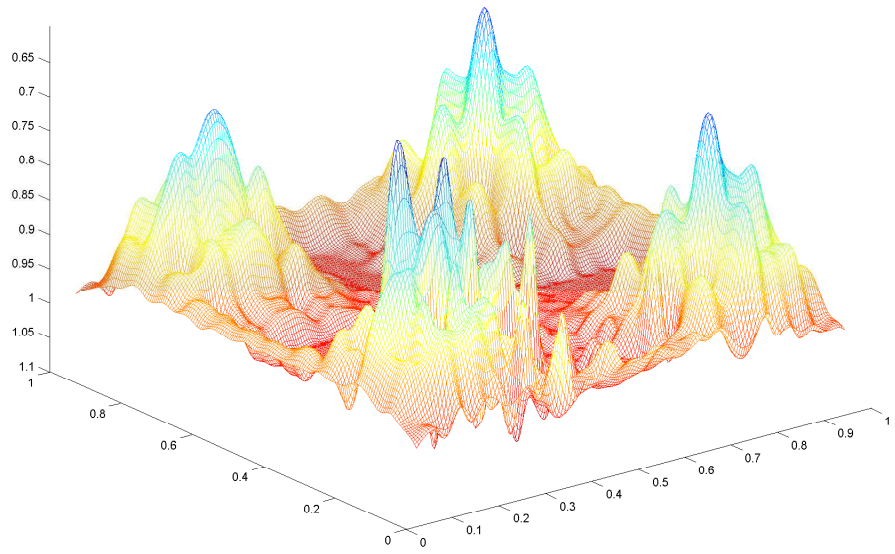

Figure 3.6: Optimal sensor placement for a random disturbance distribution

square plate by a simple modal analysis. These four locations owns good controllability level over the first few important modes of the plate. Typically the higher the modal shape considered the higher is its frequency and therefore higher is the effect of the natural passive damping. The better the actuators can affect low damping frequency/modal shape the better the overall controller performance will be. The proposed algorithm implicitly identifies such threshold of important modal shape.

The result obtained for the sensor and the coupled sensor/actuator suggests similar optimal locations. This is justified by the symmetry for the problem of sensor and actuator placement for this specific case (3.5.)

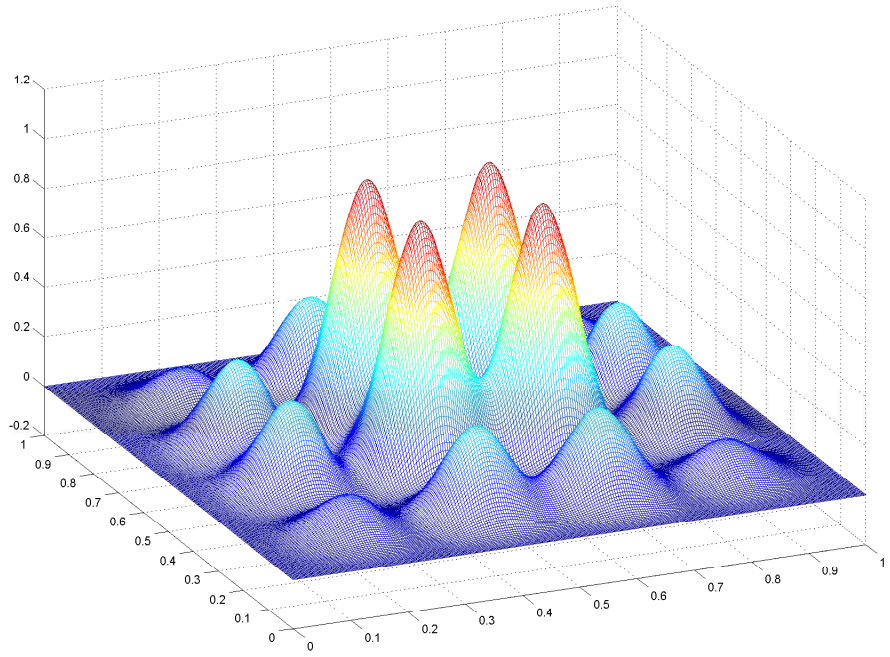

Figure 3.7: Worst spatial disturbance distribution

3.5.3 Numerical Results for Algorithm 3

The results obtained for the placement of actuators over preassigned regions of a plate are presented below. Several test were performed selecting spatial regions by using different weight functions $\widetilde{f}(\xi, \zeta)$. In general those functions can be manually determined depending on the different design requirements.

Results are presented in Figures 3.12,3.13,3.14 as a set of two pictures for each simulated test. The left side shows the 2D function $\widetilde{f}(\xi, \zeta)$ while the right one shows the associated map index J_{opt}. The use of different functions $\widetilde{f}(\xi, \zeta)$ results in different solutions for the placement problem. The weight function used should be therefore opportunely designed for each single case. Results can be compared with the previous test. It can be noticed how by using the weight matrix $\widetilde{Q}$ it is possible to select preferred spatial regions for actuator placement without compromising

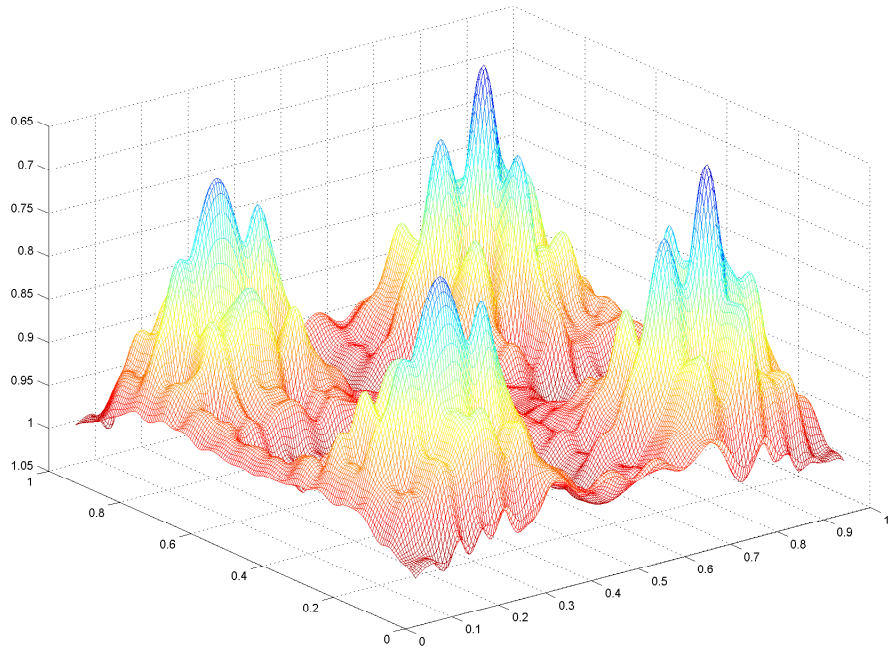

Figure 3.8: Optimal sensor placement for the worst spatial disturbance distribution

global performances. The results suggest again that the area around the quarters of the plate length represent the optimal placement. This result is congruent with the previous analysis being the geometry considered the same. It is interesting to observe in Figure 3.13 how although the central area of the plate is preassigned the optimal placements do not behave to that area, according with the results obtained from the previous sections.

The power of these strategies presented above becomes more evident when they are applied to more complex geometry. The choice of a symmetric plate was made in order to validate the proposed algorithms over a simply and well understood test case.

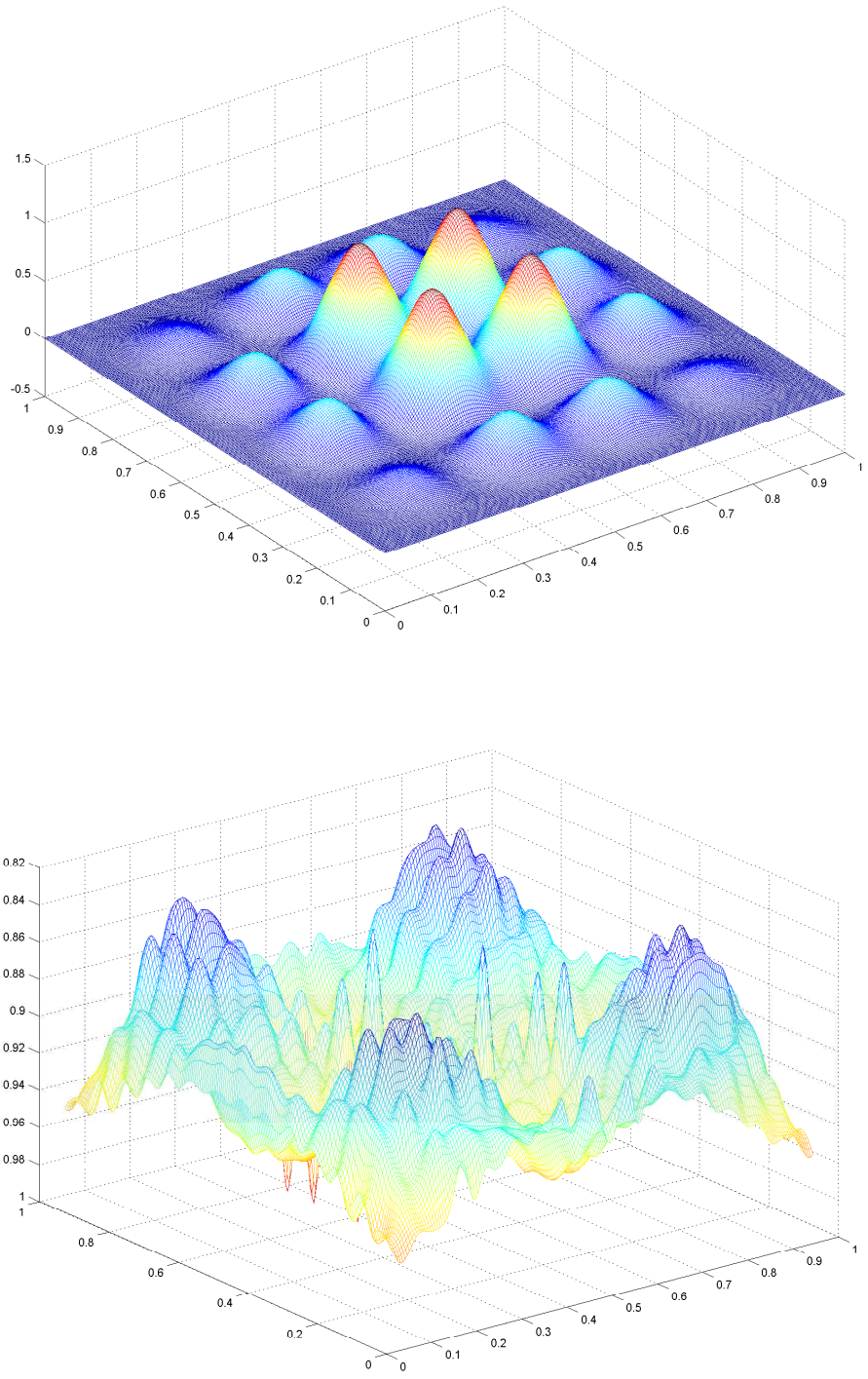

Figure 3.9: First step disturbance distribution and optimal actuator/sensor placement

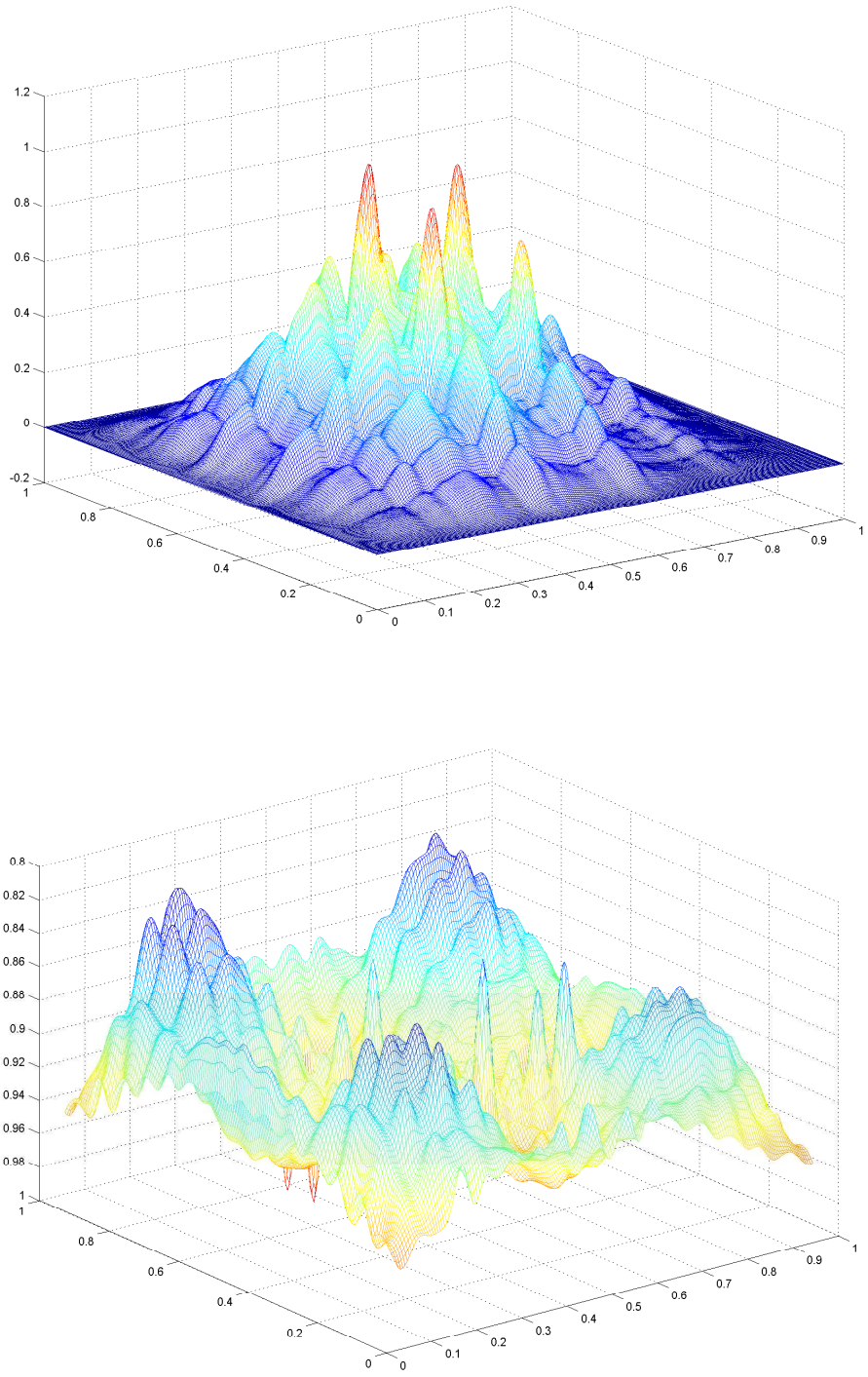

Figure 3.10: Second step disturbance distribution and optimal actuator/sensor placement

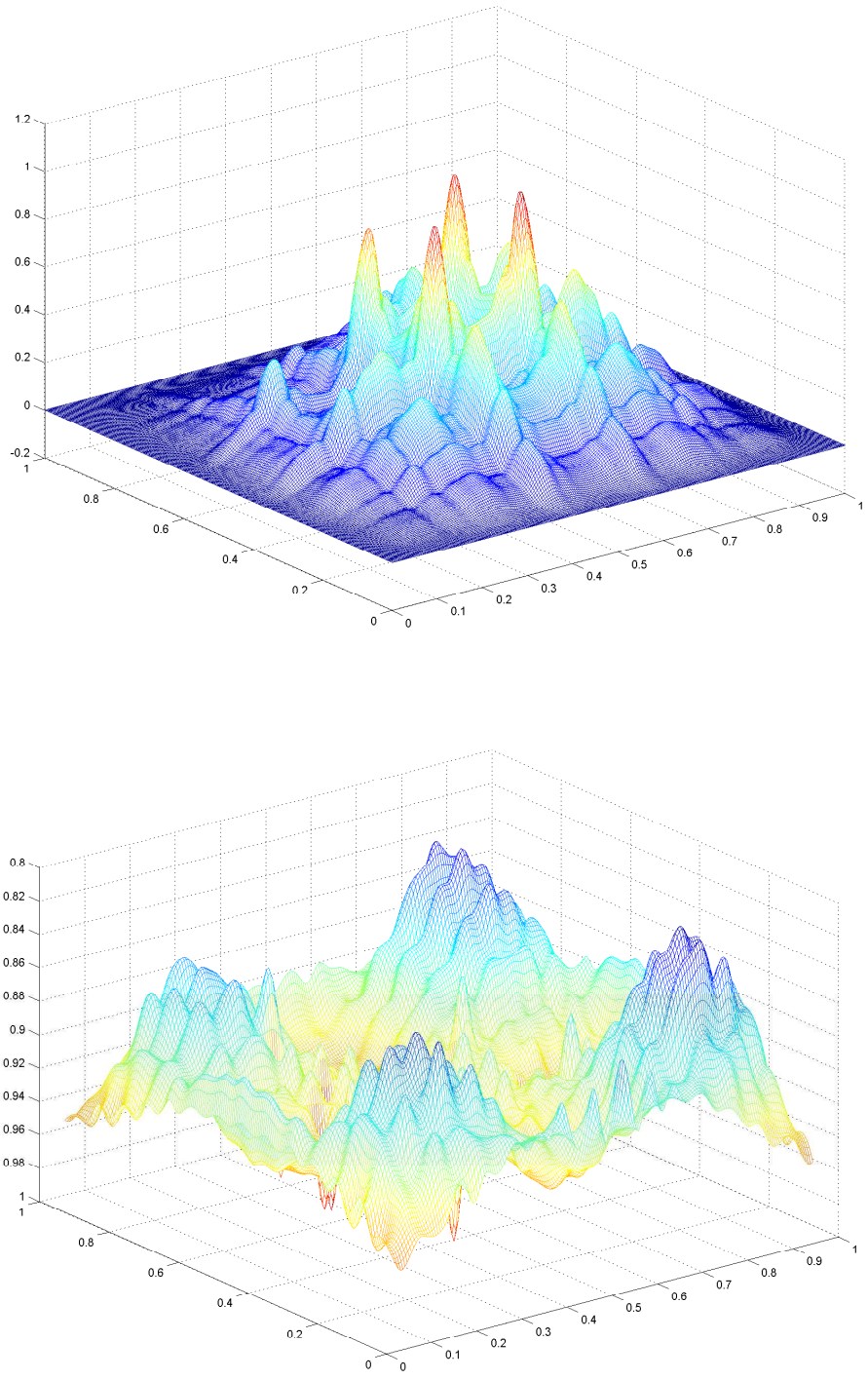

Figure 3.11: Third step disturbance distribution and optimal actuator/sensor placement

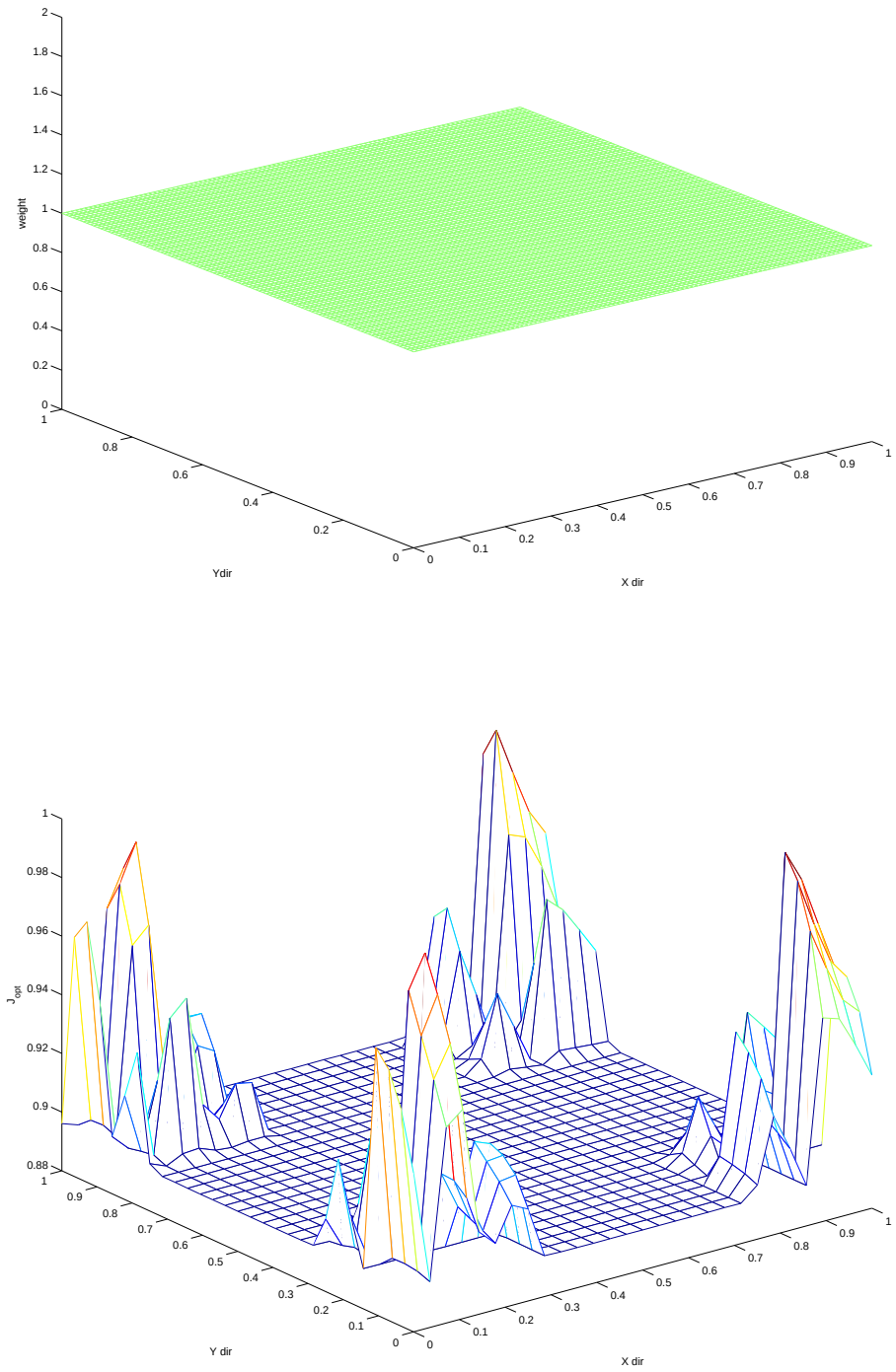

Figure 3.12: Constant weight function and corresponding $J_{opt}index$

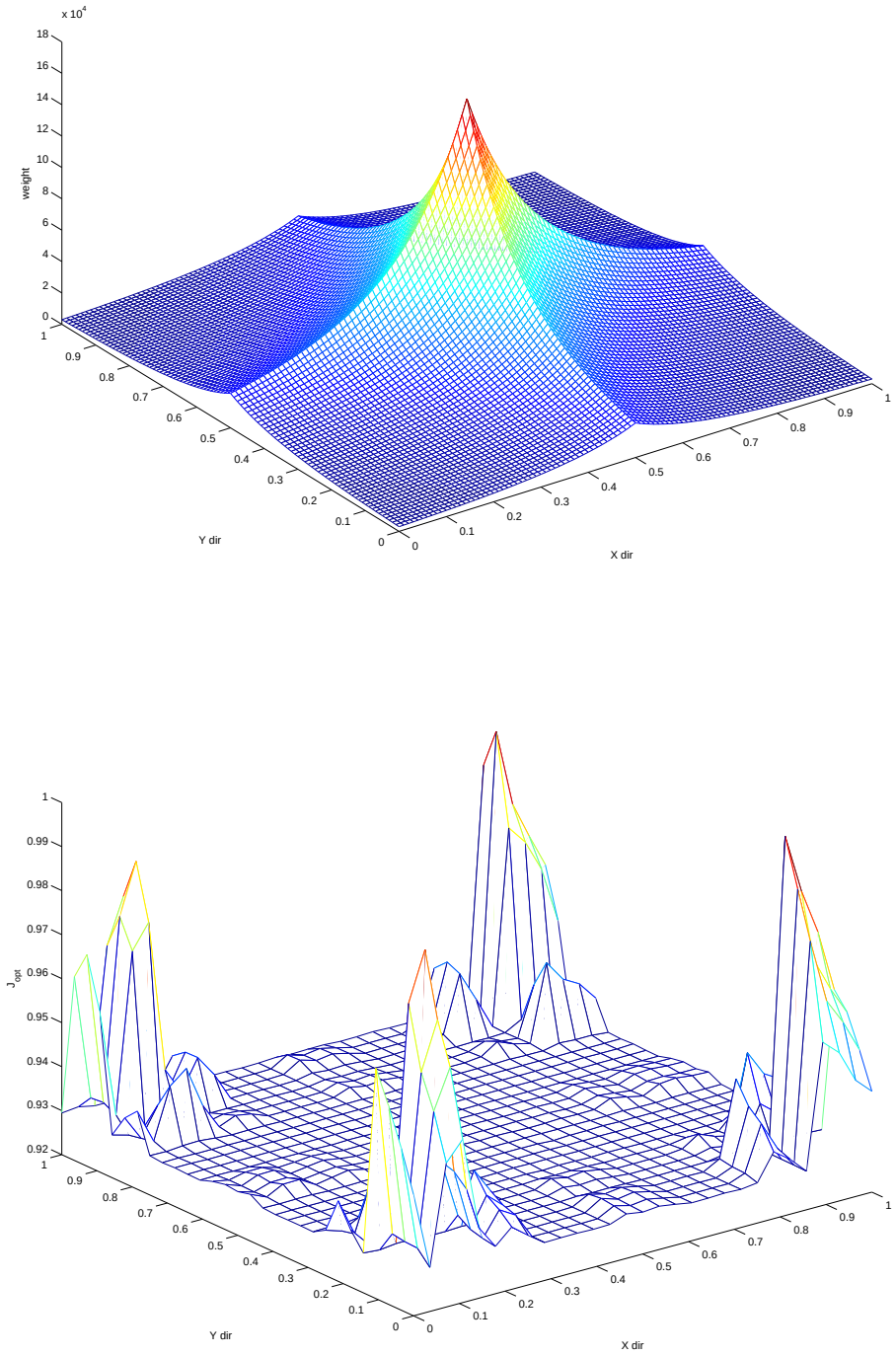

Figure 3.13: Exponential centered weight function and corresponding J_{opt} index

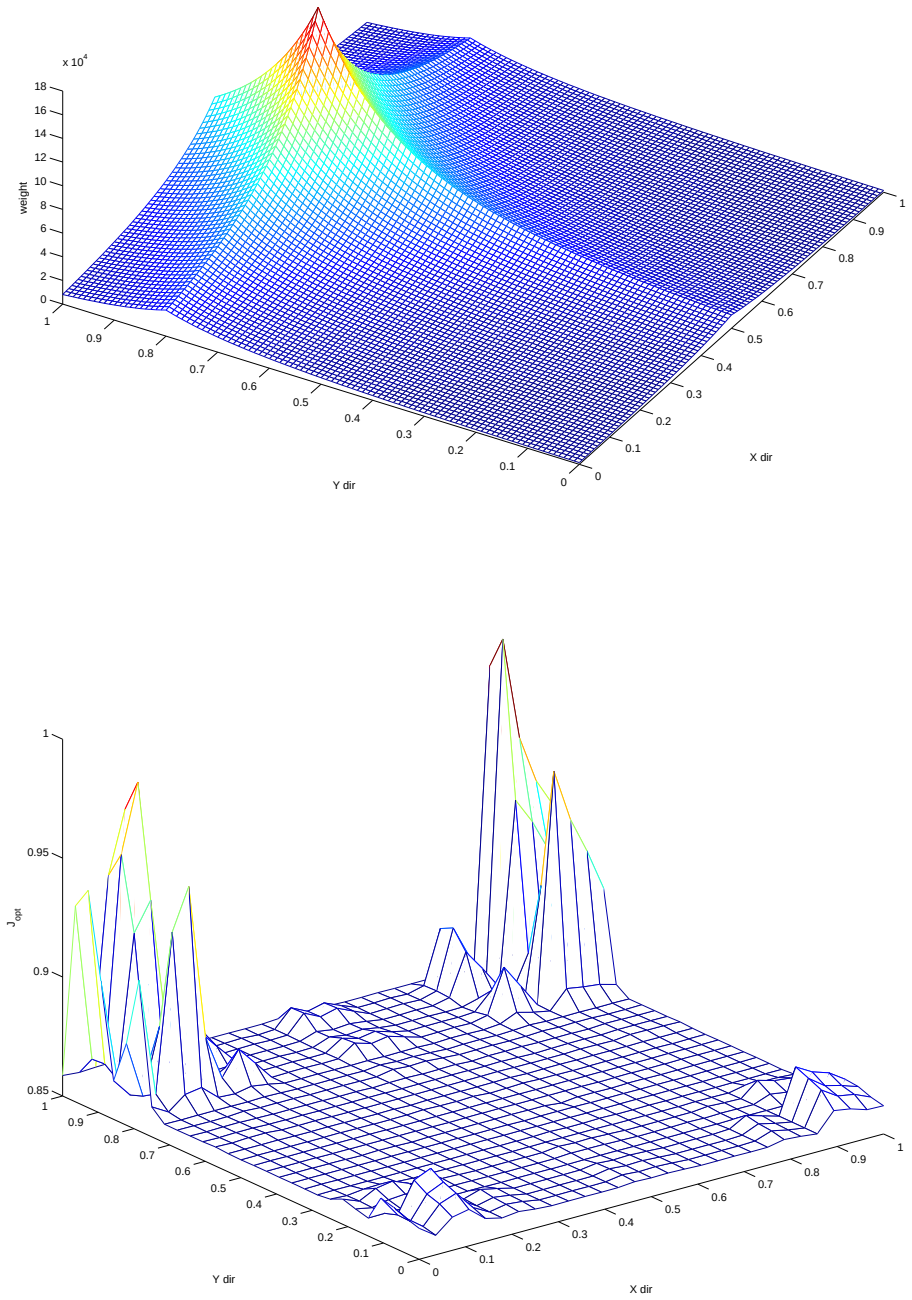

Figure 3.14: Exponential weight function and corresponding J_{opt} index

Chapter 4

Switching Strategies for Hybrid Systems

4.1 Hybrid System Overview

In the previous chapter we proposed strategies to optimally design a control system. In such control system generally it is possible to have several available actuators. Depending on the internal states and the external disturbances the use of the full set of actuators may not result in the most efficient solution. An extreme case could be encountered when the system properties are time dependent. In such cases, as for example chemical reactors, the system properties evolves in time through a sequence of stages. An actuation strategy optimal for certain stages may result in unstable behavior for different stages. In such cases it is therefore required to alternatively switch between the available control subsystems characterized by different actuation strategies.

In order to better address the problem of defining switching strategies for hybrid systems we now reformulate the model (3.1) to be

$$\begin{aligned}
\dot{x}(t) &= A_{\sigma(t)}x(t) + Ew(t) + B_{\sigma(t)}U_{\sigma(t)}(t) \\
y(t) &= C_{\sigma(t)}x(t) \\
\sigma(t) &\in \mathcal{I} = \{1, 2, \ldots, N_p\}
\end{aligned} \tag{4.1}$$

where $x(t) \in \mathbb{R}^n$ is the state vector while $U_{\sigma(t)}(t)$ represents the control signal. This term is expressed as a vector of N_p sub-signals

$U_{\sigma(t)}(t) = [u^1_{\sigma(t)}(t)\ u^2_{\sigma(t)}(t)\ \ldots\ u^{N_p}_{\sigma(t)}(t)]^T \in \mathbb{R}^{N_p}$. The index $\sigma : [0, \infty) \to \mathcal{I}$ is the switching signal which is assumed to be piecewise continuous. It represents a discrete state which indexes the (switched) state matrix A, input distribution vector B and control input U. The integer N_p denotes the number of (switch) available modes of the switched system (4.1). In this case N_p corresponds to the total number of actuating devices available on the structure. We adopt the notation used in [43] for the times a subsystem is switched in and switched out, respectively. We denote by $t_{k_r^{in}}$ and $t_{k_r^{out}}$ the time at which for the r^{th} time, the k^{th} subsystem is switched in and out or $\sigma(t^+_{k_r^{in}}) = \sigma(t^-_{k_r^{out}}) = k$. We can therefore rewrite system (4.1) as

$$\begin{aligned}
\dot{x}(t) &= A_k x(t) + Ew(t) + B_k U_k(t) \\
y(t) &= C_k x(t) \\
t_{k_r^{in}} &\leq t < t_{k_r^{out}}
\end{aligned} \tag{4.2}$$

Similarly with the notation used above E denotes the spatial distribution of disturbances while $w(t)$ is the associated temporal component, assumed to be square integrable. In general the spatial distribution of disturbances E is unknown and it may change during the time interval of interest. In other words the spatial distribution of disturbances E is time dependent. Such dependence is neglected in the notation for simplicity.

The ensuing stability analysis of the proposed switched scheme relies on already established results with the difference that we impose a specific structure on the control signals $U_k(t)$. In the proposed scheme only one actuating device is kept active over a time interval while the remaining $(N_p - 1)$ are kept dormant.

The matrix B is defined as

$$B = \left[\begin{array}{ccccccc} B^1 & B^2 & \dots & B^j & \dots & B^{N_p} \end{array} \right],$$

where $B^1 \dots B^{N_p}$ are column vectors. Each column B^j corresponds to a different actuating device. To model the switching scheme it is possible to design the control signal vector $U_{\sigma(t)}(t)$ such that only one vector component of B receives a nonzero signal while the remaining $(N_p - 1)$ ones receive the zero signal; thus

$$\begin{aligned} B_k U_k(t) &= \left[\begin{array}{ccccccc} B^1 & B^2 & \dots & B^j & \dots & B^{N_p} \end{array} \right] U_k(t) \\ &= \left[\begin{array}{ccccc} B^1 & B^2 & \dots & B^j & \dots B^{N_p} \end{array} \right] \left[\begin{array}{c} 0 \\ 0 \\ \vdots \\ u_k^j(t) \\ \vdots \\ 0 \end{array} \right] \\ &= B^j u_k^j(t). \end{aligned}$$

We assume the system's properties are being constant for each single switched subsystem. In other words, we have that the matrix A_k is constant over all interval $t_{k_r^{in}} \leq t < t_{k_r^{out}}$ and that $A_{\sigma(t)} \equiv A$.

Alternatively the switching strategy can be represented considering the control

contribution in (2.1) as a linear combination of the columns of the B matrix

$$\begin{aligned} B_{\sigma(t)}U_{\sigma(t)}(t) &= \textstyle\sum_{i=1}^{N_p} \alpha_i(t) B^i u^i(t) \\ &= B \begin{bmatrix} \alpha_1(t) & 0 & \dots & 0 \\ \vdots & \vdots & \ddots & 0 \\ 0 & 0 & \dots & \alpha_{N_p}(t) \end{bmatrix} \begin{bmatrix} u_k^1(t) \\ u_k^2(t) \\ \vdots \\ u_k^{N_p}(t) \end{bmatrix} \end{aligned} \tag{4.3}$$

this is the choice made for this work.

The term α is an array of coefficients whose elements can be either one or zero, $\alpha_i(t) \in \{0, 1\}$. We assume that only one controlling device at a time can be switched on while all the remaining ones are kept in a sleep mode. This choice implies that the vector α can have *only one* nonzero element while the others are all zero, i.e. $\sum_i^{N_p} \alpha_i(t) = 1$. In fact, in the proposed switching scheme, we only switch the coefficients $\alpha_i(t)$. To each subsystems $\sigma(t) = 1, \dots, N_p$ is associated a specific control signal $u_\sigma(t)$. In view of the above, the switching now takes the form

$$B_{\sigma(t)}U_{\sigma(t)}(t) = B \ \text{diag}\ \{\alpha_i(t)\} U_{\sigma(t)}(t).$$

Remark 4.1: Differently from most of the works referenced above, we do not investigate only switching of control signals $U(t)$. For example, the considered switching model can be used to describe the behavior of systems with mobile actuators. In those cases the full control term $BU(t)$ and not only the signal component $U(t)$ may change during the activation interval.

An extension of this approach is required when several devices are grouped together. In this case we removed the constraint $\sum_i^{N_p} \alpha_i(t) = 1$ with more than one element be different from zero or equivalently more devices, belonging to the same

group, activated at the same time.

For the output $y(t)$ we assume a common vector $C_\sigma = C$ for all the subsystems and we limit the switching only to the actuating part. The goal now is to define the optimal switching path for the subsystems, or in other words, to define the optimal time sequence of coefficients α_i. Switching strategies are presented in the following sections.

Two main parameters characterize hybrid switched systems: the subsystems' switching sequence and the switching time segments for the total time interval. In our work we assume the switching time segments to be of a constant and *a priori* decided duration. Such choice may be done arbitrarily or related to hardware design limits.

The goal is therefore to define the optimal path σ, or trajectory, to drive the given system to the equilibrium point. Without loss of generality we assume the equilibrium point to be the origin.

4.2 Cost-to-go switching policy

The goal with the first switching policy is to increase optimality for the overall switched system. To achieve this optimality we define a "cost to go" function and we look for the path σ that minimizes this cost function. The "cost to go" index is

$$J_i(\sigma) = \int_{t_0}^{t_f} [x^T(t)Qx(t) + u^T(t)Ru(t)]dt. \tag{4.4}$$

where $[t_0, t_f]$ is the total time interval considered. Due to its hybrid nature the optimization process associated with the infinite horizon problem involves complex and time-expensive computations. One may choose to divide the finite horizon interval $[t_0, t_f]$ into a number m of time subintervals of fixed duration. To solve the

problem one should then solve backwards in time N_p differential Riccati equations, each associated with one different actuator, for the last time segment m. The preceding time segment $m-1$ would require therefore the solution to $N_p \times N_p$ DREs. Continuing, one then solves $(N_p)^3$ DREs for the next interval $m-2$ and so forth. As was argued in [72, 73], the presented problem requires to solve about $(N_p)^m$ DREs with m denoting the number of time intervals. To avoid this heavy computational burden, one considers the following suboptimal control measure, reducing the computation to only N_p Algebraic Riccati Equations (AREs). In order to simplify the optimization problem the cost to go function is computed separately for each switching interval $\bar{t}_k$ to $\bar{t}_{k+1}$, as was argued in [74]. However this problem still requires to solve DREs. In order to avoid the solution of such differential equation, the following assumption is made for the index J

$$J^{opt}_{\bar{t}_k}(\sigma) = x^T(\bar{t}_k) P_\sigma x(\bar{t}_k) \tag{4.5}$$

where P_σ denotes the solution for the algebraic Riccati equation

$$A'P_\sigma + P_\sigma A + Q - P_\sigma B'_\sigma R^{-1} B_\sigma P_\sigma = 0. \tag{4.6}$$

Equation (4.5) does not provide the solution for the finite horizon problem. However it holds that

$$\lim_{T\to\infty} \widetilde{P}(t,T) = P \tag{4.7}$$

where $\widetilde{P}(t,T)$ is the solution for the corresponding differential Riccati equation. Solution of (4.4) can then be approximated by the expression (4.5), i.e. $\widetilde{P}(t,T) \backsimeq P$, provided that the interval $\Delta t = \bar{t}_{k+1} - \bar{t}_k$ is long enough to guarantee the attainment of a steady state. To verify such condition one may define a threshold τ, representing

a measure of the maximum acceptable approximation error and ensure that

$$\Delta t > \frac{\ln \tau}{\lambda_{max}}$$

where $\lambda_{max} < 0$ is the largest eigenvalue of the closed loop system and $0 < \tau < 1$. This lower bound on Δt is required to ensure, at any switching/evaluation time t_k, a sufficient converge of $\widetilde{P} \to P$. Several works can be found addressing such issue, for example on [75] is presented an explicit expression for the error $\Delta P(t) = \widetilde{P}(t) - P$.

The switching path can now be computed as

$$\sigma_{\bar{t}_k} = \arg\{ \min_{(\sigma=1,\ldots,N_p)} J^{opt}_{\bar{t}_k}(\sigma)\} \tag{4.8}$$

for any switching time $\bar{t}_k$. The two LQR parameters R and Q can be chosen to penalize the power requirements versus enhancing the stability requirements for the plant.

A Lyapunov approach is considered to study stability properties for the proposed switching scheme. Starting from the results in [43] and [37] a general stability condition for nonlinear hybrid systems is given by the following theorem.

Theorem 4.1: Given a switched nonlinear system

$$\dot{x}(t) = f_{\sigma(t)}(x(t)),$$

suppose each vector field f_i has an associated Lyapunov-like function V_i in the region Ω_i, each with equilibrium point $\overline{x} = 0$. Let $\sigma(t)$ be a given switching sequence such that $\sigma(t)$ can take the value i only if $x(t) \in \Omega_i$ and in addition

$$V_i(x(t_{i,k})) \leq V_i(x(t_{i,k-1}))$$

where $t_{i,k}$ denotes the kth time that the vector field f_i is switched in, then the previous nonlinear system is Lyapunov stable.

We apply this result to the hybrid linear system under consideration in the following lemma

Lemma 4.1: Given the switched linear system (4.1) where any closed loop subsystem σ has an associated Lyapunov-like function V_σ, such that the function V_σ is positive definite, the first derivative $\dot{V}_\sigma$ is negative definite and in addition

$$V_\sigma(\bar{t}_k) \leq V_\sigma(\bar{t}_{k-1}), \tag{4.9}$$

then the system (4.1) is Lyapunov stable.

Using the previous theorem and lemma we prove stability for the switched hybrid system under analysis in theorem 3.2

Theorem 4.2: Given the switched linear system (4.1) and applying the switching law (4.8), the resulting switching hybrid system is Lyapunov stable.

Proof: The system (4.1) is stabilizable if, with the obtained switched path σ, it is possible to define a function V that satisfies the conditions of Lemma 3.1. We choose the quadratic Lyapunov functions to be equal to the optimal value of the performance indices

$$V(\sigma) = x^T P_\sigma x = J^{opt}_{\bar{t}_k}(\sigma), \tag{4.10}$$

and therefore they are definite positive functions, by virtue of the positivity of the solution to the AREs. We apply the control law by means of the feedback gain

$$K(\sigma) = -R^{-1} B_\sigma P_\sigma, \tag{4.11}$$

where P_σ is the solution of the corresponding algebraic Riccati equation (4.6). We can then rewrite the original system (4.1), without the disturbance term, which is

generally unknown,

$$\dot{x} = A_{CL}(\sigma)x,$$

where

$$A_{CL}(\sigma) = A - B_\sigma K(\sigma). \tag{4.12}$$

The time derivative of the Lyapunov functions for such systems can be expressed as

$$\dot{V}(\sigma) = x^T \big(A'_{CL}(\sigma)P(\sigma) + P(\sigma)A_{CL}(\sigma)\big)x \tag{4.13}$$

rearranging equation (4.6) as

$$(A - B_\sigma K(\sigma))'P_\sigma + P_\sigma(A - B_\sigma K(\sigma)) = -Q - P_\sigma B'_\sigma R^{-1} B_\sigma P_\sigma \tag{4.14}$$

we arrive to

$$A'_{CL}P_\sigma + P_\sigma A_{CL} = -Q - P_\sigma B'_\sigma R_{-1} B_\sigma P_\sigma \tag{4.15}$$

Since the matrix Q is positive definite and the term $P_\sigma B'_\sigma R^{-1} B_\sigma P_\sigma$ is positive semi-definite, we have that the derivative of the Lyapunov function (4.13) is negative definite. Finally the above choice, equation (4.8), for the switching path implies also that for any switching k

$$V_\sigma(x(t_k)) \leq V_\sigma(x(t_{k-1})). \tag{4.16}$$

the conditions of Lemma 3.1 are satisfied and the switched system is proved to be stable.$\diamond$

The disturbance $Ew(t)$ was completely neglected in the previous analysis. The next step is to include the effect of disturbance in the stability investigation. We first introduce a well known result for linear system under the effect of perturbations.

Lemma 4.2: Given the system

$$\dot{x}(t) = \bar{A}x(t) + f(t)$$

where the matrix $\bar{A}$ is Hurwitz and the perturbation $f(t)$ is such that

$$f(t) : \mathbb{R}_+ \rightarrow \mathbb{R}^n$$

with

$$N_{max} = \sup_{(\forall t)} |f(t)|$$

if the perturbation is bounded, i.e. $N_{max} < \infty$, the system state is bounded and it exists a bounded Lyapunov function $V(t)$ associated with the system. If the perturbation is bounded and convergent, i.e. $\lim_{t\rightarrow\infty} f(t) = 0$, then the system state and the associated Lyapunov function are bounded and convergent.

Proof: The proof is a straightforward consequence of Theorem 3.23 in [76].$\diamond$

We can now extend this result to the more general case of switched linear systems.

Theorem 4.3: Given the switched linear system (4.1) with the unknown disturbance $Ew(t)$ and applying the switching law (4.8), if the N_p subsystems, in their closed loop form, are all stable and bounded under the disturbance $Ew(t)$, than the resulting switching hybrid system is Lyapunov stable.

Proof: The proof of this theorem is based on the idea of considering σ Lyapunov functions each one belonging to a bounded region. This assumption is equivalent to considering the following for all Lyapunov functions

$$V_\sigma(x,t) \in L_2 \text{ for all } x,\ t \text{ and } \sigma. \tag{4.17}$$

Since the decision rule from equation (4.8) ensures that the switching between the

different subsystems cannot result in any increase in term of the Lyapunov function and since each switched Lyapunov function is bounded by assumption, it results that the overall switched linear system is stable and bounded.$\diamond$

Remark 4.1: Results from the previous theorem guarantee stability for the hybrid disturbed system, provided that the condition of Theorem 4.3 are verified. However when the disturbance distribution is unknown and spatiotemporally varying, it is not possible to guarantee optimality for the full switching interval. A subsystem chosen to be optimal at the switching time t_k may not be optimal for the entire length of the switching interval$[t_k, t_{k+1})$ due to the unknown changes of the disturbance distribution.

The implicit assumption of full state availability was made for the arguments presented above. However usually only partial information of the state is available. The sensor output $y(t)$ is described as

$$y(t) = Cx(t) \tag{4.18}$$

where C is a matrix whose elements depend on the sensors properties and positions. To extend the previous results to this more general case we need to recall the equations of the state estimator (3.11). The observer (Kalman filter) provides an estimation for the full state variables set $\widehat{x}(t)$.

The algorithm proposed above can now be extended to this case. The switching rule becomes

$$\begin{cases} \hat{J}^{opt}(\sigma(t_i)) = \hat{x}^T(t_i) P_\sigma \hat{x}(t_i) \\ \sigma(t_i) = \arg\{\min\limits_{(\sigma=1,\ldots,N_p)} \hat{J}^{opt}(\sigma(t_i))\} \end{cases} \tag{4.19}$$

where $\hat{x}$ is the estimated state. Stability of the augmented switched system is investigated below based on the following assumptions:

Assumption 4.1: The entire set of subsystems, in their closed loop form, are Lyapunov stable over the entire set of switching intervals $[t_k, t_{k+1})$ for all k.

Assumption 4.2: For each subsystem, it is possible to define an observer based on (3.11), in a way such that any complete subsystem, plant and observer, is Lyapunov stable for any switching intervals $[t_k, t_{k+1})$ for all k.

Remark 4.2: At any switching time the indexes i and j are not required to be distinguished, i.e. it may happen that $i = j$. This implies that at the switching instant the optimal subsystem to be used for the next interval is the one already active.

Lemma 4.3: The augmented switched system is stable if the switching rule verifies at any time that

$$V_i(x, t_1^+) \leq V_j(x, t_1^-) \tag{4.20}$$

Proof: We first consider the first interval for $k = 0$. Assumptions 4.1 and 4.2 guarantee stability for the entire time interval $[t_0, t_1)$. Let us now assume that the switching law satisfies equation (4.20) where respectively $V_j(x, t_1^-), V_i(x, t_1^+)$ are the Lyapunov functions for the subsystem j, i active within the interval $[t_0, t_1)$ and the interval $[t_1, t_2)$. Again from Assumptions 4.1 and 4.2 and Theorems 4.1-4.3, the switched system is proved to be stable through the discontinued temporal domain $[t_0, t_{k_{max}+1}]$ $\diamond$.

Discussion: The stability problem reduces therefore to verify that condition (4.20) is satisfied. However if the switching algorithm is based on the reconstructed state from the observer then the above switching policy can guarantee only that

$$V_i(\hat{x}, t_{k+1}^+) \leq V_j(\hat{x}, t_{k+1}^-), \tag{4.21}$$

where the Lyapunov function for the i^{th} subsystem can be written as

$$V_i(\hat{x}, t) = \hat{x}^T P_i \hat{x} \tag{4.22}$$

with P_i the solution of the algebraic Riccati equation associated with the i^{th} subsystem.

In order to provide some stability arguments we define as a measure for the observer error, the expression $e = \hat{x} - x$. According with this definition it is possible to rewrite equation (4.22) as

$$V_i(\hat{x}, t) = (x + e)^T P_i (x + e) \tag{4.23}$$

or

$$V_i(\hat{x}, t) = x^T P_i x + \Delta V_i(e, x) \tag{4.24}$$

where $\Delta V_i(e, x) = x^T P_i e + e^T P_i x + e^T P_i e$, and equation (4.21) can be rewritten as

$$V_i(x, t_{k+1}^+) + \Delta V_i(e, x) \leq V_j(x, t_{k+1}^-) + \Delta V_j(e, x). \tag{4.25}$$

Two cases that guarantee stability for the switched system can be individuated. The first possible case is verified when the terms $\Delta V(i, e, x)$ and $\Delta V(j, e, x)$ are identical. This is equivalent to stating that $P_i = P_j$ and it may occur in accordance with Remark 4.2. Moreover, provided that $|\Delta V_j - \Delta V_i| \ll |V_j - V_i|$, than verifying equation (4.21) may be equivalent to verifying equation (4.20).

Stability can be ensured also in this second case. Defining a percentage threshold $\tau_{\%}$ proportional to the absolute value of the difference $|V_j - V_i|$ and such that $\tau_{\%} = 50\%|V_j - V_i|$ then equation (4.21) implies also equation (4.20) if it is verified that $\max(|\Delta V_i|, |\Delta V_j|) < \tau_{\%}$.

Remark 4.3: A priori knowledge of the observer error, usually unavailable, is required to ensure the condition described above. However to ensure stability for the system a sufficiently long switching interval should be defined. A determinant factor defining such length is the convergence speed for the combined observer and plant.

Remark 4.4: Achievement of stability, by ensuring conditions (4.21) and (4.20), for the case of an input-output feedback, does not imply any optimality. This is due to the impossibility of detecting the actual smallest Lyapunov function (or performance index J) for the switched system as described for the switching algorithm above

The switching procedure is reassumed in the algorithm below

Algorithm 4 Cost-to-go switching rule

1: divide the interval $[t_0, t_f]$ into m subintervals, each with duration $\Delta t = \frac{t_f - t_0}{m}$.

2: for each B^i, corresponding to each of the N_p actuating devices, solve the N_p AREs

$$A^T P_i + P_i A - P_i B^i R^{-1} (B^i)^T P_i + Q = 0$$

3: at each t_k consider the cost-to-go

$$J_k = \int_{t_k}^{\infty} x^T(\tau) Q x(\tau) + R u^2(\tau)\, d\tau$$

4: at the beginning of each interval $[t_k, t_k + \Delta t)$ find the minimum of the optimal values of the quadratic indices corresponding to each actuating device

$$B^{opt} = \arg \min_{(B^1, \ldots, B^{N_p})} x^T(t_k P_k x(t_k)$$

5: deactivate all devices and only activate the B^{opt} device; supply it with the control signal

$$u^{opt}(t) = -R^{-1}(B^{opt})^T P_{opt} x(t) \quad t \in [t_k, t_k + \Delta t).$$

4.3 Minimum system energy switching policy

This switching algorithm is based on mechanical energy properties of the system. The objective is again to find the optimal way, between a set of possible choices, to stabilize and drive the system to the equilibrium state. In a similar way to the strategy presented above we defined a performance index to be minimized; now we chose the system's energy $E(x,t)$ to be that index. In other words we chose to minimize the index

$$J(x,t) = E(x,t) = \frac{1}{2}x^T(t)Gx(t) \tag{4.26}$$

where the matrix G characterizes the components of the mechanical energy for the system.

The expression $E(x,t)$ refers to the open loop energy for the system and does not include the contribution from the actuators. In other words, the index represents the conservative mechanical energy associated with system (4.1). Minimizing the mechanical energy implies stabilizing the plant itself and driving the states to the origin. The methodology here presented can be used also if it is required to drive the state to a different final value ($x_{desired}(t) \neq 0$). A simple variable transformation allows to opportunely redefine the energy index for different final values.

The index $J(t)$ or equivalently the system's mechanical energy, calculated at the switching time t_i, assumes the same value for each of the available N_p subsystems. Mechanical energy is indeed calculated for the open loop system and does not account for the external contributions provided from the actuators. However the next switching time predicted energy $J(t_{i+1})$, depends on the control force applied during the interval $\Delta t = t_{i+1} - t_i$. Therefore, at any switching time t_i,to each separate subsystems σ corresponds a different expected performance index $J_\sigma(t_{i+1})$.

The strategy is therefore to turn on at each switching time t_i the subsystem that

minimizes the estimated energy index $J(t_{i+1})$. The switching policy described is synthesized in the following expression

$$\sigma(t_i) = \arg\{\min_{(\sigma=1..N_p)} J_\sigma(t_{i+1})\} \tag{4.27}$$

In order to solve the optimization problem (4.27) it is required to calculate the estimation of $J(t_{i+1})$ at the switching time t_i. Using a first order expansion we have

$$J(t_{i+1}) = J(t_i) + \frac{\delta J_\sigma}{\delta t}\Big|_{t_i} \Delta t + 0(\Delta t^2) \tag{4.28}$$

where $\frac{\delta J_\sigma}{\delta t}\big|_{t_i} = \frac{\delta E(x,t)}{\delta t}\big|_{t_i}$.

Applying this idea to the linear system (4.1) we obtain the following expressions for the derivative of J

$$\frac{\delta J_\sigma}{\delta t}\Big|_{t_i} = \frac{1}{2}x^T(\bar{t_i})(A^TG + GA)x(\bar{t_i}) + x^T(\bar{t_i})GB_\sigma U(\bar{t_i}) \tag{4.29}$$

The switching path $\sigma(t)$ is therefore defined by combining together equations (4.27),(4.28) and (4.29).

Remark 4.5: Since the terms $x^T(\bar{t_i})(A^TG + GA)x(\bar{t_i})$ and $x^T(\bar{t_i})Gx(\bar{t_i})$ are the same for any subsystem, the choice of the optimal path σ is based only on the term $x^T(\bar{t_i})GB_\sigma U(\bar{t_i})$.

The strategy described presents evident similarity with the model predictive control technique MPC [77, 78]. In particular the switching logic is based on energy state prediction along a set of receding finite horizon segments. MPC is widely used and although this approach is not optimal, in practice it has given very good results.

The switching interval was chosen to be of a constant length, fixed a priori. Such choice, also known as dwell time, allows to practically ensure stability for the

switched system in despite of the global efficiency. When all the subsystems are exponentially stable this result is achieved by allowing a sufficiently long interval between switches. On the other hand the lack of flexibility in switching times may result in excessive long use of a subsystem that is not anymore the most efficient [39, 79]. However on this specific case limits for the switching interval length arise due to system's properties as shown in the following lemma

Lemma 4.4: An upper bound for the admissible Δt can be obtained by expanding equations (4.26),(4.28) and (4.29) as shown below

$$\begin{aligned} &J(t_{i+1}) = \tfrac{1}{2}x^T(t_i)Gx(t_i)+ \\ &\Delta t\left[\tfrac{1}{2}x^T(t_i)(A^TG+GA)x(t_i) + x^T(t_i)GB_\sigma U(t_i)\right] \end{aligned} \tag{4.30}$$

if the control signal is defined as

$$U(t_i) = -K_\sigma x(t_i) \tag{4.31}$$

where K_σ is the control gain associated with the σ subsystem then equation (4.30) can be rewritten as

$$J(t_{i+1}) = \frac{1}{2}x^T(t_i)\left[G + \Delta t(A^TG + GA - 2GB_\sigma K_\sigma)\right]x(t_i). \tag{4.32}$$

We assume that the open loop system is stable. This implies that the following equality is verified

$$A^TG + GA = -Q. \tag{4.33}$$

By substituting this in the previous equation we obtain

$$J(t_{i+1}) = \frac{1}{2}x^T(t_i)\left[G - \Delta t(Q + 2GB_\sigma K_\sigma)\right]x(t_i). \tag{4.34}$$

The maximum admissible Δt must be such that the matrix $[G - \Delta t(Q + 2GB_\sigma K_\sigma)]$ is positive definite. It can be noticed that the condition found does not depend on the state variables $x(t)$ and therefore holds also when only the estimated state information $\widehat{x}(t)$ is available.

Remark 4.6: To ensure a good approximation for (4.28), the switching interval Δt should be small. However such length cannot be arbitrarily small. Mechanical limitations and computational time may introduce a lower bound for the choice of Δt. When such case arise to achieve a better accuracy an higher order approximations should be used on computing the value of $J(t_{i+1})$. This case is considered below with the second order.

$$J(t_{i+1}) = J(t_i) + \frac{\delta J_\sigma}{\delta t} \mid_{t_i} \Delta t + \frac{1}{2} \frac{\delta^2 J_\sigma}{\delta t^2} \mid_{t_i} \Delta t^2 + 0(\Delta t^3). \tag{4.35}$$

with the assumption that, within each time interval Δt, the state's variable $x(t)$ are continuous functions in R^n.

The stability arguments for this switching rule are presented below.

Theorem 4.4: The following switched system

$$\dot{x}(t) = Ax(t) + B_{\sigma(t)}U(t) \tag{4.36}$$

with the switching law (4.27) is Lyapunov stable if the open loop matrix A is stable.

Proof: Defining the common Lyapunov function

$$V(x,t) = E(x,t) = J(x,t) \tag{4.37}$$

we have for the time derivative of the Lyapunov function

$$\left(\frac{\delta V(x,t)}{\delta t}\right)_{\sigma} = \left(\frac{\delta J(x,t)}{\delta t}\right)_{\sigma} \tag{4.38}$$

and substituting (4.31) and (4.33) in (4.29) we show that

$$\left(\frac{\delta V(x,t)}{\delta t}\right)_{\sigma} \leq 0, \ \ \forall \sigma \tag{4.39}$$

moreover the switching rule (4.27) ensures that at any switching time t_i it has activated the subsystem $\sigma(t_i)$ that results in the most negative value for $\frac{\delta V(x,t)}{\delta t}\diamond$.

Lemma 4.5: For the more general case of (4.1) the switching rule (4.27) guarantees stability if:

- All the possible subsystems N_p are bounded
- The prediction for the energy index $J(t)$ is sufficiently accurate at any switching time

Similarly to what done above the switching algorithm is reassumed below

Algorithm 5 Minimum system energy switching policy

1: divide the interval $[t_0, t_f]$ into m subintervals, each with duration $\Delta t = \frac{t_f - t_0}{m}$.
2: at the beginning of each interval $[t_k, t_k + \Delta t)$ find the predicted value of J at the next switching time (t_{k+1})
3: find the optimal device to be used by solving

$$B^{opt} = \arg \min_{(B^1,\ldots,B^{N_p})} J(t_{k+1}))$$

4: deactivate all devices and only activate the B^{opt} device.

We can now add some more details for the specific structural case considered here. It is possible to explicit the energy index J for the investigated example. First

we consider for each closed loop subsystems the feedback control law $u_\sigma(t) = K_\sigma x(t)$, with the gain K optimally computed for each subsystems. The energy matrix G in this mechanical system is defined as

$$G = \begin{bmatrix} K & 0 \\ 0 & M \end{bmatrix}. \tag{4.40}$$

By computing the index J as described above we obtain for this particular application the following expression

$$J(t_i) = \frac{1}{2}\dot{X}_{mn}^T(t_i)M\dot{X}_{mn}(t_i) + \frac{1}{2}X_{mn}^T(t_i)KX_{mn}(t_i)$$

where the $X_{mn}, \dot{X}_{mn}$ are the state variables displacement and velocity and the derivative of J is

$$\frac{\delta J_\sigma}{\delta t}\Big|_{t_i} = \frac{1}{2}(\ddot{X}_{mn}^T(t_i)M\dot{X}_{mn}(t_i) + \dot{X}_{mn}^T(t_i)M\ddot{X}_{mn}(t_i))$$

$$+\frac{1}{2}(\dot{X}_{mn}^T(t_i)KX_{mn} + X_{mn}^TK\dot{X}_{mn}(t_i))$$

4.4 Local maximum deviation switching policy

In this section we introduce a third switching strategy. The idea is to identify the area of the structure where the effects from the disturbance are more relevant. In other words to identify the most perturbed spatial region of the structure. The supervisor select then the closest available actuator to such area in order to locally address the vibration state. The algorithm is summarized below.

The proposed algorithm requires a substantial knowledge of the vibration state for the structure. This requirement can be satisfied by introducing an observer as done above or either providing a network of sensors collocated over the structure. Since the switching path is determined by comparing the vibration levels only close

Algorithm 6 Local maximum deviation switching policy

1: At the time $t_k - \frac{\Delta t}{20}$ start sampling the absolute values from the sensors' readings

2: At the switching time t_k:

1. process the samples from the sensor network and define the average for any sensor's sampling
2. find the absolute maximum value between the available sampling sets and its corresponding sensor's position $(\xi_s, \zeta_s)^{max}$
3. clear the sampling sets and maintain only the information $(\xi_s, \zeta_s)^{max}$

3: Identify the closest actuator to this area solving the optimization problem

$$\sigma(t_i) = \arg\{\min_{\sigma \in \Theta} F_{dist}(t_i, p_k)\} \tag{4.41}$$

where $F_{dist}(t_i, p_k)$ is the distance function

$$F_{dist}(t_i, p_k) = |(\xi_s, \zeta_s)^{max} - (\xi_{p_k}, \zeta_{p_k})| \tag{4.42}$$

4: Switch on the actuator found for the full length $t_{k-1} - t_k$

to the available actuators, placing the sensors in proximity to the actuators allows us to avoid the use of a dedicated observer in order to reconstruct the required information.

The most important aspect of this approach is the simplicity in terms of implementation and the reduced computational power required, important factors over the final design feasibility.

The absence of constraints for the switching law makes impossible to guarantee *a priori* stability for the global system. However it is possible to prevent unstable behavior by ensuring that all the subsystems are exponentially stable and the switching interval length is longer than the average decay time for the slowest subsystem.

Remark 4.7: It is possible to guarantee stability for the switched system by

Table 4.1: Numerical simulation: piezo coordinates over the plate

PZT 1	$0.1242m, 0.2301m$
PZT 2	$0.8054m, 0.2301m$
PZT 3	$0.1242m, 0.7899m$
PZT 4	$0.8054m, 0.7899m$

introducing the following additional constraint. Define a set of Lyapunov functions $V_\sigma(t)$ associated with the N_p subsystems and ensure that the choice obtained from (4.41) verify also that

$$V_\sigma(\bar{t}_k) \leq V_\sigma(\bar{t}_{k-1}), \tag{4.43}$$

it is then possible to use the stability arguments presented in the previous section.

4.5 Numerical results

The strategies described above were first validated through a set of numerical simulations presented in this section. The test case considered is again the flexible plate introduced in chapter three.

Four piezo are considered available on the simulated plate. Table 4.1 provides the piezo's coordinates.

Only three of these piezoelectric patches are used to control the plate while the forth one is used as a sensor. In the first two switching strategies the sensor information is required to build an estimation for the state variables. This estimation is then used to define both the switching path and the control law.

An exception is made for the third switching strategy. In particular for this approach it is required a network of sensors that provides information from the overall plate or at least from the areas in proximity of the available actuators. In order to satisfy such requirement all four piezo were used for active control. Moreover

each of the simulated piezo/actuator were also assumed to be working as a sensor. In other words once the piezo positions are assigned and the B_2 matrix is defined the sensors component is obtained simply by imposing $C_2 = B_2^T$.

The numerical code was implemented using $Matlab$® on a standard PC machine (2GHz, 1Gb).

The mass and stiffness matrix for the plate are obtained again with the discrete approach described in chapter two. The dynamics of the plate is described by the first order system (4.1). In addition it is necessary to simulate also the dynamics of the observer, described by equation (3.11).

The solution for this coupled system of differential equations (4.1),(3.11) was obtained by using the ordinary differential equation toolbox available in $Matlab$®. In particular an external cycle of switching intervals was defined and for each switching interval the system of differential equations was solved by using the available toolbox.

The plate is subjected to an external, time varying disturbance. In particular we vary the spatial distribution of such disturbance. This is done by considering different spatial distribution for the disturbance E_1 and switching between these on a random or a predesignated base. Figures 4.1,4.2,4.3 show some of the spatial disturbance distributions used in these simulations. Those distributions are however unknown to the controller.

Results are shown in the next figures. The plots represent the kinetic energy for the open loop system, the closed loop system without switching and the switched closed loop system. The switching intervals were chosen of a fixed length both for the actuators and the disturbance components. In particular the control switching law was computed every two simulated seconds while the disturbance was switched any simulated second.

The results from the numerical simulations are shown in the next set of figures.

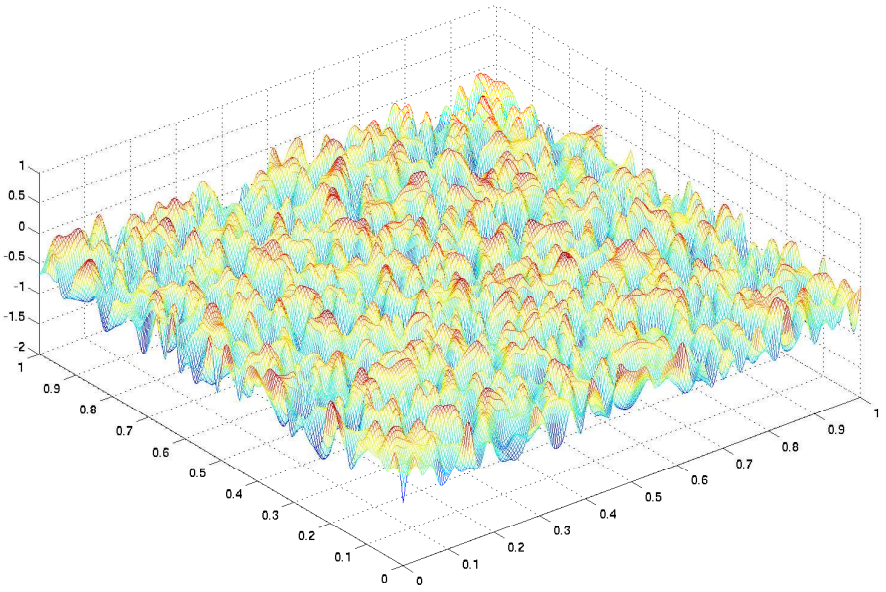

Figure 4.1: First spatial disturbance distribution

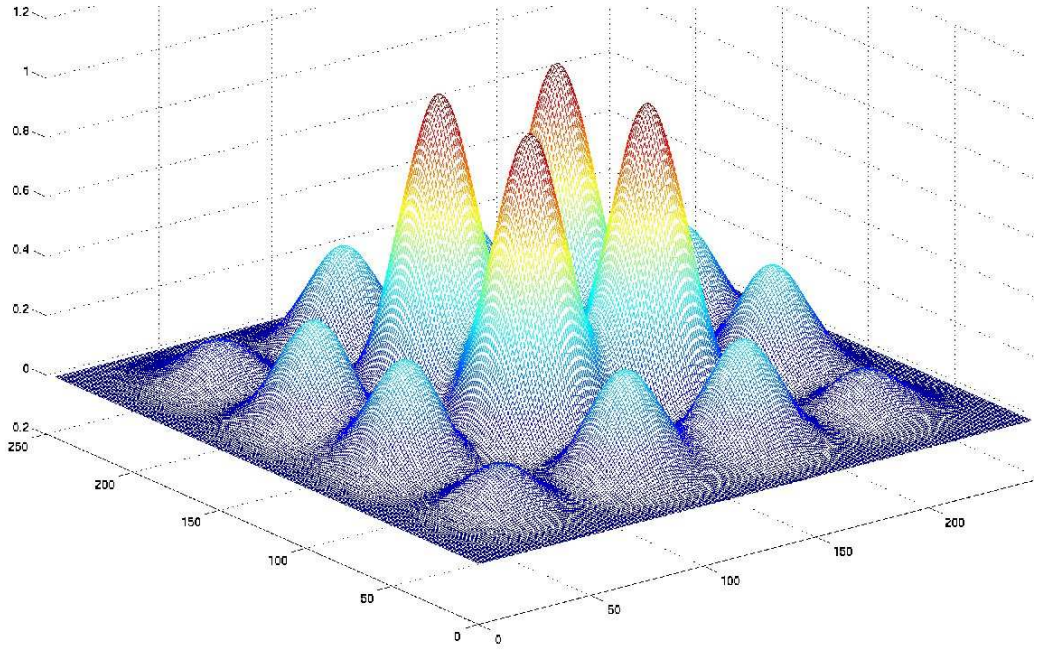

Figure 4.2: Second spatial disturbance distribution

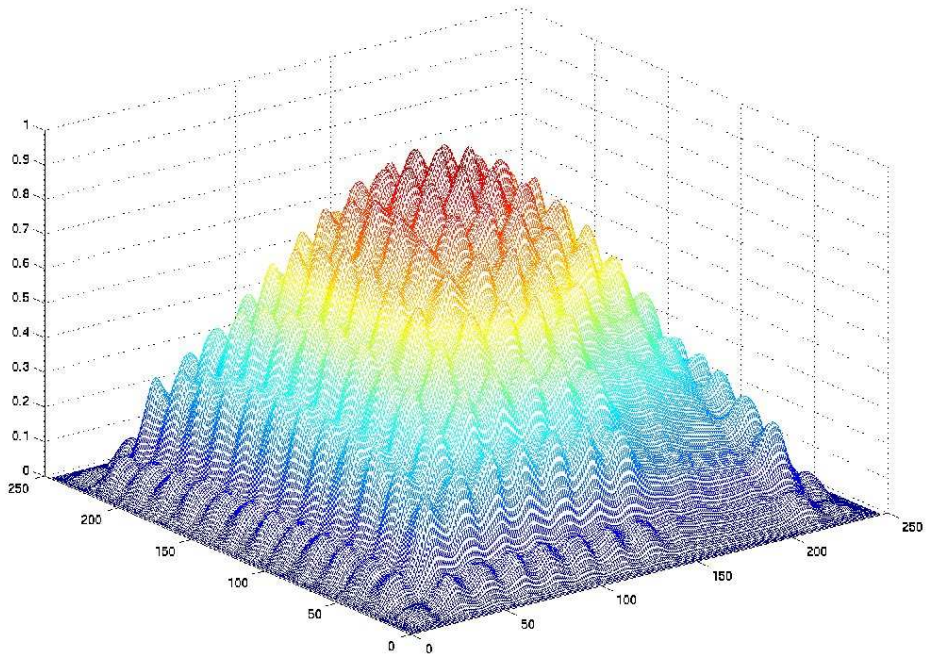

Figure 4.3: Third spatial disturbance distribution

Two simulations for each switching strategy are presented. The difference between the two simulations is related to the effects of different sequences of disturbance distributions. The preassigned spatial disturbance distribution were randomly switched during the simulations. This was done to better simulate the uncertainty associated with the disturbance effects. The open loop, closed loop and closed loop case with switching were however simulated with the same sequence of disturbances for each test.

The first two figures show the results obtained using the "Cost to go" switching rule. By comparing the three curves it results evident the beneficial effect of the switching. The second pictures depicts the results obtained with the minimum energy switching policy. Similarly to the previous switching law also for this second case the improvements due to the switchings are tangible. The different levels of

high frequency fluctuations in the pictures are related to the different averaging interval used. Finally the third pictures set shows the results obtained using the max deviation rule. In this last case the optimality for the actuation strategy cannot be guarantee. However the results still indicate additional benefits from the use of a switched controller.

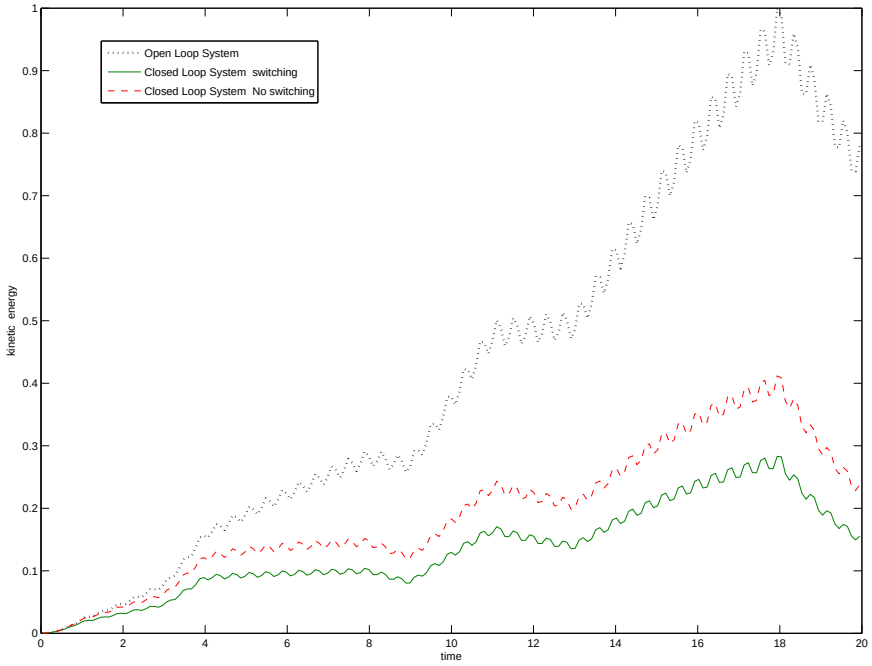

Figure 4.4: Kinetic energy:cost to go switching rule

4.6 Experimental results

The switching strategies described above were also validated on an experimental test case. The test case chosen is a cantilever aluminum plate. The choice of a cantilever boundary condition was made in order to limit the system rigidity and enhance the effects of disturbance/control moments. This was a necessary choice

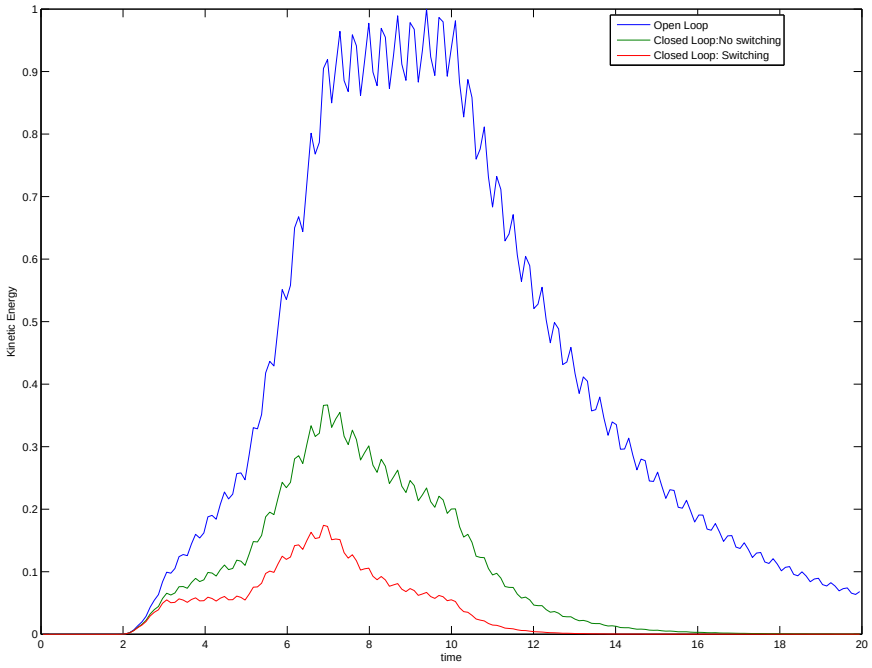

Figure 4.5: Kinetic energy:cost to go switching rule, test 2

due to the limited strength of the available actuators.

The experimental set up is shown in Figure 4.10

The control and disturbing moments were delivered by piezoelectric patches. Eight piezoelectric patches were affixed in collocated position (four each side of the plate) as showed in picture 4.10. Three of the four patches of the front side were used to deliver the control action while the fourth one was used as sensing device. The information from such sensor was used to generate the estimated state variables $\widehat{x}(t)$ for the system and subsequently the feedback-based control law u(t). The estimated state variables are also used from the control strategies to define the switching path. This is the case for the Cost to go rule and the Minimum energy system rule.

For the Maximum deviation switching rule additional sensing information is required. In particular sensors should be available in correspondence of each actuator.

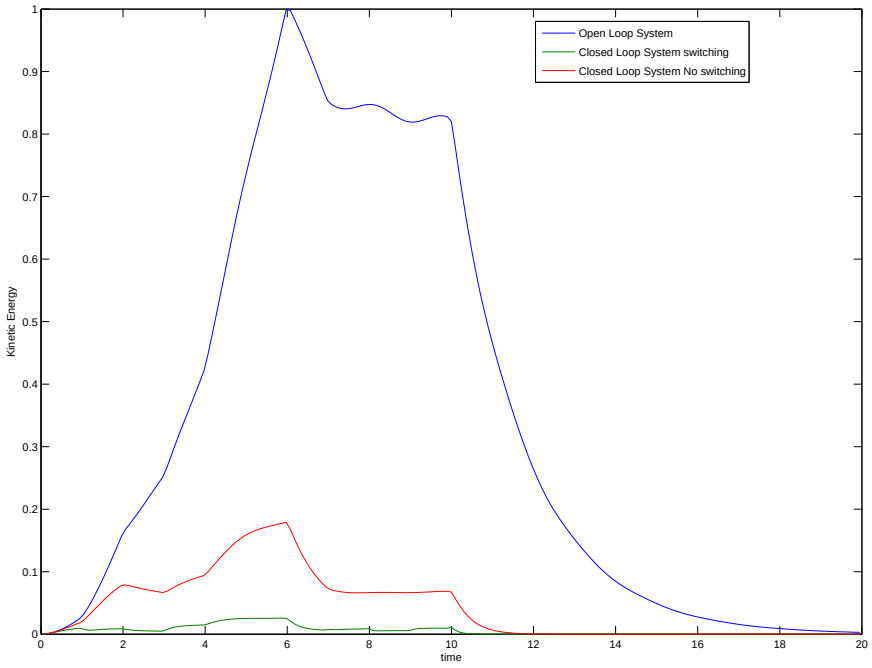

Figure 4.6: Kinetic energy:minimum energy switching rule

In order to satisfy this condition three additional accelerometers were affixed on the plate in proximity of the actuators. The fourth piezo on the front side is still used as a sensor. The information is used to generate the feedback law $u(t)$. With reference to the notation introduced above three controlling subsystems are available on the described configuration $N_p = 3$.

The length for each interval between two successive switching was chosen to be $\Delta t = 1s$. This choice, in our case arbitrary made, may in general be related to several factors such as mechanical switching limitation, avoiding chattering, fast change in time for the disturbance etc etc.

The four collocated actuators on the rear side of the plate are all dedicated to simulate a disturbing moment acting over the plate. Disturbance characteristics are assumed not to be available for the switching controller. The moving disturbance

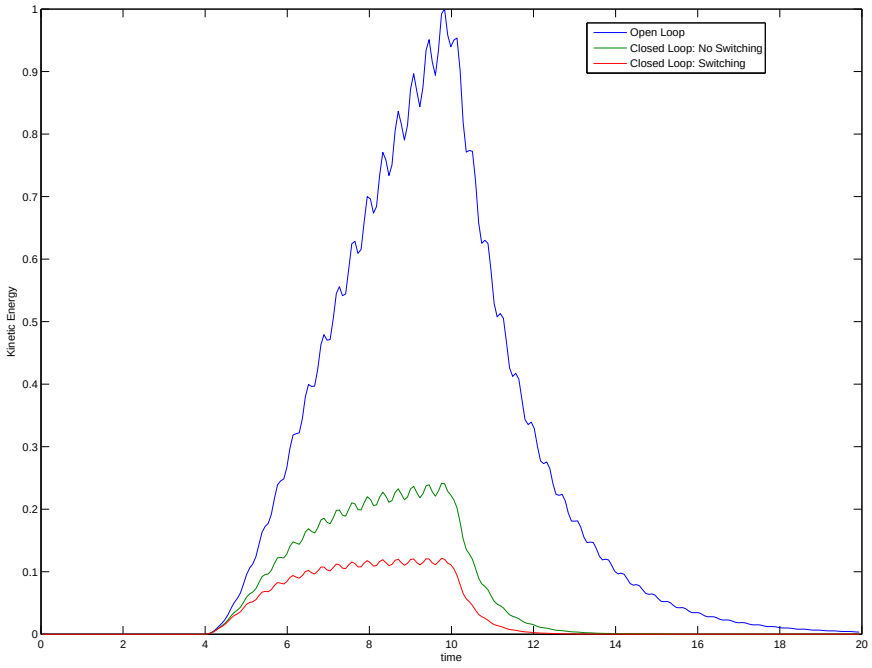

Figure 4.7: Kinetic energy:minimum energy switching rule, test 2

is simulated using only one actuator at time and switching between the remaining according with a predetermined activation sequence. The interval length chosen for the disturbance switching is $\Delta t_{dist} = 3s$. The temporal disturbance component $w(t)$ was chosen to be a sinusoidal signal with a frequency of $244Hz$. This frequency was found to be the one that maximizes the effect of the disturbance over the plate. Mechanical properties of the plate and the piezoelectric patches are listed in the table 4.2 A discrete model for the plate is required in order to implement the switching controller and the control law. In particular mass, stiffness and damping matrixes must be calculated for the considered case, according with the approach presented in chapter two. The damping matrix is obtained trying to match the experimental frequency response with the model frequency response.

Figure 4.11 shows the input/output response from the discrete model compared

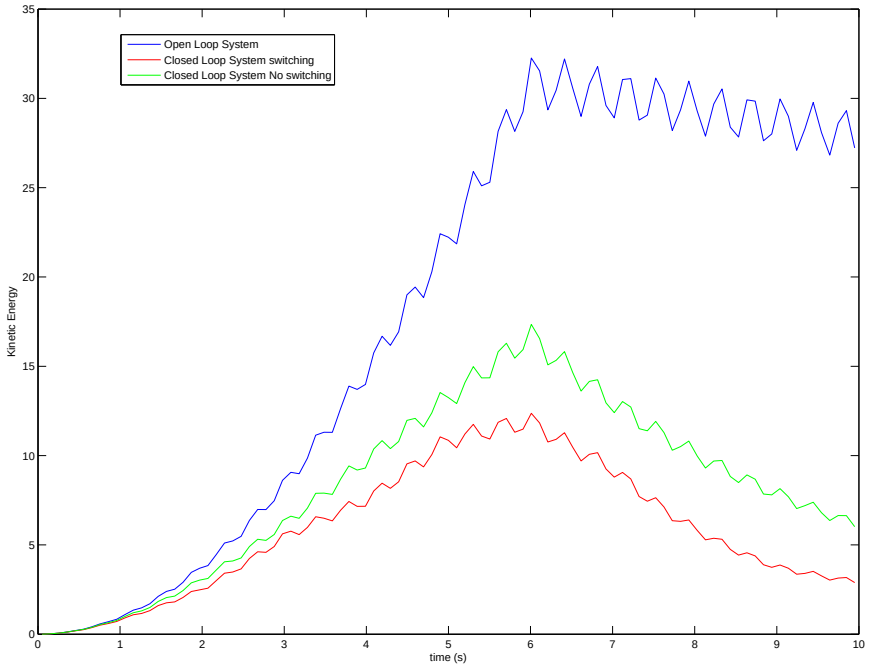

Figure 4.8: Kinetic energy:max deviation switching rule

with the experimental values.

Few discrepancies from the numerical and experimental model can be noticed; those are due to the limits associated with the choice made for the damping matrix D.

Simulink® package was used to create the virtual model for the switched controller while dSPACE® ACE1103 Kit was used to interface the hardware (plate and actuators/sensors) and computer.The computer used for implementing real-time control was a 2GHz Pc with 1G of memory while the sampling rate for the discrete model on real time models was $\frac{1}{1500}s$.

Theoretically higher sampling rates would guarantee a better efficiency over higher natural frequencies. However due to hardware limitations the effect of delays between the sensor readings and the control law signal are not anymore negligible

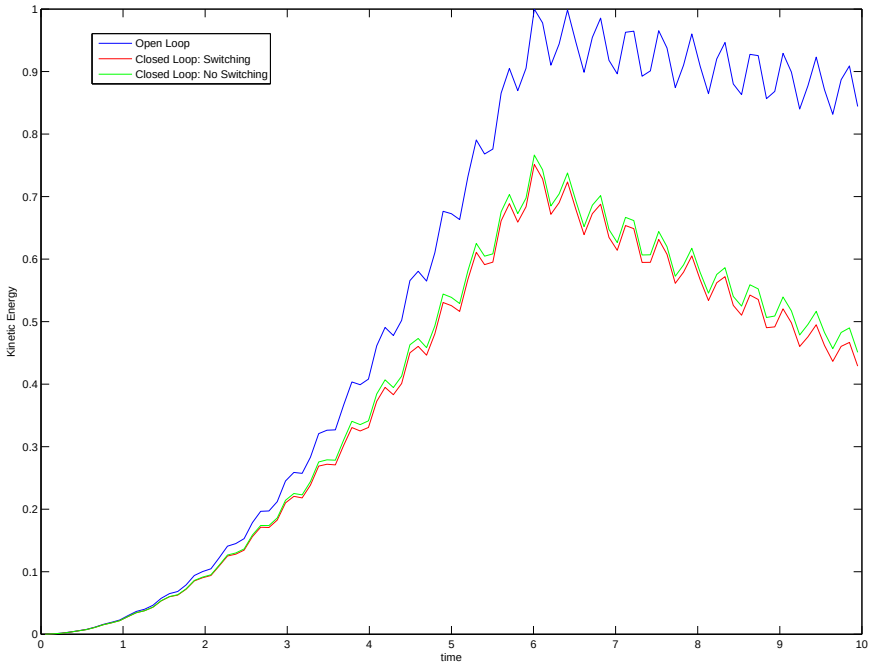

Figure 4.9: Kinetic energy:max deviation switching rule

for higher sampling times. According with such limitation it is necessary to filter the high frequency content that cannot be processed by the available hardware. In particular the frequency content higher than 1KHz is discarded both for the sensor readings input and the control law output. This is done by using a Butterworth Low-Pass anti-aliasing filter. In addition a signal conditioner is used to amplify the control signal before it is sent to the actuators. The complete experimental set up, shown in picture 4.12, includes the Pc, the *DSpace*® board, two filters and two signal conditioner.

The complete experimental apparatus is schematized in figure 4.20

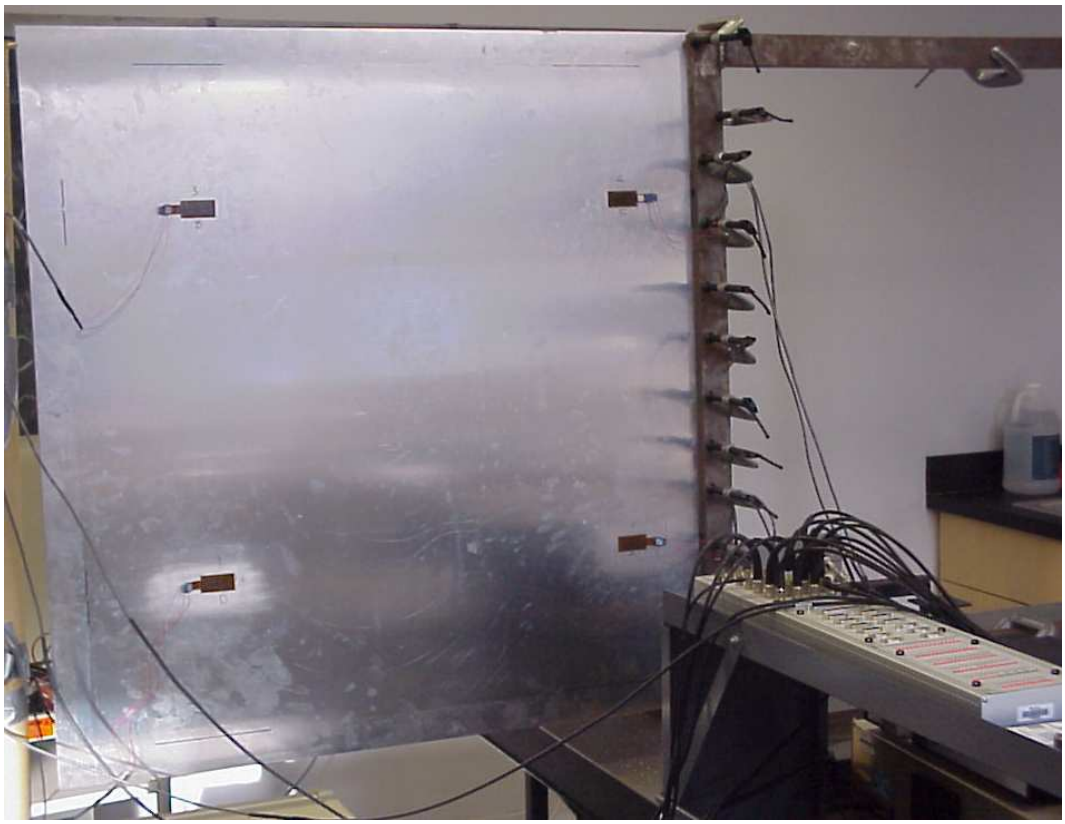

Figure 4.10: The experimental set up

4.6.1 "Cost to go" policy

In this section we present the experimental results obtained by defining the switching strategy according with the "Cost to go" rule. The control moment is applied to the structure by only one of the actuators at time according with the activation sequence defined on real time. Two different cases were considered for this strategy. First only two actuators were alternatively used to perturb the system. This is equivalent to use two different spatial distribution disturbance to destabilize the structure. The second part of this test was done, similarly to the previous case, by using all the four back side actuators to alternatively generate four different spatial distributions disturbance.

Table 4.2: Plate and PZT properties

Plate length	1.052m
Plate height	1.108m
Plate thickness	0.001635m
Plate density	$2.69 \times 10^3 Kg/m^3$
PZT length	0.0508m
PZT height	0.016078m
PZT thickness	0.00075m

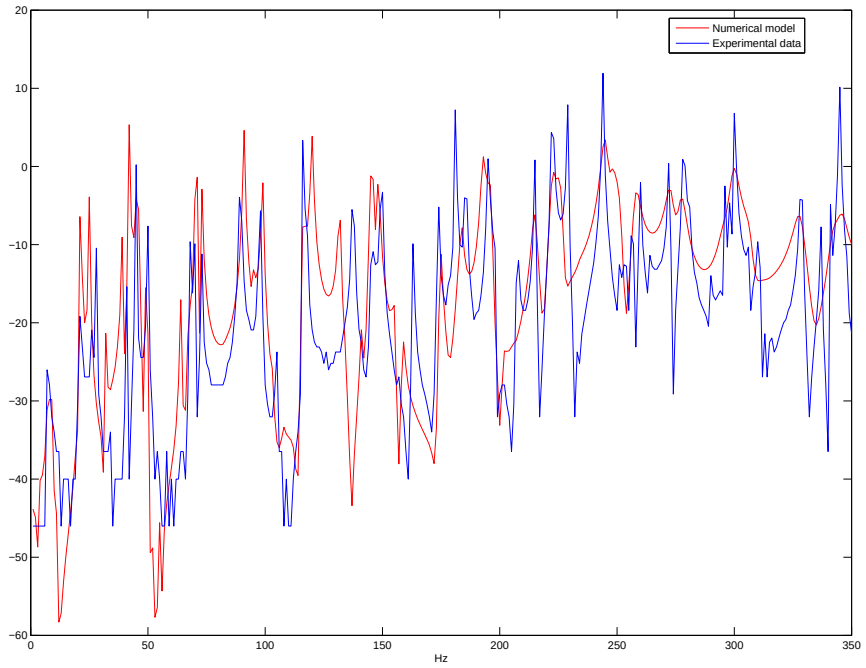

Figure 4.11: Input/output response for numerical and experimental model

Figure 4.14 shows part of the Simulink model implemented for this switching strategy. The top window contains the main part of the model. This includes the switching time component, the feedback laws for the available actuators and the dedicated observer for the switching controller. The bottom window contains the first layer of the switching controller model.

Results for both cases are shown in Figures 4.15,4.16. It can be noticed the im-

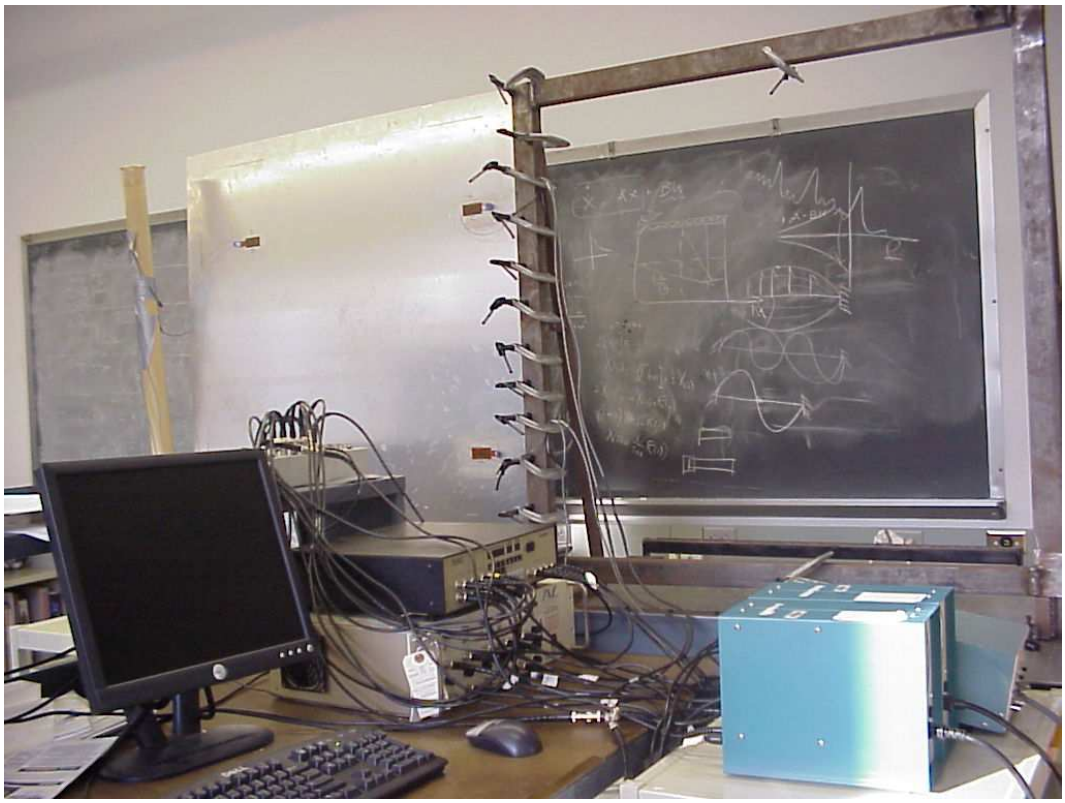

Figure 4.12: Experimental set up

proved control efficiency for the switched controller. The switched solution provides up to 50% additional vibration reduction compared with the traditional controller performance. We observe that the traditional controller becomes unstable under the effect of the moving disturbance. Moreover it can be seen as its efficiency drops to zero and the vibration level for the closed loop without switching reaches the same level as the open loop system.

In order to test the robustness of this switching policy we performed an extreme initial conditions test. The plant was driven to an unstable behavior by implementing a closed loop cycle with a positive gain feedback. The plate itself is a stable plant due to the its intrinsic damping properties. The energy provided by the used actuator can be completely dissipated or in other words that the actuator is not strong enough to break the plate. Because of this conditions the plate vibration for

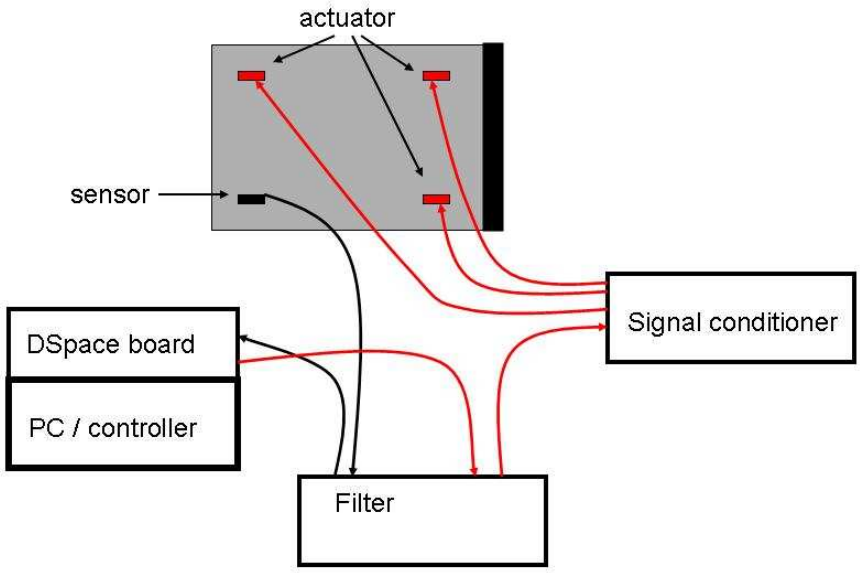

Figure 4.13: Scheme of the experimental apparatus

the unstable closed loop results higher than the open loop but still a bounded value. Once the plate vibration had reached its maximum level for this unstable condition the switched control system was turned on. Figure 4.17 shows the vibration levels for such case.

The blue curve represent the system with no active control while the red line depicts the vibration level for the closed loop. The mechanical energy for the red curve is higher than the open loop case for the first part of the test. This is due to the induced unstable behavior. Once the switching controller is turned on the system gains stability and the vibration is reduced below the open loop levels.

A different analysis for the performance of such strategy can be done by looking at the frequency domain. The following pictures depict the power spectra of the sensor output signal. In other words we now look at the energy content of different

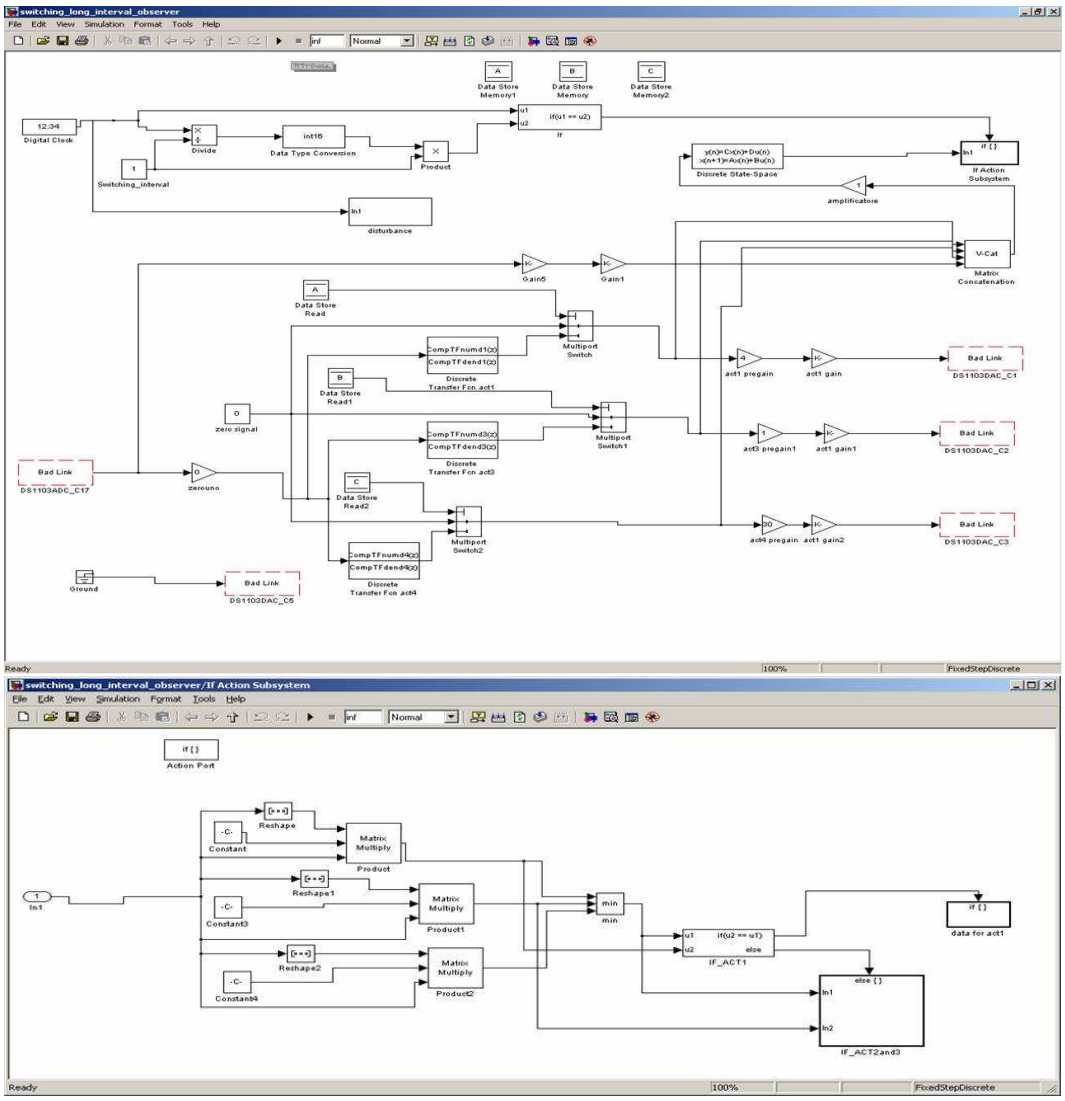

Figure 4.14: Simulink model: Cost to go policy

frequencies. Again the open loop, closed loop without switching and switched case are compared.

The comparison is shown in Figure 4.18. The energy peak located at $224Hz$ is a direct consequence of the choice made for the disturbance. As specified above the disturbance time component is a sinusoidal signal at $224Hz$. It is possible to identify the benefit associate with the use of a switched controller for such dominant frequency, as highlighted on the picture.

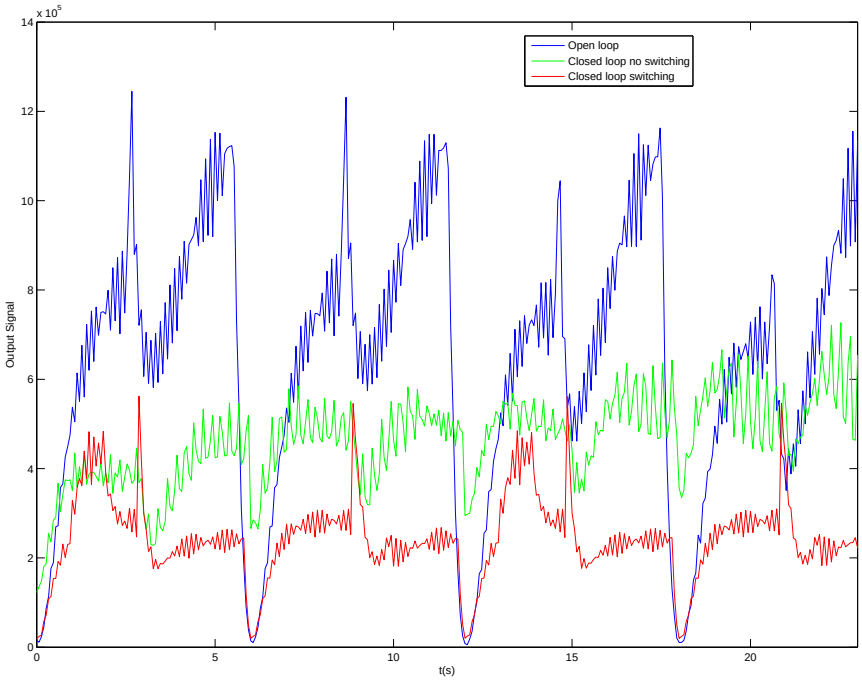

Figure 4.15: Cost to go policy with two disturbance distributions

An interesting case is shown in Figure 4.19. The power spectra are relative to the test case where four possible spatial disturbance distributions were alternated. Recalling the time domain results showed above in this case the traditional closed loop could become instable under the effect of the switching. Observing picture 4.19 it is possible to note the instability effects on the extra energy peeks for the non switched case.

4.6.2 "Minimum energy" policy

The third switching strategy was experimentally validated with a similar set of tests. Only one actuator at time is switched on to provide the control moment. A single PZT device is used as sensor. The information obtained from the sensor is processed to define the switching law $\sigma(t)$ and the control signal $u(t)$. Differently from the

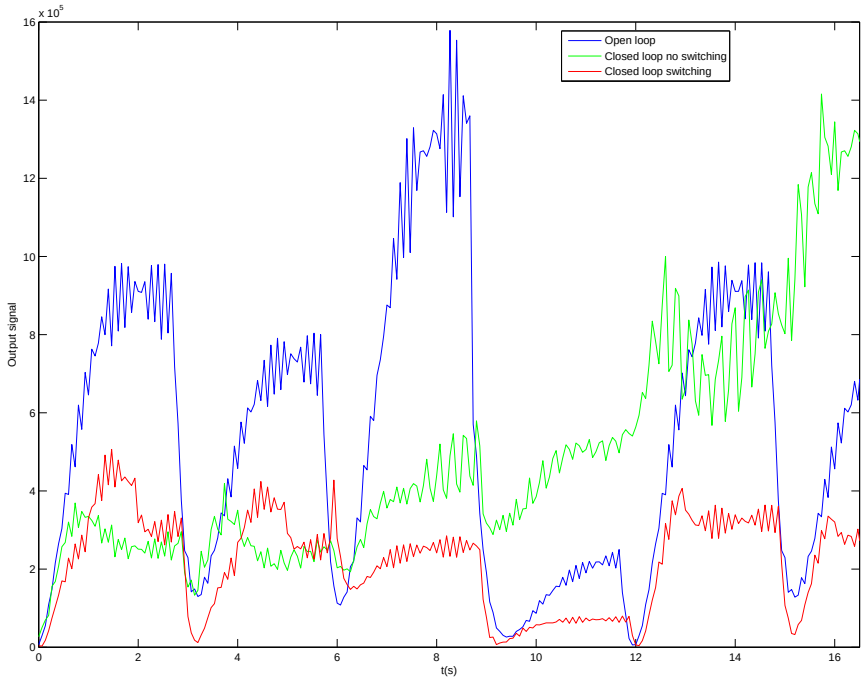

Figure 4.16: Cost to go policy with four disturbance distributions

previous case the switching sequence is now obtained by minimizing the energy state for the system, as described on section 4.3. The Simulink architecture for this case is analogous to the Cost to go policy because of the similarity of input requirements for the switching controller.

In Figures 4.20,4.21 similarly to the above pictures, the output signal for the open loop, closed loop no switching and closed loop with switching is depicted. The two "closed loop no switching" curves (green lines) in the left and right figures are obtained choosing a different patch as fixed actuator. It can be notices how in the left case the device chosen results to be less optimal than the one used for the second test (right picture). However in both cases the switched controlling system (red lines) performs more efficiently than the traditional closed loop. A substantial improvement in vibration reduction is achieved with the introduced switching.

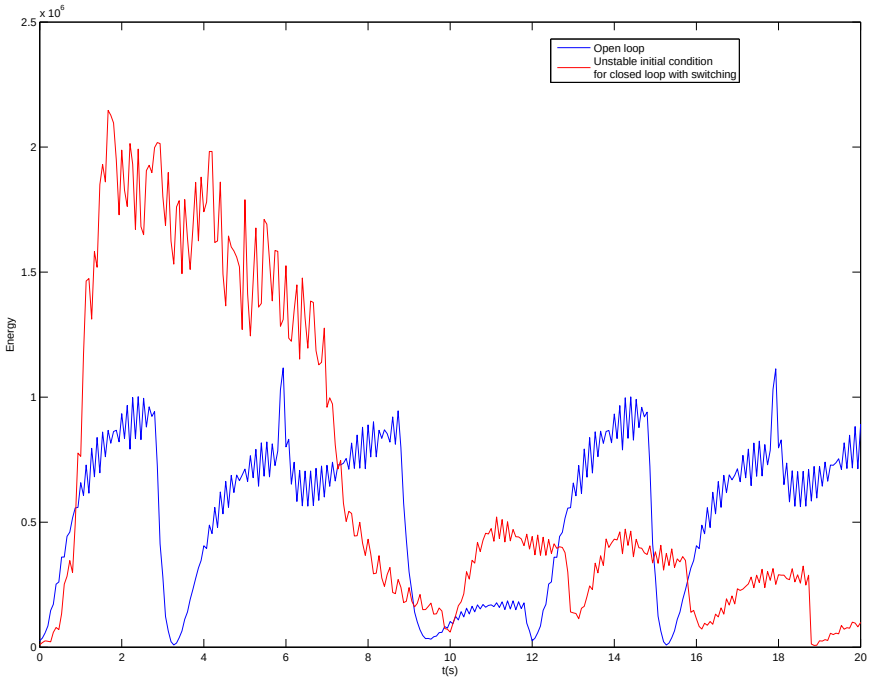

Figure 4.17: Cost to go policy: unstable initial condition

Similarly to what done above for the first switching strategy we now analyze the frequency domain. Power spectra for the open loop, closed loop and closed loop with switching are shown in picture 4.22.

Again the improvement achieved by introducing the switched controller is evident.

4.6.3 Local maximum deviation switching policy

The last experimental test was done using the local maximum deviation rule to define the switching path $\sigma(t)$. In order to implement this algorithm it is required a network of sensors located in proximity to the controlling actuators. Three accelerometers were used to build such network; according to the switching strategy, these sensing devices were located in proximity to the three actuating devices (PZT actuators).

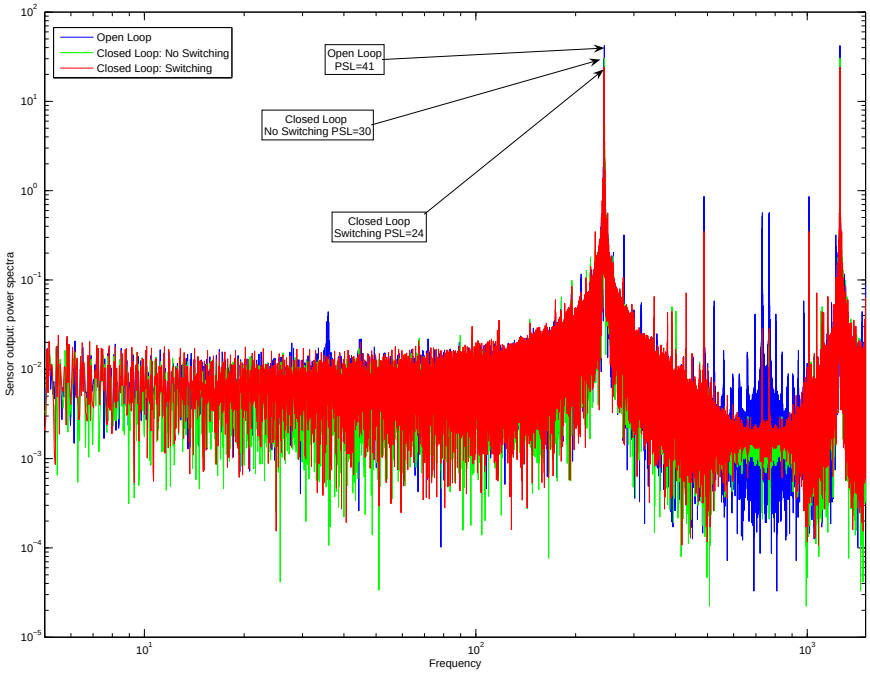

Figure 4.18: Power spectra for sensor output

Figure 4.24 shows the Simulink model for this switching rule. Similarly to what done above the first window contains the main part of the model while the switching controller is modelled in the second window. The main difference is that in this case the switching controller does not require a dedicated observer but only the direct readings from the three designed sensors.

In analogy with the previous section the three cases, open loop, closed loop without switching and closed loop with switching are compared. Figure 4.23 depicts the norm of the output signal (PZT sensor information) from the plant for these three cases. Experimental results are in full agreement with results from the numerical investigation previously described. The vibration level are substantially reduced when the switching controller is kept active respect to the case without switching. It is also interesting to observe how the unsteady character of the disturbance affects

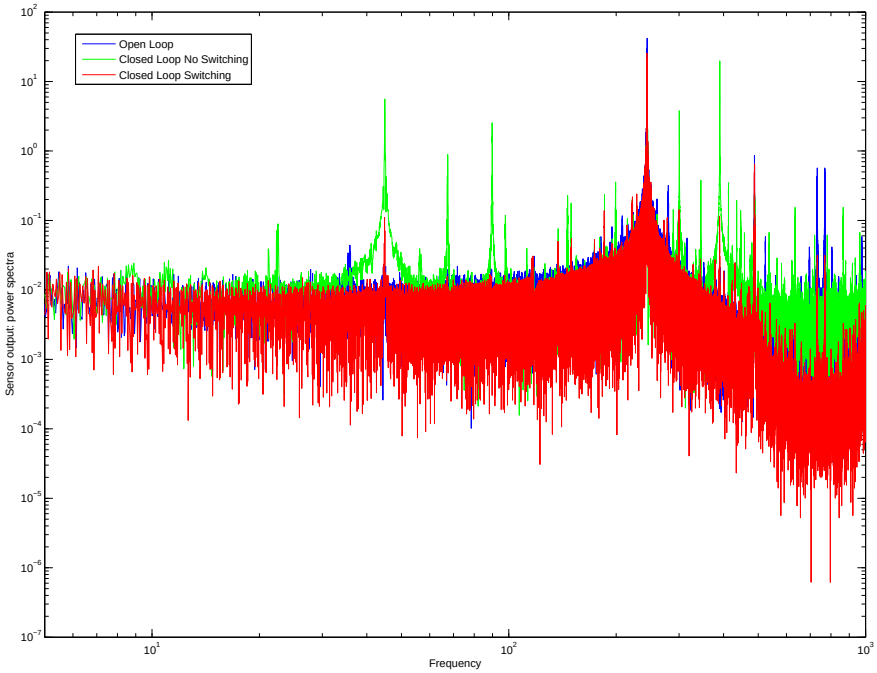

Figure 4.19: Power spectra for sensor output, case with instability

the open loop behavior. The switching results to decrease the intrinsic systems's stability.

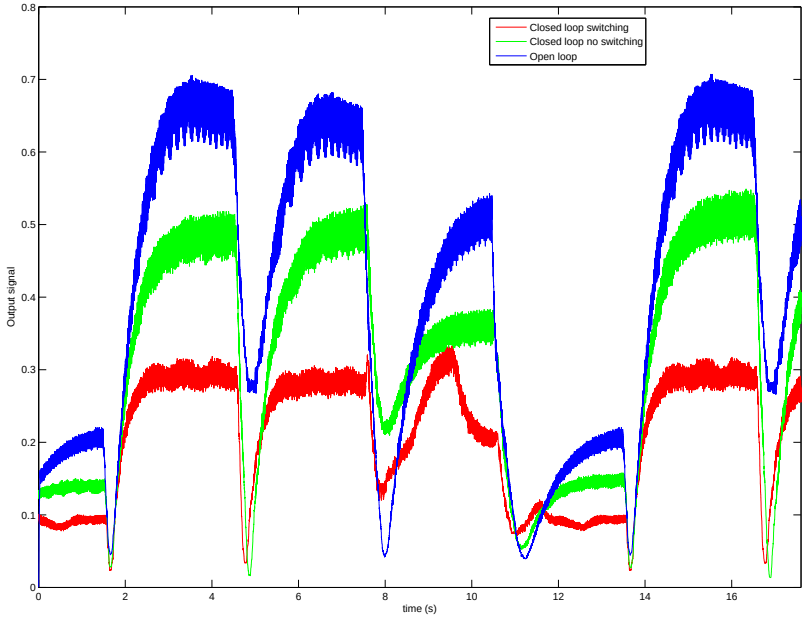

Figure 4.20: Minimum energy switching policy

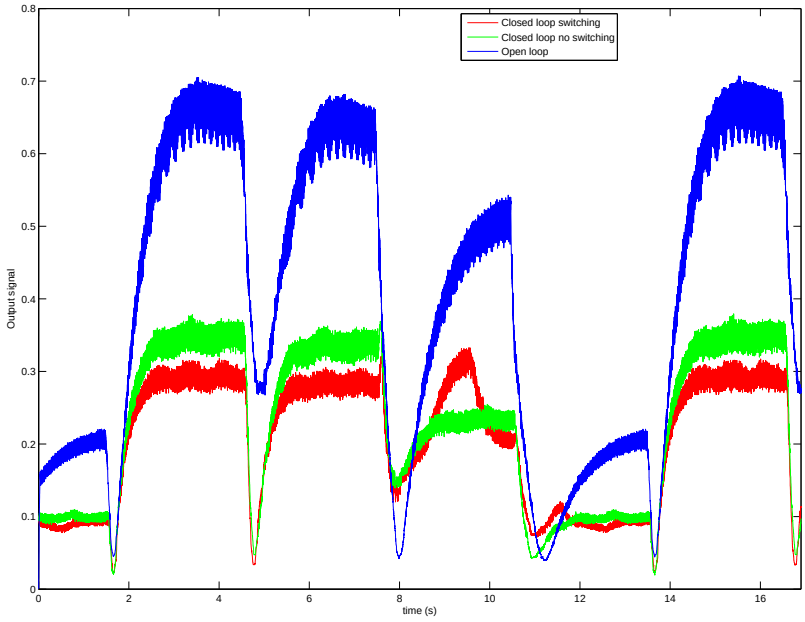

Figure 4.21: Minimum energy switching policy, alternative fixed piezo

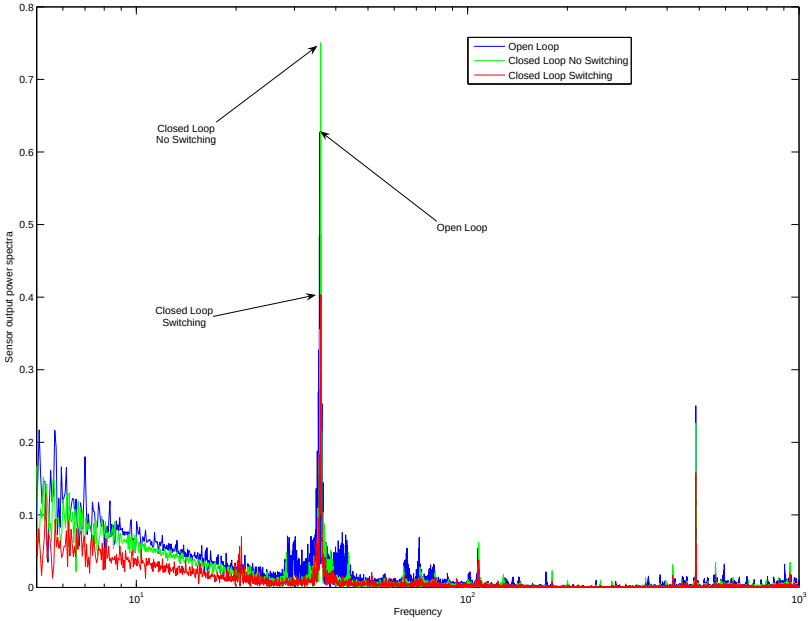

Figure 4.22: Power spectra for sensor output with minimum energy policy active

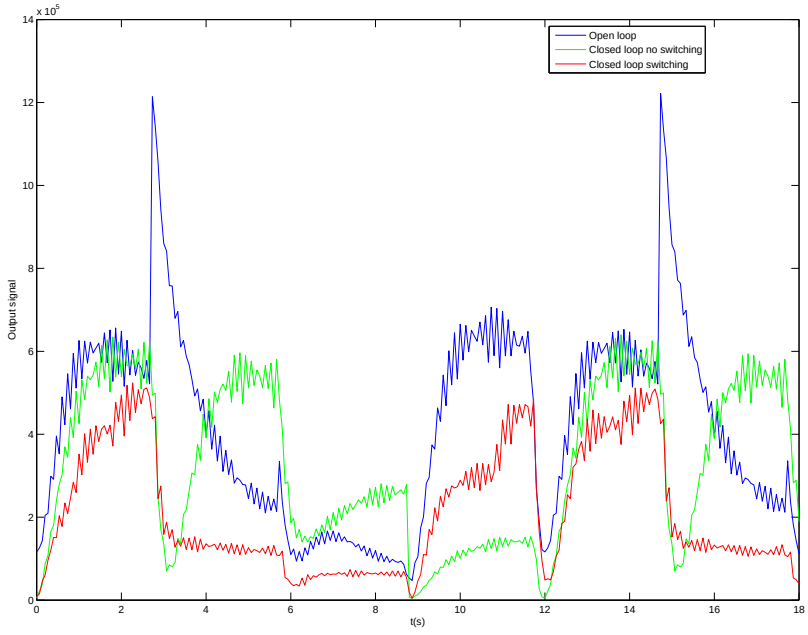

Figure 4.23: Local maximum deviation switching policy

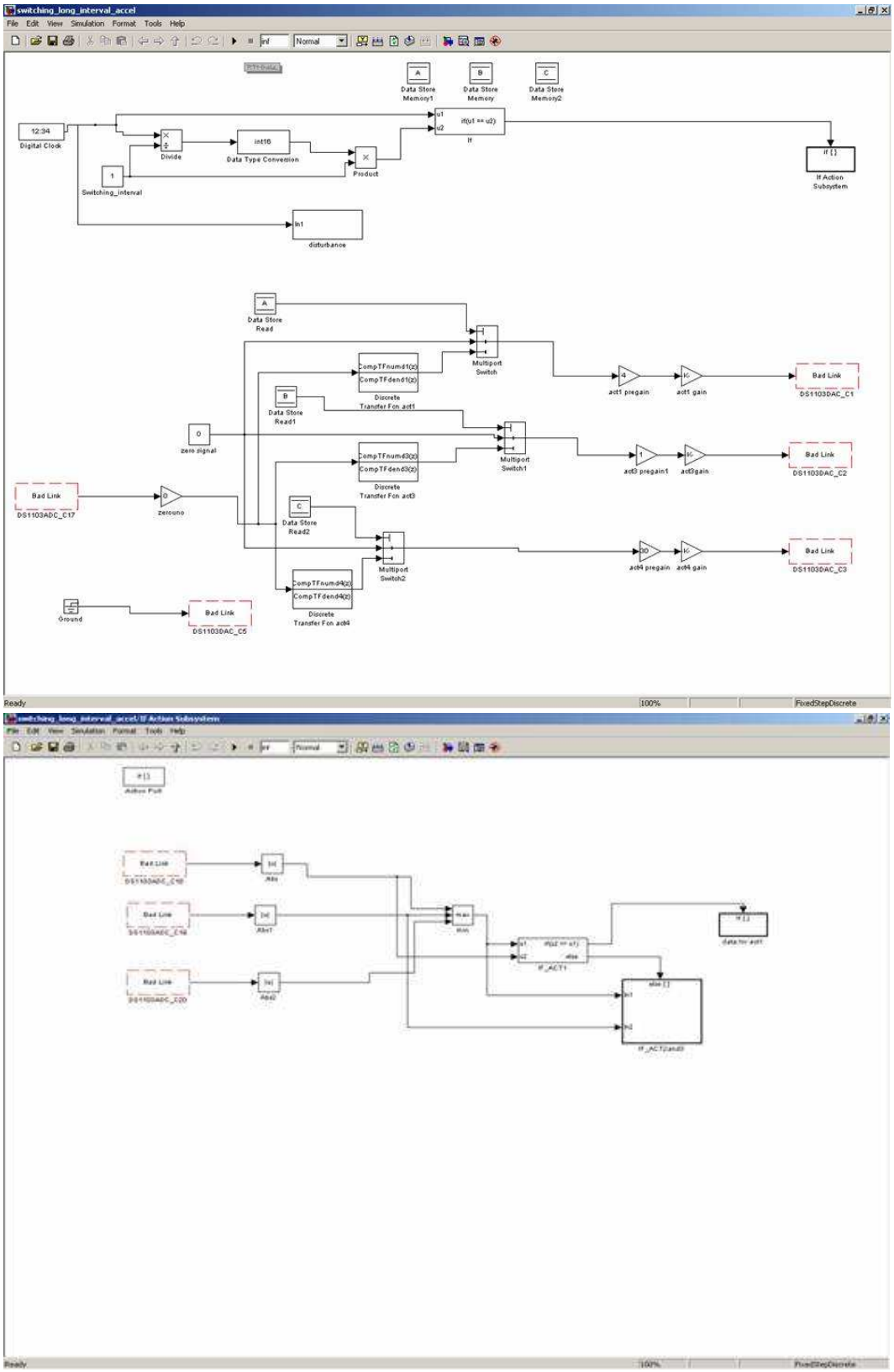

Figure 4.24: Simulink model: Maximum deviation rule

Chapter 5

Conclusion and Future Developments

In this comprehensive study the problem of vibration control for flexible structure was investigated. First, the issue of designing a network of actuators and sensors was considered. In order to accomplish such task the desired positions for sensors and actuators had been identified. Three different approaches to determine the optimal placement for controlling devices have been proposed. The three proposed strategies address different typology of situations that can occur in structural vibration problems. The first case considered was the simultaneous placement of several actuating devices. The proposed solution for this case guarantees controllability over a fixed number of modal shapes, providing an easy way to simultaneously locate the devices. With the second strategy, the influence of disturbances over the optimal actuator and sensor placement process was introduced. The algorithm described provides robustness against a known spatial distribution of disturbance. The next step was to introduce the worst admissible scenario for the disturbance. The placement algorithm simultaneously guarantees robustness and optimality. Finally, in the

third case, a strategy was proposed to address the problem of actuator placement over preassigned spatial regions.

The described algorithm provides both improvement in spatially localized control action and global performance. These approaches were validated by numerical simulations.

In the second part of this work the problem of activation strategies for hybrid systems was discussed. In particular, three different control strategies to define activation sequences for the available actuators were considered. The algorithms proposed were validated both numerically and experimentally. Similar to the previous part of this work, a vibration control problem was chosen as a test case to validate these strategies. A flexible plate with affixed actuating and sensing devices was selected to be the switched system. The idea was to reduce the power requirements by efficiently using only a subset of the controlling devices. The goal was therefore to identify the most optimal sequence of controllers to be used along the operational interval. Traditional and switched controller performances were compared and the improvement obtained by introducing the switching controller was evident. Similar results were obtained both from numerical simulations and experimental tests. Experimental tests showed that by using the cost to go switching policy, vibration level was reduced up to 50% with respect to the traditional controller levels.

In this work, vibration control schemes were investigated in detail for flexible 2D structures, however the proposed approaches can be extended to *any* plant whose dynamics can be described by a second order linear system. In particular a possible extension for the proposed switching strategies could include the control of unmanned autonomously vehicles (UAV). The same principle used here could be applied to generate optimal trajectories for the UAV by removing the restriction of spatially fixed actuators and sensors. The vehicle could be seen as a moving

actuator or sensor who's position is the output variable in the optimization process.

Consider for example the case of marine oil (or other pollutant) spilling. In such case a set of autonomous vehicle, able to detect the spilling perimeter and provided with a reactant foam or floating barriers, could be use to contain the spilling. In this case the strategies proposed in this work could be used to obtain a sequence of positions (or in other words a trajectory) for each vehicle such that its sensing ability is maximized. The proposed approaches would also minimize the required energy to power the vehicles by optimizing their trajectories.

Another future development is the extension of the switching laws to non linear systems. This step would remove the limit associated with linearized models expanding significantly the range of applicability. Switched strategies could be used, for example, in active flow control, allowing a significant reduction for power consumption and an overall improvement of system efficiency.

Bibliography

[1] K. Billah and R. Scanlan, "Resonance, tacoma narrows bridge failure, and undergraduate physics textbooks," *American Journal of Physics* **59**, p. 118124, 1991.

[2] J. D. Irwin and E. R. Graf., *Industrial noise and vibration control*, Englewood Cliffs, N.J. : Prentice-Hall, 1979.

[3] A. W. Burton, "Active vibration control in automotive chassis systems," *Computing & Control Engineering Journal* **4**, pp. 225–232, 1993.

[4] B. Riley and M. Bodie, "An adaptive strategy for vehicle vibration and noise cancellation," *Proceedings of the IEEE 1996 National Aerospace and Electronics Conference* **2**, pp. 836–843, 1996.

[5] R. Shoureshi, J. Vance, and R. Gasser, "Automotive applications of active noise and vibration control," *Proceedings of the IEEE International Symposium on Industrial Electronics* **3**, pp. 1071–1076, 1997.

[6] R. C. Bremer, *A practical treatise on engine crankshaft torsional vibration control*, Warrendale, PA : Society of Automotive Engineers, 1979.

[7] S. Viswamurthy and R. Ganguli, "Modeling and compensation of piezoceramic actuator hysteresis for helicopter vibration control," *Sensors and Actuators, A: Physical Elsevier* **135**, pp. 801–810, 2007.

[8] S. Wang, "Free vibration analysis of skew fibre-reinforced composite laminates based on first-order shear deformation plate theory," *Elsevier Science* **63**, pp. 525–538, 1997.

[9] Z. Shi, G. Ma, and Q. Hu, "A hybrid control scheme of vibration reduction of flexible spacecraft during attitude maneuver," *1st International Symposium on Systems and Control in Aerospace and Astronautics* **2006**, pp. 169–174, Jan. 2006.

[10] H.-P. Xie, S. Kalaycioglu, and R. Patel, "Control of residual vibrations in the space shuttle remote manipulator system," *Proceedings - IEEE International Conference on Robotics and Automation* **4**, pp. 2759–2764, 1997.

[11] G. Song, V. Sethi, and H. Li, "Vibration of civil structures using piezoceramic smart materials: A review," *Engineering Structures* **28**, pp. 1513–1524, Elsevier 2006.

[12] A.-P. Wang and Y.-H. Lin, "Vibration control of a tall building subjected to earthquake excitation," *Journal of Sound and Vibration* **299**, pp. 757–773, Elsevier Science 2006.

[13] R. S. Jones, *Noise and vibration control in buildings*, New York : McGraw-Hill, 1984.

[14] D. Halim and S. O. R. Moheimani, "Experiments in spatial h_∞ control of a piezoelectric laminate beam," *Lecture notes in control and information sciences* **268**, pp. 103–122, 2001.

[15] D. Halim and S. O. R. Moheimani, "Spatial resonant control with collocated piezoelectric actuator/sensor pairs," *Proceedings of the American Control Conference* **3**, pp. 1960–1965, 2001.

[16] G. Paolo, C. Rolando, and B. Edoardo, "Control of beam vibrations by means of piezoelectric devices: theory and experiments," *Composite structures* **50, no. 4**, pp. 373–381, 2000.

[17] Y. Yu, *Vibration of elastic plates: linear and nonlinear dynamical modelling of sandwitches, laminated composites, and piezoelectric layers*, Springer Verlag, New York, 1995.

[18] A. Sadri, R. Wynne, and J. Wright, "The design and implementation of robust strategies for active vibration control," *Proceedings of the American Control Conference* **6,**, pp. 3465–3469, (Philadelphia) 1998.

[19] Z. C. Qiu, X. M. Zhang, H. X. Wu, and H. H. Zhang, "Optimal placement and active vibration control for piezoelectric smart flexible cantilever plate," *Journal of Sound and Vibration* **301**, pp. 521–543, 2006.

[20] R. C. H. del Rosario and R. C. Smith, "Lqr control of thin shell dynamics: Formulation and numerical implementation," *Journal of Intelligent Material Systems and Structures* **9**, pp. 301–320, 1998.

[21] A. K. Jha and D. J. Inman, "Optimal sizes and placements of piezoelectric actuators and sensors for an inflated torus," *Journal of Intelligent Material Systems and Structures* **14**, pp. 563–576, 2003.

[22] P. Gaudenzi and Y. Shindo, "Modelling of smart structures," *Computers and Structures* **83**, p. 11511152, 2005.

[23] H. T. Banks, R. C. Smith, and Y. Wang, *Smart Material Structures: Modeling, Estimation and Control*, Wiley-Masson, New York, 1996.

[24] A. Preumont, *Vibration Control of Active Structures: An Introduction*, Kluwer Academic Publishers, Dordrecht-Boston, 1997.

[25] V. Sethi and G. Song, "Multimode optimal vibration control of flexible structure using piezoceramics," *International Symposium on Intelligent Control* **299**, pp. 216–221, Taipeei, Taiwan, 2004.

[26] J.Lin and W.-Z. Liu, "Experimental evaluation of a piezoelectric vibration absorber using a simplified fuzzy controller in a cantilever beam," *Journal of Sound and Vibration* **296**, pp. 567–582, 2006.

[27] J. Fei and Y. Fang, "Active feedback vibration suppression of a flexible steel cantiliver beam using smart materials," *International Symposium on Intelligent Control* **299**, pp. 89–92, Taipeei, Taiwan, 2004.

[28] M. van de Wal and B. de Jager, "A review of methods for input/output selection," *Automatica* **37**(4), pp. 487–510, 2001.

[29] C. S. Kubrusly and H. Malebranche, "Sensors and controllers location in distributed systems-a survey," *Automatica* **21**, pp. 117–128, 1985.

[30] R. Rana, H. Gupta, and T. Singh, "Application of controllability measure for actuator placement in a civil engineering structure," *Proceedings IEEE Conference on Control Applications* **0-7803-3876-6/97**, pp. 553–558, (Hartford, CT) 1997.

[31] S. Moheimani and T. Ryall, "Considerations on placement of piezoceramic actuators that are used in structural vibration control," *Proceedings of the 38th IEEE Conference on Decision and Control* **2**, pp. 1118–1123, Piscataway, NJ 1999.

[32] D. Chmielewski, J. Peng, and A. Manthanwar, "Convex methods in actuator placement," *Proceedings of the 2002 American Control Conference* **6**, pp. 4309–4314, Danvers, MA 2002.

[33] A. Arabyan and S. Chemishkian, "H_∞ optimal mapping of actuators and sensors in flexible structures," *Proceedings of the 37th IEEE Conference on Decision and Control* **1**, pp. 821–826, Tampa, Florida Dec 1998.

[34] F. Chee, A. Savkin, T. Fernando, and S. Nahavandi, "Optimal H^∞ insulin injection control for blood glucose regualtion in diabetic patients," *IEEE Transaction on Biommedical Engineering* **52**, pp. 1625–1631, October 2005.

[35] P. Mhaskar, N. El-Farra, and P. Christofides, "Predictive control of switched nonlinear systems with scheduled mode transitions," *IEEE Transactions on Automatic Control* **50**, pp. 1670–1680, November 2005.

[36] G. Stewart and G. Dumont, "Finite horizon based switching between stabilizing controllers," *Proceedings of the 2006 American Control Conference* , pp. 1550–1556, June 14-16, 2006.

[37] R. Decarlo, M. Branicky, S. Pettersson, and B.Lennartson, "Perspectives and results on the stability and stabilizability of hybrid systems," *Proceedings of the IEEE* **88**, pp. 1069–1082, July 2000.

[38] C. Seatzu, D. Corona, A.Giua, and A. Bemporad, "Optimal control of continuous-time switched affine systems," *Transactions on Automatic Control IEEE* **51**, pp. 726 – 741, 2006.

[39] J. P. Hespanha, D. Liberzon, and A. S. Morse, "Hysteresis-based switching algorithms for supervisory control of uncertain systems," *Automatica : the journal of IFAC, the International Federation of Automatic Control* **39, no. 2**, pp. 263–272, 2003.

[40] D. Borrelli, A. Morse, and E. Mosca, "Discrete-time supervisory control of families of two degrees of freedom linear set point controllers," *IEEE Transactions on Automatic Control* **44**, pp. 178–181, 1999.

[41] A. Bemporad, F. Borrelli, and M. Morari, "Piecewise linear optimal controllers for hybrid systems," *Proceedings of the American Control Conference. 2* **2**, pp. 1190–1194, 2000.

[42] T. Hanselmann, A. Zaknich, L. Noakes, and A. Savkin, "A hybrid dynamical system with robust switching control by action dependent heuristic dynamic programming," *IEEE International Joint Conference on Neural Networks* **3**, pp. 1779–1804, 2004.

[43] N. El-Farra, P. Mhaskar, and P. Christofides, "Output feedback control of switched nonlinear systems using multiple lyapunov functions," *Systems & Control Letters* **54**, pp. 1163–1182, 2005.

[44] J. Hespanha and A. Morse, "Switching between stabilizing controllers," *Automatica* **38**, pp. 1905–1917, 2002.

[45] Z. Sun, "Combined stabilizing strategies for switched linear systems," *IEEE Transactions on Automatic Control* **51**, pp. 666–674, 2006.

[46] G. Zhai, D. Liu, J.Imae, and T. Kobayashi, "Lie algebraic stability analysis for switched systems with continuous-time and discrete-time subsystems," *IEEE Transactions on Circuits and Systems* **53**, pp. 152–156, 2006.

[47] M. Margaliot, "Stability analysis of switched systems using variational principles: An introduction," *Automatica* **42**, pp. 2059–2077, 2006.

[48] S.Yoshikawa, A. Bogue, and B. Degon, "Commercial application of passive and active piezoelectric vibration control," *Proceedings of the Eleventh IEEE International Symposium on Applications of Ferroelectrics, 1998. ISAF 98.* , pp. 293 – 294, Aug. 1998.

[49] V. G. S. Sethi, "Multimode optimal vibration control of flexible structure using piezoceramics," *Proceedings of the 2004 IEEE International Symposium on Intelligent Control, 2004.* , pp. 216 – 221, 2004.

[50] E. Ventsel and T. Krauthammer, "Thin plates and shells : theory, analysis, and applications," 2001.

[51] L. Meirovitch, *Dynamics and Control of Structures*, John Wiley & Sons, Inc., New York, 1990.

[52] A. Leissa, *Vibration of Plates*, Acoustical Society of America, Melville NY, 1993.

[53] A. Preumont, *Vibration Control of Active Structures: An Introduction*, Kluwer Academic Publishers, Dordrecht-Boston, 1997.

[54] R. C. Smith, *Smart Material Systems: Model Development*, SIAM, Society for Industrial and Applied Mathematic, Philadelphia, PA 19104 USA, March 2005.

[55] P. M. Prenter, *Spline and Variational Methods*, Wiley-Masson, New York, 1975.

[56] W. Gawronski, *Advanced Structural Dynamics and Active Control of Structures*, Springer, New York, 2004.

[57] R. D. Blevins, *Formulas for Natural Frequency and Mode Shape*, Krieger Publishing Company, Melbourne Florida, 1979.

[58] M. Balas, "Active control of flexible systems," *Journal of Optimization Theory and Applications* **23**, pp. 415–436, 1978.

[59] J. Bontsema and R. Curtain, "A note on spillover and robustness for flexible systems," *IEEE Transaction on Automatic Control* **33**, pp. 567–569, 1988.

[60] F. Wang, D. Li, and G. Tang, "Robust optimal sensor configuration for modal sensing," *First International Symposium on Systems and Control in Aerospace and Astronautics (IEEE Cat. No.06EX1168C)* , pp. 67–71, 2006.

[61] D. Halim and S. R. Moheimani, "An optimization approach to optimal placement of collocated piezoelectric acutators and sensors on a thin plate," *Mechatronics* **13**, pp. 27–47, 2003.

[62] C. Chantalakhana, "Stability improvement of modal controllers for suppressing beam vibrations using a hybrid control scheme," *IEEE ICIT '02. 2002 IEEE International Conference on Industrial Technology* **1**, pp. 549–554, 2002.

[63] Y. Sugiyama, T. Katayama, E. Kanki, K. Nishino, and B. Akesson, "Stabilization of cantilevered flexible structures by means of an internal flowing fluid," *Journal of Fluids and Structures* **10**, pp. 653–661, 1996.

[64] H. D. and M. S. O. R., "Compensating for the truncation error in models of resonant systems that include damping," *Proceedings of the 41st IEEE Conference on Decision and Control* **3**, pp. 3390 – 3395, 2002.

[65] K. Zhou and J. Doyle, *Essential of Robust Control*, Prentice Hall, Englewood Cliffs, 1997.

[66] B. Anderson and J. Moore, *Optimal Control: Linear Quadratic Methods*, Prentice Hall, Englewood Cliffs, 1990.

[67] S. Han, "A globally convergent method for nonlinear programming," *Journal of Optimization Theory and Applications* **22**, p. 297, 1977.

[68] M. Powell, "The convergence of variable metric methods for nonlinearly constrained optimization calculations," *Nonlinear Programming 3* **Academic Press**, 1978.

[69] J. J. More, "Gradient projection techniques for large-scale optimization problems," *Proceedings of the 28th IEEE Conference on Decision and Control* **1**, pp. 378 – 381, 1989.

[70] G. Yu, Z. Yanlin, and W. Zengxin, "A descent nonlinear conjugate gradient method for large-scale unconstrained optimization," *Applied mathematics and computation* **187, no. 2**, pp. 636 – 644, 2007.

[71] J. W. Herrmann, "A genetic algorithm for minimax optimization problems," *Proceedings of the 1999 Congress on Evolutionary Computation* **2**, pp. 1099–1103, 1999.

[72] O. V. Iftime and M. A. Demetriou, "Optimal control for switched distributed parameter systems with application to the guidance of a moving actuator," in *Proceedings of the 16th IFAC World Congress*, (Prague), July 4-8 2005.

[73] M. A. Demetriou and O. V. Iftime, "Finite horizon optimal control of switched distributed parameter systems with moving actuators," in *Proceedings of the 2005 American Control Conference*, (Portland, OR), June 8-10 2005.

[74] M. A. Demetriou, "Optimal switching policy of smart actuators in flexible structures," in *Proceedings of SPIE's 8th Annual International Symposium on Smart Structures and Materials and NDE for Health Monitoring and Diagnosis*, **4326**, pp. 220–231, (San Diego), 2001.

[75] F. M. Callier, J. Winkin, and J. L. Willems, "On the exponential convergence of the time-invariant matrix riccati differential equation," *Proceeding of the 31st Conference on Decision and Control* , pp. 1536–1537, 1992.

[76] Z. Sun and S. S. Ge, *Switched Linear Systems: Control and Design*, Springer, New York, NY 10013, 2005.

[77] P. Mhaskar, N. H. El-Farra, and P. D. Christofides, "Stabilization of nonlinear systems with state and control constraints using lyapunov-based predictive control," *Systems & Control Letters* **55, Issue 8**, pp. 650–659, 2006.

[78] Garcia, Prett, and Morari, "Model predictive control: theory and practice," *Automatica* **25**, pp. 335–348, 1989.

[79] D. Liberzon, *Switching in Systems and Control*, Springer, New York, NY 10013, 2003.